Characteristics of fluid electrical conductivity (FEC) profiles associated with a contaminant plume in porous and weathered basement aquifer systems

Malefa Florence Moleme

Student number: 2008013569

Submitted in fulfilment of the requirements for the degree
Doctor of Philosophy
majoring in Geohydrology
at the Institute for Groundwater Studies
in the Faculty of Natural and Agricultural Sciences
at the University of the Free State

Supervisor: Prof Modreck Gomo

02 October 2023

DECLARATION

I, Malefa Florence Moleme, declare that the thesis I herewith submit to the Institute for Groundwater Studies in the Faculty of Natural and Agricultural Sciences at the University of the Free State, in fulfilment of the doctoral degree, Doctor of Philosophy, majoring in Geohydrology, is my independent work, and that I have not previously submitted it for a qualification at another institution of higher education. In addition, I declare that all sources cited have been acknowledged by means of a list of references.

…………………………………….

Malefa Florence Moleme

02 October 2023

ABSTRACT

The fluid electrical conductivity (FEC) profiling method has been commonly applied to aid in the compilation of site-specific conceptual models and understanding of the subsurface environment. Although research has recently been conducted to help improve the knowledge and understanding of the evolution of FEC profiles under natural and saline contaminated environments within the fractured-rock aquifer system, a research gap still exists for such studies in other aquifer types. The type of aquifer system plays a significant role in determining the migration patterns and behaviour of contaminants. Therefore, it is expected that the evolution of FEC profiles in different aquifer systems will vary, and this needs to be understood. It is against this background that this research aimed to investigate the behaviour of FEC profiles associated with a saline contaminant plume in typical unconfined porous and weathered basement aquifer systems, using laboratory-based aquifer models. This was done to improve the conceptual understanding of contaminant migration within these aquifer systems, which will essentially improve the interpretation of their FEC profiles. To achieve this, two physical models were developed in the laboratory to represent an unconfined porous aquifer system and a weathered basement aquifer system. The performance of the models was evaluated and tested, and subsequently used to investigate the progression of FEC profiles associated with a saline contaminant plume. The outcome of the laboratory tests was also verified in the field. This study also explored the effects that the distance of a source from a monitoring point would have on the shape of FEC profiles. Unlike previous studies which conducted the FEC profiling technique under induced groundwater flow, this study investigated the efficiency of a non-invasive approach of applying the method under natural gradient conditions. From the analysis of profiles obtained within the two simulated aquifer systems conceptual profiles were developed. Within the unconfined porous aquifer system, FEC profiles recorded from the borehole located closer to the source were notably different from the FEC profiles recorded from a borehole positioned further away from the source, thus it was evident that the distance of a monitoring point from the source influenced the orientation of the plume, and ultimately the resulting FEC profile. This brought to light the phenomenon of “plume orientation”. The orientation of the plume is usually disregarded in groundwater models and assessments, however this research showed that it is an important aspect which can be used to assist with FEC data interpretation and contaminated site characterisation studies.

The orientation of the plume was strongly influenced by the magnitude of the forces acting upon it, primarily the gravitational and advection force. Closer to the source, the plume took on a vertical to sub-vertical orientation, whereas as the plume continued to migrate further away from the source it aligned with the flow lines of the system which resulted in a horizontal orientation. From the analysis of the weathered basement aquifer system two distinct signatures were identified and conceptualised: the low FEC profile and the elevated FEC profile. The low FEC profile not only represented a profile captured under natural conditions in the absence of contamination, but also represented a profile that would be observed when the majority of the contaminant has passed the borehole and the system was in the process of re-establishing initial conditions. It had three distinct zones: the weathered zone, transition zone, and the impermeable zone. The elevated FEC conceptual profile was associated with contaminated groundwater conditions within the weathered basement aquifer system. It had two distinct zones: the weathered zone and the impermeable zone.

Keywords: Aquifer; Borehole profiling; Conceptual profile; Contaminant plume; Fluid electrical conductivity; Groundwater flow; Mass transport; Natural water; Non-invasive approach; Porous media; Tracer breakthrough curve; Unconfined porous aquifer system; Weathered basement aquifer system

ACKNOWLEDGEMENTS

I would like to express my deepest gratitude and appreciation to the following people:

- My academic supervisor, Prof Modreck Gomo, for his constant motivation, tireless technical and academic guidance, and his overall commitment and support which contributed greatly towards my academic development.
- My parents, Molefi Joseph and Morakane Sina, my siblings Lebohang and Sebabatso, and my aunt Soni Justina Kholotsa, for their continued and immeasurable support throughout my academic career and for being a great inspiration to me.
- The University of the Free State for funding this project, and the Institute for Groundwater Studies (IGS), for providing the proper administrative facilities to undertake this study.
- Above all, I acknowledge the grace of God upon my life and wish to thank Him for making everything possible.

TABLE OF CONTENTS

LIST OF FIGURES

LIST OF TABLES

LIST OF ABBREVIATIONS AND ACRONYMS

ATV	Acoustic tele-viewer
BH	Borehole
EC	Electrical conductivity
EM	Electromagnetic
FEC	Fluid electrical conductivity
NaCl	Sodium chloride
ORP	Oxidation-Reduction-Potential
OTV	Optical tele-viewer
PVC	Poly-vinyl chloride
SI	International System of Units
SP	Self-potential
TLC	Temperature-level-conductivity

Chapter 1
INTRODUCTION

1.1 Background

In contaminated land studies the knowledge and understanding of migration patterns within the subsurface environment is an important aspect which can assist with finding appropriate remediation approaches. The fluid electrical conductivity (FEC) profiling method has been widely applied to provide insight on the subsurface environment, this includes locating groundwater flow zones during groundwater sampling (Gomo and Vermeulen 2015; Gomo et al., 2017), identifying karst aquifers (Smart and Worthington, 2003), assisting in the understanding of solute mass transport properties (Xu et al., 1997), and the development of conceptual site models (Worthington and Smart, 2017). The method has also been identified as one of the most effective tools used to obtain information on the basic aquifer hydraulic characteristics, without the complexities of other alternative methods such as packer tests (Doughty and Tsang, 2005; Tsang et al., 1990).

Traditionally, the FEC profiling method entails replacing fluid within the borehole with fluid which has a contrasting EC to that of the water in the formation (Tsang et al., 1990). Thereafter, repeated profiling cycles are performed with an EC probe over the length of the water column in order to detect zones that are experiencing changes in EC. The obtained time function EC measurements are then used for the estimation of hydraulic properties (Beauheim and Pedler, 2009; Doughty and Tsang, 2005; Moir et al., 2014; Tsang et al., 1990).

While the FEC profiling technique has been in use for over a decade for various site characterisation purposes, its application has mostly been in fractured-rock aquifer systems (Beauheim et al., 1997; Doughty et al., 2013; Gebrekristos, 2007; Gomo, 2009; Kurikami et al., 2008 and Pacome, 2010), and very little research has been devoted towards understanding FEC responses in other aquifer systems. The type of aquifer system plays a crucial part in determining the behaviour of contaminants and their migration patterns. Therefore, it is expected that the evolution of FEC profiles obtained in different aquifer systems will vary.

Although research has recently been conducted to help improve the knowledge and understanding of the evolution of FEC profiles under natural and saline contaminated environments within the fractured-rock aquifer system (Moleme, 2017; Moleme and Gomo, 2018), a research gap still exists for such studies in other aquifer systems. It is against this background that the aims of this research are based.

1.2 Aims and objectives

The aim of this study is to assess the behaviour of FEC profiles associated with a saline contaminant plume, in typical unconfined porous and weathered basement aquifer systems using laboratory-based aquifer models and field tests. This was done to improve the conceptual understanding of contaminant migration patterns within these aquifer systems, and to essentially improve the interpretation of their FEC profiles. Additionally, this study aims to investigate if the distance of a contaminant source (injection point) from a borehole has any effects on the evolution of FEC profiles.

These aims will be achieved through the following objectives:

1. Designing and constructing physical models that are representative of typical unconfined porous and weathered basement aquifer systems.
2. Simulating two groundwater flow conditions; natural water flow and contaminated groundwater conditions.
3. Testing the extent to which the physical models can simulate real systems based on literature.
4. Once the physical models are deemed adequate, using them to assess, monitor and develop FEC profiles under controlled laboratory conditions.
5. Conducting the laboratory tests multiple times using varying salt concentrations to assess repeatability.
6. Conducting field tests to verify the results obtained in the laboratory.

Since the unconfined porous aquifer system is the most ideal and homogeneous system, it will be used to investigate the effects that a monitoring borehole’s distance from a contaminant source has on the resulting FEC profiles.

Unlike previous studies which conducted the FEC profiling method under induced groundwater conditions (Beauheim and Pedler, 2009; Doughty and Tsang, 2002, 2005; Doughty et al., 2005; Mohr and Smith, 2019; Tsang et al., 1990), this study will explore the efficiency of a non-invasive approach, namely conducting FEC profiling under natural gradient conditions during the laboratory tests.

1.3 Significance of the research

The structure of an aquifer system is expected to influence the shape of the resulting FEC profile. In recent years research has been conducted to help improve the understanding and interpretation of FEC profiles associated with diverse groundwater conditions within the fractured-rock aquifer system (Moleme, 2017; Moleme and Gomo, 2018). However, such studies still have not been conducted in other aquifer systems.

Therefore, as its primary outcome this study intends to provide insight on the characteristics of FEC profiles under diverse groundwater conditions in unconfined porous and weathered basement aquifer systems, and ultimately produce conceptual profiles which may be referred to as guidelines during the interpretation of FEC profiles obtained in such systems.

1.4 Thesis structure

This study is divided into six chapters inclusive of this introduction (Chapter 1), which presents the aims, objectives, significance of the study and the general structure of the thesis. Chapter 2 provides a review on the literature available on borehole profiling methods, with a primary focus on the FEC profiling method, its basic principles, application, analytical and numerical solutions. The physical characteristics of unconfined porous and weathered basement aquifer systems, groundwater flow and mass transport properties in porous media, as well as various hydrogeological test models are also discussed in this chapter.

In Chapter 3 the methods and materials of the laboratory tests are presented. This includes the design and construction of the physical models, the application of tracer breakthrough tests to assess the performance of the models, and details on the FEC profiling method set-up. Thereafter the chapter discusses the results obtained from the laboratory tests.

Chapter 4 reports on the tests conducted in the field to verify the outcome of the laboratory tests. This includes the description of the sites used, methods and materials, and the results and discussions. Chapter 5 presents the conceptual profiles obtained from the porous, and weathered basement aquifer tests. Chapter 6 offers a summary and conclusions for the study and provides recommendations for further studies. Lastly, a reference list is documented, followed by the appendices.

Chapter 2
THEORETICAL BACKGROUND

2.1 Introduction

The focus of this theoretical background section is to provide a brief review on borehole profiling methods, with a primary focus on the FEC profiling method - its principles, applications, and analytical tools. A review on the mass and transport processes in typical porous media is also included because it is these processes, together with the hydraulic properties of the formation that influence the shape of FEC profiles. Additionally, a brief review on the classification of hydrogeological models and the effects of scaling in modelling is discussed.

2.2 Hydrogeological borehole profiling methods

Borehole profiling refers to the process of measuring the physical, structural, and chemical properties of penetrated geological formations (Wonik and Olea, 2007). This can be done by lowering a probe into the borehole using a wireline cable or rope. The measurements are recorded as a function of depth and may be taken continually or discretely within the borehole.

Hydrogeological borehole profiling methods can be used to determine (a) physical parameters such as density, dielectric constant, electrical resistivity, and velocity of elastic waves; (b) geometric parameters such as azimuth, dip, orientation of fractures, bedding planes and joints; (c) conditions of the borehole i.e. casing, screens and cementation; and (d) water quality parameters such as pH, EC, temperature, and Oxidation Reduction Potential (ORP).

Hydrogeological borehole profiling can be divided into geophysical, geochemical, and flowmeter profiling techniques. The methods are primarily differentiated based on their distinct principles, specific profile, the required borehole conditions as well as the information that can be obtained from them. This sub-section will briefly discuss these profiling methods.

2.2.1 Geophysical profiles

Geophysical borehole profiling allows for an in-situ determination of groundwater and physical properties of the rock strata. Its use and applications have been extensively researched in environmental studies (Keys, 1989; Taylor et al., 1990), hydrogeological assessments

(Jorgensen and Petricola, 1995; Mares et al., 1994; Repsold, 1989), geological investigations (Doverton and Prensky, 1992), and salt-freshwater research (Hwang et al., 2004). These methods are commonly based on physical properties indirectly related to contrasts in the subsurface such as layer contact zones, change in rock properties or inflow zones (Wonik and Hinsby, 2006). The most commonly used geophysical borehole profiling methods in groundwater studies are the acoustic, optical, electromagnetic, and electrical methods.

2.2.1.1 Acoustic profiling method

The acoustic profiling method has been used to determine the compressional velocity of rocks adjacent to the borehole as a function of depth along the borehole since the early 1960s. The method was developed to be comparable to porosity profiling using a variety of equipment, such as density and neutron profiling probes (Zemanak et al., 1970). In this technique the profile would produce compressional velocity values averaged over a certain volume, with compensation being made for borehole effects such as drilling damage, diameter, and invasion.

As of recently acoustic profiles can also be obtained using a combination of an acoustic source and several receivers. The source is either a magnetostrictive or piezoelectric device which generates signals into the borehole fluid, and the receivers are piezoelectric crystals which translate transmitted pressure waves into electromagnetic signals that can then be transmitted up the profiling cable. A profiling tool centralized in the borehole is used to take measurements (Paillet et al., 1992).

Acoustic profiling is generally conducted in open boreholes with fluid. The method can detect fracture zones and help determine the lithological classification of the rock sequence, if the rock matrix velocity is known, porosity can also be determined using the method. To obtain photographic-like images of the borehole wall an acoustic tele-viewer (ATV) probe is used. The ATV imaging system makes use of an ultrasonic pulse-echo configuration with a 0.5 – 1.5 MHz transducer. The amplitude and transit time of the reflected acoustic signal are recorded as photographic-like images as shown in Figure 2-1C and D. The transit time data can also be used to produce high resolution caliper profiles as shown in Figure 2-1A and B. The most commonly used ATV tools may range from 1.7 to 3.7 m in length and 40 to 50 mm in diameter (Williams and Johnson, 2004), they can be applied in water or light mud filled intervals in boreholes.

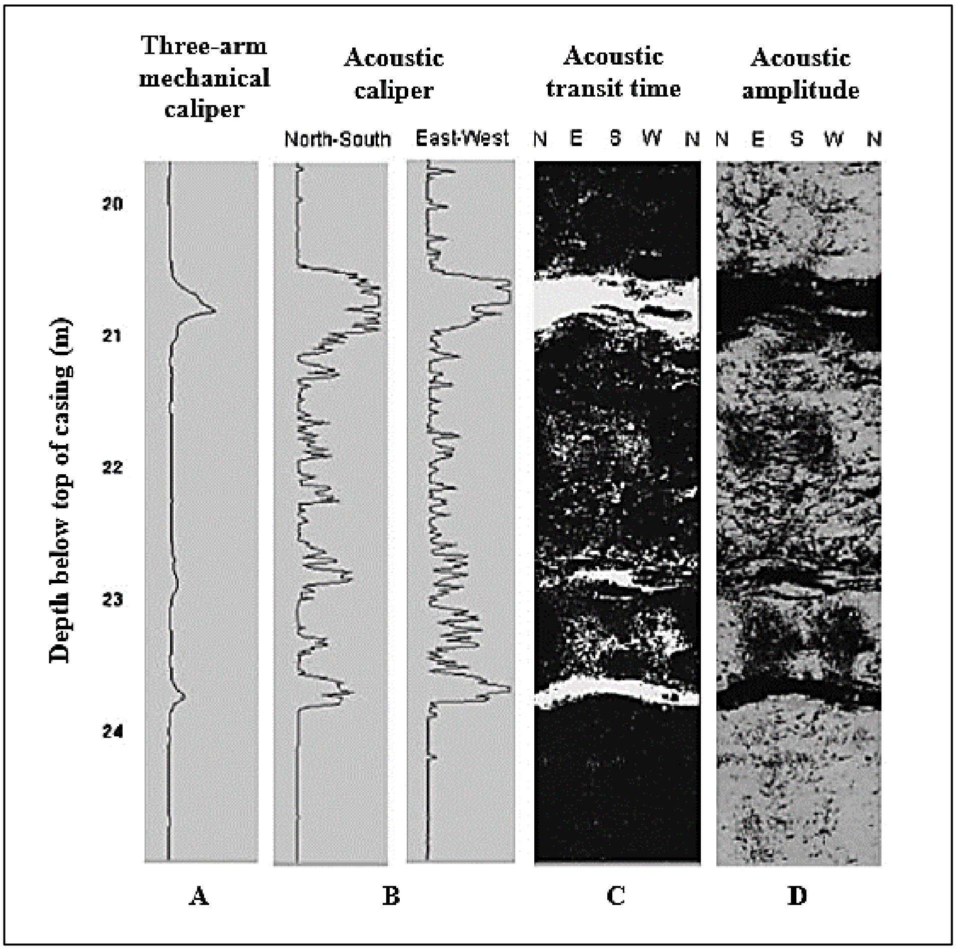

Figure 2-1 (A) Three arm mechanical acoustic profile, (B) acoustic caliper profile, (C) acoustic transit time profile, and (D) acoustic tele-viewer images obtained in a 150 mm diameter borehole.

Source: Williams and Johnson, 2004.

The acoustic profiling method has been found to be effective even in environments that are usually hostile to downhole probes such as complex geothermal reservoirs. According to Lacy and Smith (1989), acoustic emissions can be used to detect and determine the geometry of fractures in the reservoirs which assists in the understanding and interpretation of their nature.

2.2.1.2 Optical profiling method

Although the first optical tele-viewer (OTV) was developed in 1987, their use in groundwater studies only became popular in the mid-to late 1990s. OTV imaging systems make use of a charge coupled device camera to measure the intensity of the colour spectrum; a hyperbolic or conical reflector contained in a transparent cylindrical window to focus the 360jslice of the borehole wall in the camera's lens; and ring lights to illuminate the borehole (Gochioco et al., 2002). The intensity of the light can be adjusted in most OTV devices.

The optical image scan is sent up the profiling cable as an analog signal and digitised either downhole or up-hole and sent up as a digital signal. Lithology and structural features such as bedding planes, fractures, and foliation can be viewed directly on the OTV images. OTV imaging systems can function in dry or clear water-filled boreholes, and the quality of the images can be significantly affected by muddy water, bacterial growth, chemical precipitation, and other conditions that affect the clarity of water in the borehole (Williams and Johnson, 2004). Although fractures can generally be recognised on both acoustic and optical images, they are more apparent and easier to distinguish under a range of conditions in acoustic images i.e. cloudy borehole water, dark coloured rocks, and coated borehole walls. However, optical images allow for direct viewing of the correlation between lithological and structural features as shown in Figure 2-2. Therefore, both the acoustic and optical imaging systems have their individual advantages and drawbacks, the decision of which method to apply should be determined by the objectives of the study.

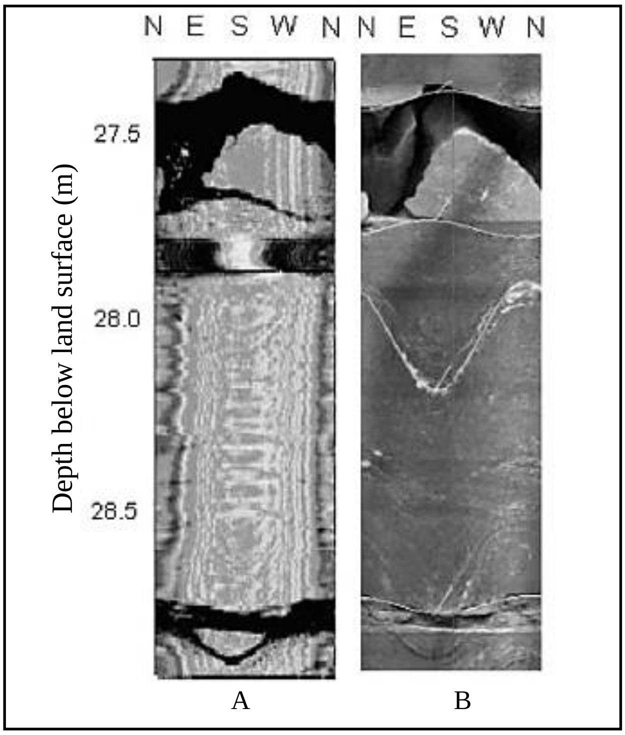

Figure 2-2 (A) An acoustic and (B) optical tele-viewer image of a 75 mm diameter borehole drilled in a gneiss.
Source: Stumm et al., 2001.

2.2.1.3 Electromagnetic profiling method

Electromagnetic (EM) profiling methods have been extensively applied in geo-hydrological studies to assist with contaminant mapping (DeSimone and Barlow, 1993), groundwater salt tracking (Church and Friesz, 1993), lithological classification of the rock sequence (Maute, 1992), and identification of subsurface structural features (Spies, 1996; Wonik and Hinsby, 2006). They can be applied in boreholes that are dry or filled with water, and unlike electrical methods they can also be used in boreholes with plastic casing (Smits et al., 1993; Spies, 1996).

When identifying lithology or structural features, parameters such as electrical conductivity and resistivity are measured. These parameters are determined using either an induction or susceptibility tool. Although low frequency electrode tools have been widely used, high electrode tools such as induction tools have become the most preferred resistivity tool due to their efficacy in lithology with high resistivity (i.e. oil-based muds) and their precision at greater depths (Spies, 1996).

An induction device operates with a transmitter coil and two or more receiver coils. The transmitter coil generates an alternating magnetic field around the borehole which induces electrical eddy currents proportional to the conductivity of the rock. The receiver coils are wound in the opposite direction thus making the net free-space signal zero (Doll, 1949). Over the years, additional transmitter or receiver coils have been added onto the device to improve sensitivity in deeper formations (Barber and Rosthal, 1991; Martin et al., 1984; Wonik and Hinsby, 2006). Improved electronics and processing software have also made it possible to measure the small "out of phase signal" also referred to as the X-signal, thus enabling compensation to be made for the skin effect during data interpretation (Brown et al., 1985).

2.2.1.4 Electrical profiling method

Electrical profiling methods are applied in fluid-filled boreholes. They are used to obtain the electrical resistivity of rocks which when coupled with other physical parameters can help develop lithological profiles (Maute, 1992; Ward, 1980). While some electrical profiling tools record self-potential, others use numerous electrode configurations to determine resistivity.

Self-potential (SP) originates from a range of sources including filtration (electro-kinetic potential) and gradients in ionic concentrations (electrochemical potential). The SP measurement entails the recording of the potential difference between an electrode at the surface and an electrode in the borehole (Doll, 1949; Wyllie, 1948). The electrochemical potential is derived from two solutions with different salinity such as the formation fluid and the mud filtrate. The difference between the two concentrations creates an ionic current path through the formation into adjacent beds with different electrochemical properties, thus forming a closed current path through the borehole (Spies, 1996). The electrochemical potential is usually greater than the electro-kinetic potential which relies greatly on the conductivity of the fluid (Gondouin and Scala, 1958).

In conventional borehole resistivity profiling techniques i.e. micro-log and electro-log, a four-electrode array is used to determine the resistivity of the rock. A constant current is initiated into the rock between two current electrodes in the profiling tool. The potential recorded between the two potential electrodes is proportional to the electrical resistivity of the rock. The measured value which is referred to as the "apparent resistivity" depends on the overlying and underlying rocks, the adjacent rock, and the size of the borehole (Rauen and Lastovickova, 1995). The apparent resistivity can be used to derive the "true" resistivity using master curves (Spies, 1996). Figure 2-3 shows the typical borehole electrical profiles derived from a sedimentary sequence using various electrical profiling probes.

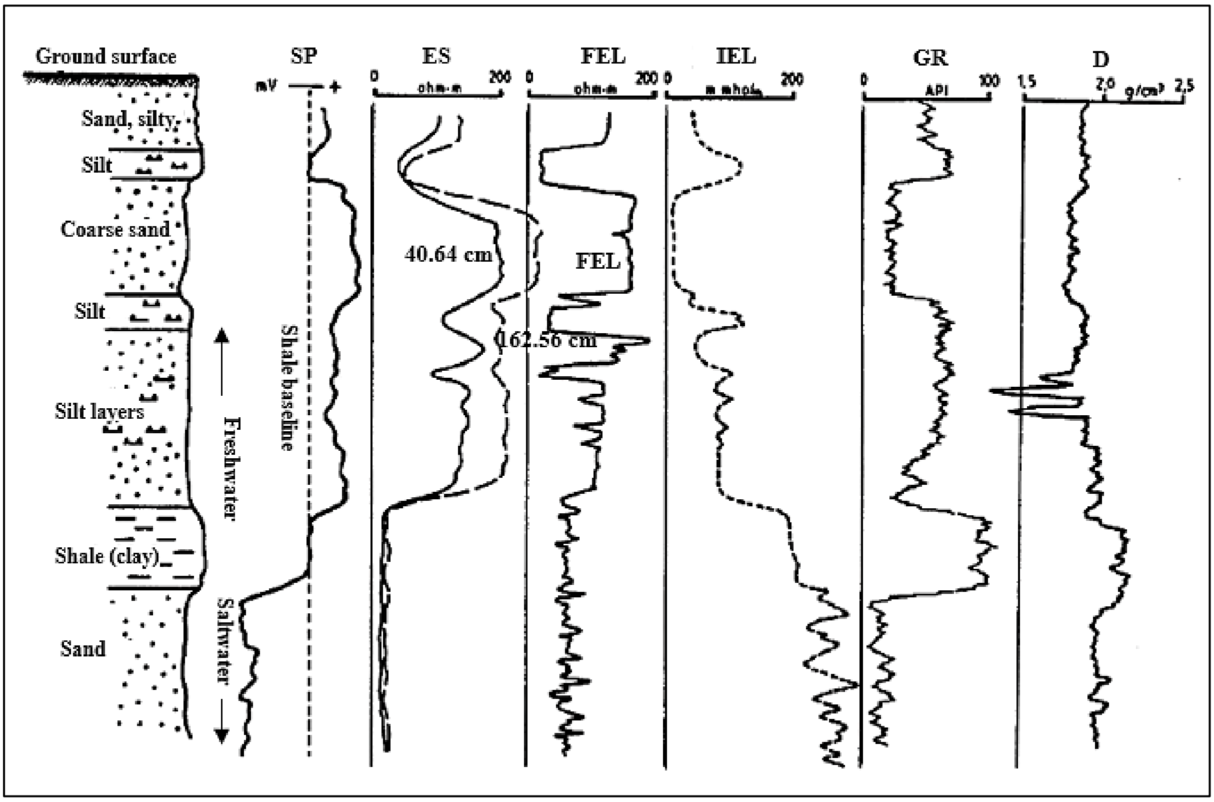

Figure 2-3 Borehole electrical profiles derived from a sequence of sedimentary rocks. SP: Self-potential; ES: Electric profile; FEL: Focused electric log; IEL: Induction log.

Source: Repsold, 1989.

2.2.2 Geochemical profiles

Geochemical borehole profiling is conducted in boreholes with drilling fluid or water. When using this method various geochemical parameters can be measured using a suitable profiling tool i.e. a parameter specific or multi-parameter tool. These parameters include pH, reduction potential (Eh)/ ORP and fluid electrical conductivity (FEC). Among these the FEC parameter profiling technique is the most commonly used because it has proven to be effective, efficient, readily available and relatively inexpensive. This method entails lowering a manual or automated EC probe into the borehole column to obtain electrical conductivity and groundwater level measurements simultaneously. The measurements can be recorded either as the probe is being lowered down into the borehole or pulled upwards towards the surface. The temperature values of fluid can be obtained simultaneously with FEC and groundwater measurements using a hand-held Temperature-Level-Conductivity (TLC) probe. The obtained profiles can be used to give an indication of the vertical movement of the fluid within the borehole (Wonik and Hinsby, 2006).

Since the FEC profiling method is the most commonly applied geochemical profiling method, as well as the method employed in this study, additional information on its principles, application and analysis is provided in Section 2.3.

2.2.3 Flowmeter profiles

Borehole flowmeters are downhole tools that are commonly used to measure the magnitude of axial flow in the borehole. Profiles of axial flow during ambient conditions can assist in determining the direction of the vertical hydraulic gradient, locate hydraulically active fractures and assess cross contamination among different geologic units (Molz et al., 1994). Profiles of axial flow during induced flow conditions can aid in locating vertical positions of borehole screens, measure hydraulic conductivity profiles and identify hydraulically active fractures.

The propeller of the flowmeter is turned by water flowing through the meter, and revolutions are recorded. Any water movement caused by the movement of the tool is corrected during data processing. The radius of the borehole has a significant influence on the measurements recorded, therefore when using flowmeters in open boreholes they should always be coupled with caliper profiling tools. A caliper has one or more arms with springs to stabilise the ends of the arms against the borehole walls (Wonik and Hinsby, 2006). These tools require clear water because suspended and high viscosity matter affects their functionality.

Flowmeters range from impeller flowmeters which require high velocity to rotate their blades (Hill, 1990), to electromagnetic and heat-pulse flowmeters which can be applied under velocities as low as 10^{-3} meters per second (Hess, 1986; Molz et al., 1994; Kazumasa et al., 2006). Figure 2-4 shows a caliper, fluid-temperature, and heat-pulse interpretation profiles.

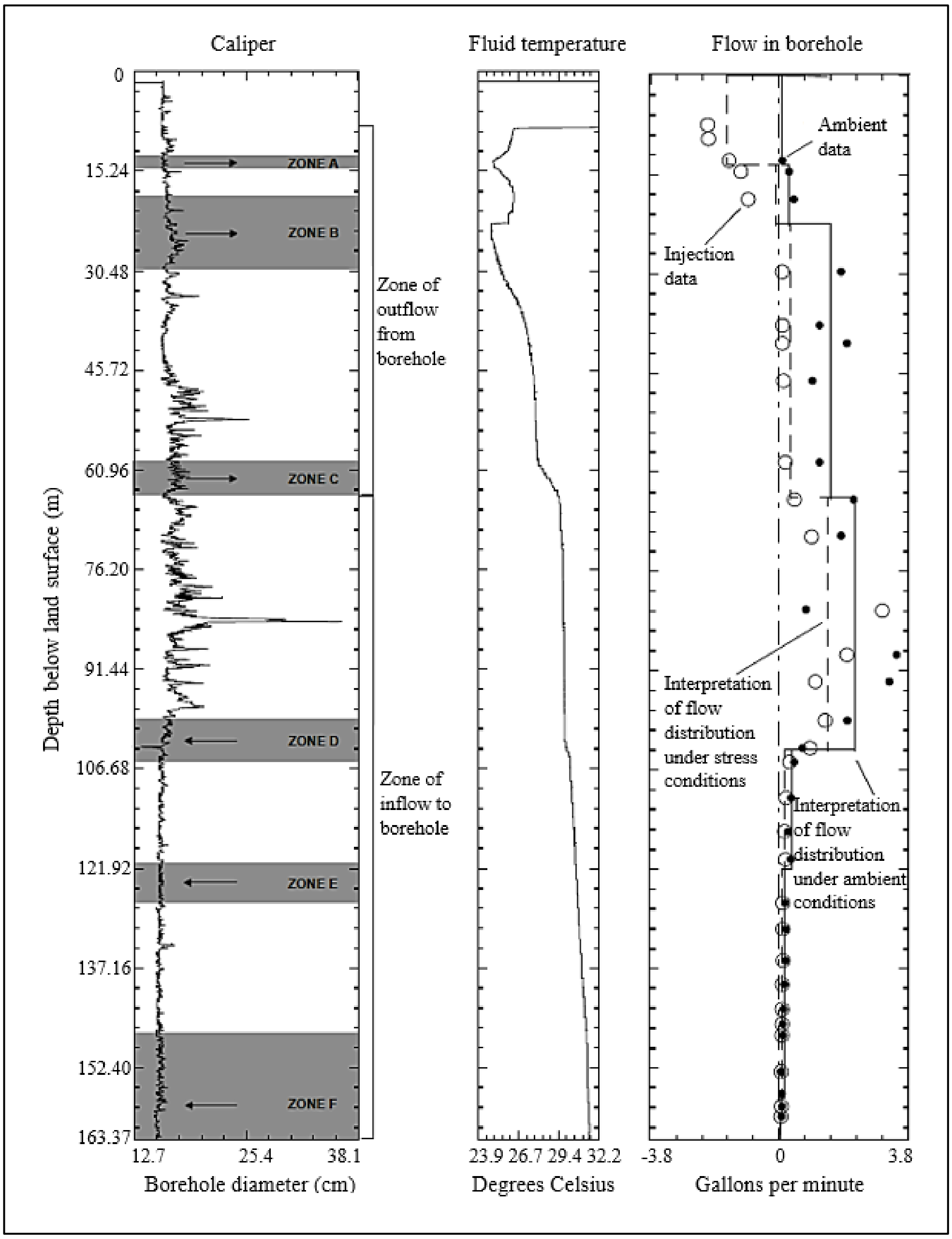

Figure 2-4 A caliper, fluid-temperature, and heat-pulse flowmeter interpretation profiles.

Source: Robledo et al., 1997.

The interpretation of flowmeter profiles is not always simple. Although six water-bearing zones were noted in Figure 2-4 these are not easily observed – especially if the profiles are interpreted in isolation. This is usually attributed to rugged borehole walls which can cause large scattering in data, particularly in intervals that have the greatest flow. It is for this reason that flowmeter profiling is often coupled with other profiling tools, such as an acoustic tele-viewer.

Table 2-1 is a summary of the discussed profiling methods, their required borehole conditions, information that can be obtained from them, known drawbacks as well as references for additional information.

Table 2-1 Comparative table of commonly used borehole profiling methods in hydrogeology.

Method	Log Type	Required Borehole Condition	Information Obtained	Drawbacks	References
Acoustic	• Acoustic waveform • Acoustic borehole tele-viewer	Uncased holes with fluid. Acoustic tele-viewer can be used in muddy water.	• Saturated porosity • Orientation and character of fracture openings and bedding.	• Measures matrix porosity instead of total porosity. • Damage to the borehole wall may affect fracture interpretation.	Paillet et al., 1992; Williams and Johnson, 2004; Zemanak et al., 1970.
Optical	• Borehole camera • Optical borehole tele-viewer	Uncased or cased, dry or clear water.	Borehole construction, secondary porosity, caving, slope and fracture detection.	No information can be obtained in muddy or cloudy water, and dark mineral bands mimic fractures.	Gochioco et al., 2002; Stumm et al, 2001; Williams and Johnson, 2004.
Electro-magnetic	• Induction • Susceptibility	PVC cased holes with or without fluid.	Lithology and detects fractures.	Influenced by fluid resistivity and bed boundaries.	Brown et al., 1985; Church and Friesz, 1993; DeSimone and Barlow, 1993; Doll, 1949; Smits et al., 1993; Spies, 1996.
Electrical	• Self-Potential • Resistivity	Screened holes with fluid.	Identification of the thickness of permeable zones, and determines water quality.	Influenced by fluid resistivity and bed boundaries; effect of reduction-oxidation.	Maute, 1992; Rauen and Lastovickova, 1995; Gondouin and Scala, 1958; Spies, 1996; Ward, 1980; Wyllie, 1948.
Fluid	Water quality	Screened holes with fluid.	Fracture position, lithology, and geochemical parameters.	Requires a contrast in solutes in borehole versus formation.	Doughty and Tsang, 2005; Tsang et al., 1988, 1989, 1990; Moir et al., 2014; Moleme and Gomo, 2018.
Flow	• Caliper • Temperature	Cased holes with clear fluid.	Vertical movement in borehole	Suspended and high viscosity matter prevents proper functioning;	Hess, 1986; Hill, 1990; Molz and Young, 1993; Robledo et al.,

				rugged borehole walls produce data scattering.	1997; Wonik and Hinsby, 2006.

2.3 The FEC profiling method, its principles, applicability, and analysis

The FEC profiling method was proposed by Tsang et al. (1990) to determine depth locations of hydraulically active zones, assess the salinity of the incoming fluid, and evaluate transmissivity at each feed point. The method has been used in numerous studies to help locate conductive zones intercepted by a borehole, and to determine other hydraulic features that control water quality (Doughty and Tsang, 2005; Moir et al., 2014; Moleme and Gomo, 2018; Pacome, 2010). This method has been found useful in both deep aquifer studies (Kelly et al., 1991; Marschall and Vomvoris, 1995) as well as shallower aquifer studies (Bauer and LoCoco, 1996; Evans, 1995; Pedler et al., 1992).

When comparing it to other alternative methods Tsang et al. (1990) described the FEC profiling method as more precise than flow meters, and less complex and more efficient than packer tests. This is because flowmeter logs are strongly affected by borehole radius variations. Thus, to improve data accuracy additional instruments and resources which are not always available are required (i.e. a caliper log has to be run to calibrate the results, packers need to be used, or the flow meter needs to be coupled with other profiling tools such as an acoustic tele-viewer). Additionally, there is a low flow rate limit below which conventional flowmeter logs are no longer useful. Although heat pulse flowmeters have been developed to measure much lower flow velocities than conventional flowmeters, they also require the use of an inflatable packer to direct flow through the heat pulse flowmeter to produce more accurate results (Molz et al., 1994; Kazumasa et al., 2006).

2.3.1.1 Electrical conductivity

Electrical conductivity (EC) also referred to as specific conductance, is a measure of the ease with which electrical current can pass through an aqueous solution. Although its measurement unit as defined by the International System of Units is Siemens per metre ($S.m^{-1}$), due to the low conductivity values of natural water submultiples of $S.m^{-1}$ such as micro-Siemens per centimetre ($\mu S.cm^{-1}$) or milli-Siemens per metre ($mS.m^{-1}$) are generally used instead (Pacome, 2010).

The EC of fluid is mainly dependent on the presence of ions, their valence, total concentration, flexibility, and relative concentration. The EC of a material increases with its increase in impurity (Keller and Frischknecht, 1966) and pure water is commonly regarded as a non-conductor due to its notably low conductivity. It is for this reason that EC can provide valuable indications of changes in the composition of water primarily its total dissolved ions (McNeely et al., 1979). Additionally, EC offers a good measure of the inorganic chemistry quality of groundwater since solutions of most inorganic salts, acids and bases are relatively good conductors (APHA, 1998).

2.3.1.2 Basic principles of the fluid electrical conductivity profiling method

First, the borehole water is replaced with deionized water or fluid with a constant salinity distinctly different from that of the formation water (Tsang et al., 1990). It is essential to know the natural EC values of the formation water as this will provide guidance to the levels of salinity necessary to produce distinct profiles. Subsequently the borehole is pumped at a low flow rate which causes formation water to enter it through inflow zones. The changes in salinity as a function of depth are then measured using an EC probe as shown in Figure 2-5. The pump is generally placed at the shallow part of the borehole below the anticipated drawdown of the water level.

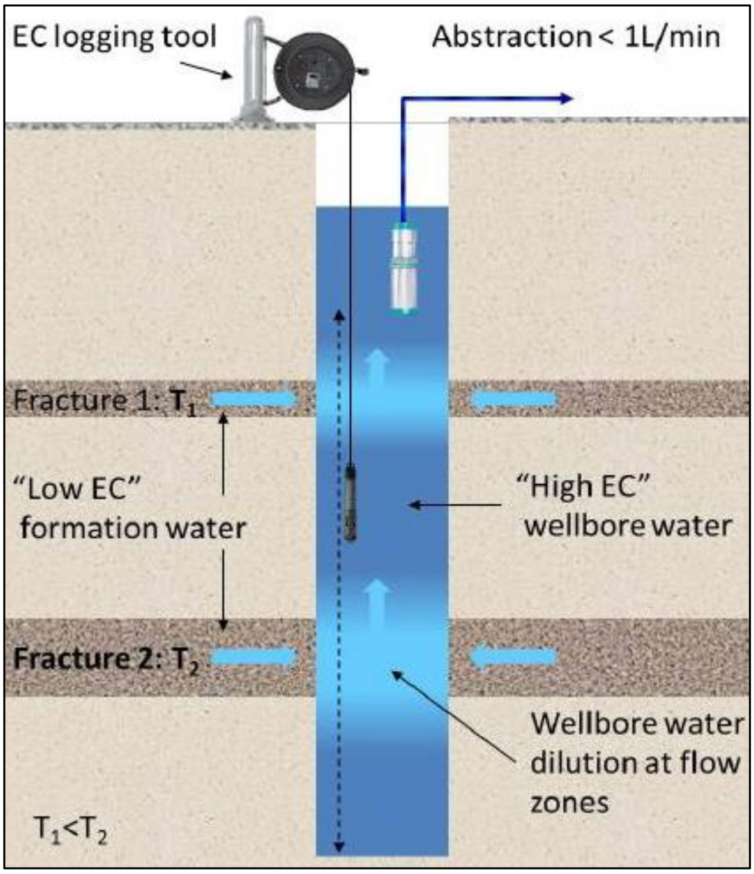

Figure 2-5 A typical FEC profiling set-up.

Source: Mohr and Smith (2019).

Thereafter a series of FEC versus depth profiles at different times are recorded and analysed. The changes in FEC noted during profiling reflect the shared effects of two factors: the EC of flowing water, and the magnitude of the flow- which is directly related to the hydraulic gradient and transmissivity (Beauheim and Pedler, 2009).

Although the application of the FEC profiling method has been deemed efficient, cost effective and versatile, the interpretation of FEC profiles has often been found to be inconsistent across various studies which has led to immense confusion. This could be because no guidelines have been developed to aid in the interpretation of these profiles. The anomaly observed in Figure 2-6 A was associated with a zone with limited porosity and absence of an inflow zone, whereas the one in Figure 2-6 B was concluded to be indicative of an inflow zone. Often these conclusions are made without any supporting evidence either from drilling logs or multiparameter readings.

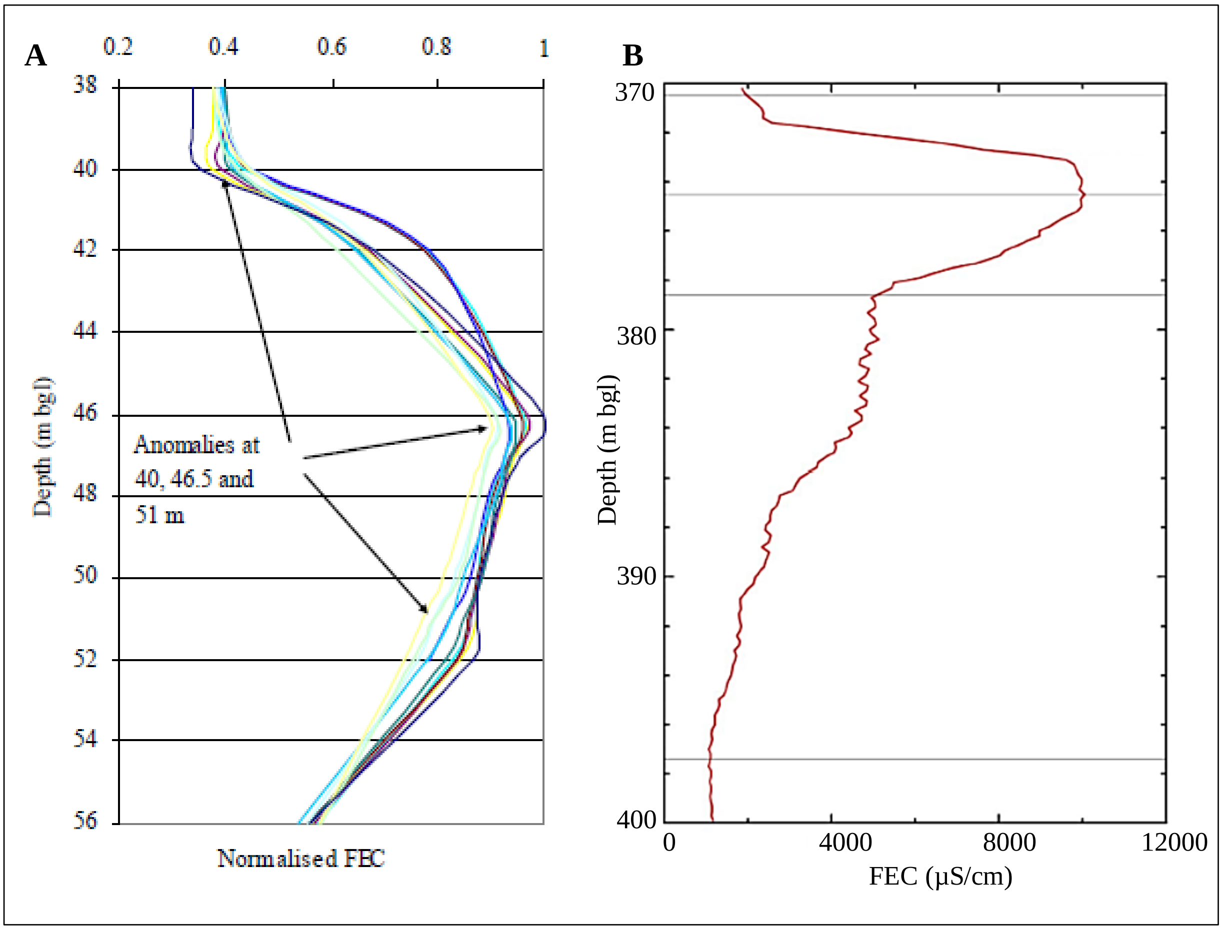

Figure 2-6 Examples of FEC profiles recorded in the field. The anomaly observed in A was attributed to a zone with limited porosity, whereas B was attributed to the presence of an inflow zone.

Source: (A) Usher et al., 2008 and (B) Beauheim and Pedler, 2009.

It is a common trend to associate anomalies in FEC profiles with a fractured aquifer system, with little or no consideration for the lithology or construction of the borehole. Anomalies are not only analogous to fractured aquifer systems, insufficient cuttings in the borehole casing could limit the inflow of water from the surrounding sedimentary aquifer into the borehole, thus resulting in an FEC profile response similar to that of a fracture. Beyond this, proper guidelines are needed to show typical FEC profiles associated with various aquifer systems.

Further details on the principles of the FEC method can be found in Doughty and Tsang (2000, 2002), Doughty et al. (2005), Gomo (2009), Kurikami et al. (2008), Moleme and Gomo (2018), Pedler et al. (1990) and Tsang et al. (1990). It is important to highlight that unlike previous studies that conventionally obtained FEC profiles under induced groundwater conditions, this current study used a non-invasive approach, and obtained FEC profiles under natural gradient conditions without pumping the system.

2.3.1.3 Application of numerical and analytical tools

Three main approaches are available for the analysis of FEC data (1) Mass Integral Analysis, a method that integrates individual profiles over the entire profiled interval to provide an estimate of the ion mass in place as a function of time, which can offer useful constraints on the direct fitting process (Doughty and Tsang, 2005); (2) BORE, a numerical model that can determine the evolution of FEC profiles in a borehole or borehole section and compares model results to profiles obtained in the field (Doughty and Tsang, 2000; Hale and Tsang, 1988; Tsang and Doughty, 1985); and (3) Multi-rate Analysis FEC analysis, which allows for the analysis of multiple sets of FEC profiles obtained under varying pumping rates (Tsang and Doughty, 2003). The three analysis tools are described in more detail below.

2.3.1.3.1 Mass Integral Analysis

When incoming formation water has distinctly higher EC values compared to the water in the borehole, the resulting FEC profiles will show high-salinity peaks in zones where water is entering the borehole. The height of the peaks at any time is dependent on the product $q_i (C_i - C_0)$, where q_i is the inflow rate, C_i the inflow concentration, and C_0 is the initial borehole concentration. For simplicity, the height of the peaks is referred to as the concentration profile (C_z), it represents the ion concentration of the borehole fluid as a function of depth.

For early-time data, prior to inflow peaks interfering with each other, mass conservation requires that at time *t*, the ion mass represented by the i^{th} concentration peak, M_i(t) be expressed as:

$$M_i(t) = q_i(C_i - C_0)t \qquad \textit{Equation 2-1}$$

Where:

t = Time [T];

q_i = Inflow rate [LT^{-1}];

C_i = Inflow concentration [ML^{-3}]; and

C_0 = Initial borehole concentration [ML^{-3}].

Thus, the area under i^{th} *C(z)* peak can be given by:

$$A_i = \int [C(z) - C_0] dz = \frac{M_i(t)}{\pi r^2} = \frac{q_i(C_i - C_0)t}{\pi r^2} \qquad \textit{Equation 2-2}$$

Where:

A_i = Area [L^2];

C_0 = Initial borehole concentration [ML^{-3}];

t = Time [T];

r = Borehole radius [L];

q_i = Inflow rate [LT^{-1}]; and

C_i = Inflow concentration [ML^{-3}].

Löw et al. (1990) showed that Equation 2-2 is valid regardless of whether there is flow entering the peak from below or not, as long as the concentration of that flow is the same as the initial concentration. To estimate the product $q_i (C_i - C_0)$, the area is calculated by integrating the ion concentration profile in the vicinity of the i^{th} feed point at a series of times. Usually less accurate integrals are obtained from very early time profiles which have small peaks. Thus, it is recommended that the largest non-interfering peaks are used to estimate the $q_i (C_i - C_0)$ product.

Generally, outflow points do not produce distinct signatures that enable them to be easily identified. Doughty and Tsang (2005) described how the Mass Integral Analysis could also be applied to help locate outflow points by observing changes in ion mass in the borehole section.

If a borehole section with one or multiple outflow points above one, or multiple inflow points is considered, and the feed-point concentration and strength is assumed not to change over time, then the procedure would be as follows: Each *C(z)* profile is integrated over the entire borehole section to obtain the area (*A(t)*) under the *C(z)* profile at time *t*. Thereafter, *A(t)* is multiplied by the mean borehole cross-sectional area to determine ion mass in place at time *t*, which is represented as the mass integral *M(t)*. Mass integral (*M(t)*) is then plotted against *t*. Before the concentration front reaches outflow points, *M(t)* is linear, with slope:

$$S_{early} = \sum_{\text{in}} q_i (C_i - C_0) \qquad \textit{Equation 2-3}$$

When the concentration front finally reaches an outflow point, a decrease in the slope of *M(t)* is observed due to the ion mass leaving the borehole at that point. When the concentration front passes the uppermost outflow point, *M(t)* becomes linear again, with slope:

$$S_{late} = \sum_{\text{in}} q_i (C_i - C_0) - \sum_{\text{out}} q_i (C_{maxi} - C_0) \qquad \textit{Equation 2-4}$$

Since steady-state concentration does not change at the outflow point and all these outflow points are above the inflow points, all outflow C_{maxi} values equal the steady-state concentration at the uppermost inflow point, which is represented as C_{max}. Thus, the above equation is simplified as follows:

$$S_{late} = S_{early} - (C_{max} - C_0) \sum_{\text{out}} q_i \qquad \textit{Equation 2-5}$$

In order to determine the aggregate outflow rate, this is rearranged to yield:

$$\sum_{\text{out}} q_i = \frac{S_{early} - S_{late}}{C_{max} - C_0} \qquad \textit{Equation 2-6}$$

Thereafter, the *C(z)* profiles are studied to determine the times when (1) *M(t)* becomes nonlinear, and (2) *M(t)* becomes linear again as shown in Figure 2-7. The leading edge of the concentration front at (1) identifies the deepest outflow point, z_{max}.

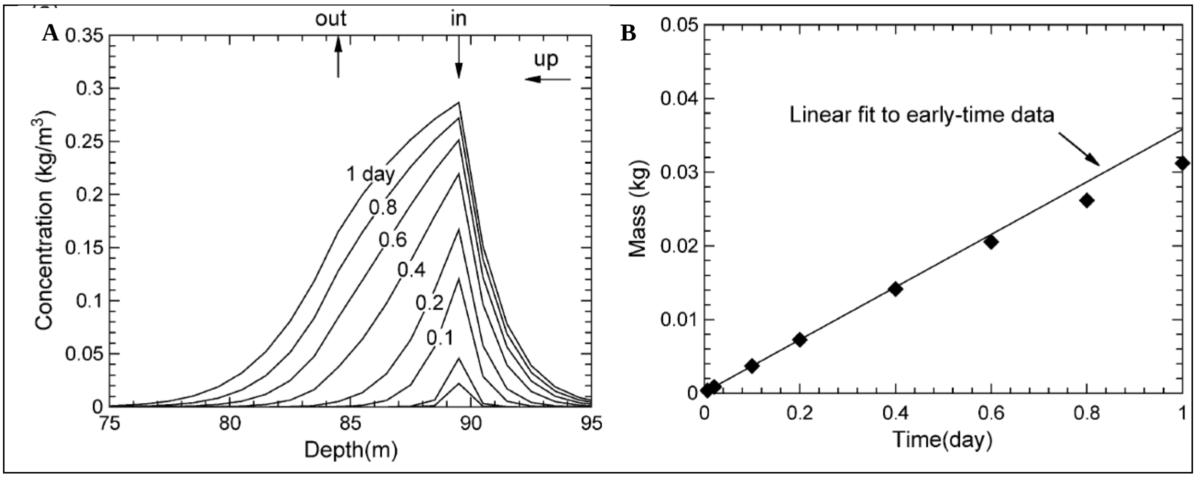

Figure 2-7 Mass Integral Analysis method applied over a short time: (A) simulated concentration profiles; and (B) *M(t)* integral and linear fit to early points.
Source: Doughty and Tsang (2005).

2.3.1.3.2 BORE

BORE is a numerical approach to FEC analysis (Hale and Tsang., 1988; Tsang, 1985). The code produces FEC profiles given different inflow parameters (i.e. inflow concentrations, positions, and inflow rates) by carrying out a forward calculation. The code also analyses solute dilution within the borehole to determine ambient horizontal flow velocity in the formation. With the advancement of numerical modelling BORE was improved to provide interactive modification of model parameters, accommodate current operating systems, and provide graphical comparisons between field and model data, the enhanced version is called BORE II (Doughty and Tsang, 2000).

BORE II also extended the range of applicability by considering multiple outflow and inflow zones, overlapping or isolated FEC peaks, time-varying feed-point strengths and concentrations, early-time and late-time behaviour and relationship of dispersion and advection in a borehole (Doughty and Tsang, 2005; Doughty et al., 2008).

Figure 2-8 illustrates a series of simulated idealised concentration profiles developed using BORE II for a borehole pumped from the top, containing feed points with a constant $q_i > 0$, constant C_i, $C_0 = 0$, and $t_{0i} = 0$.

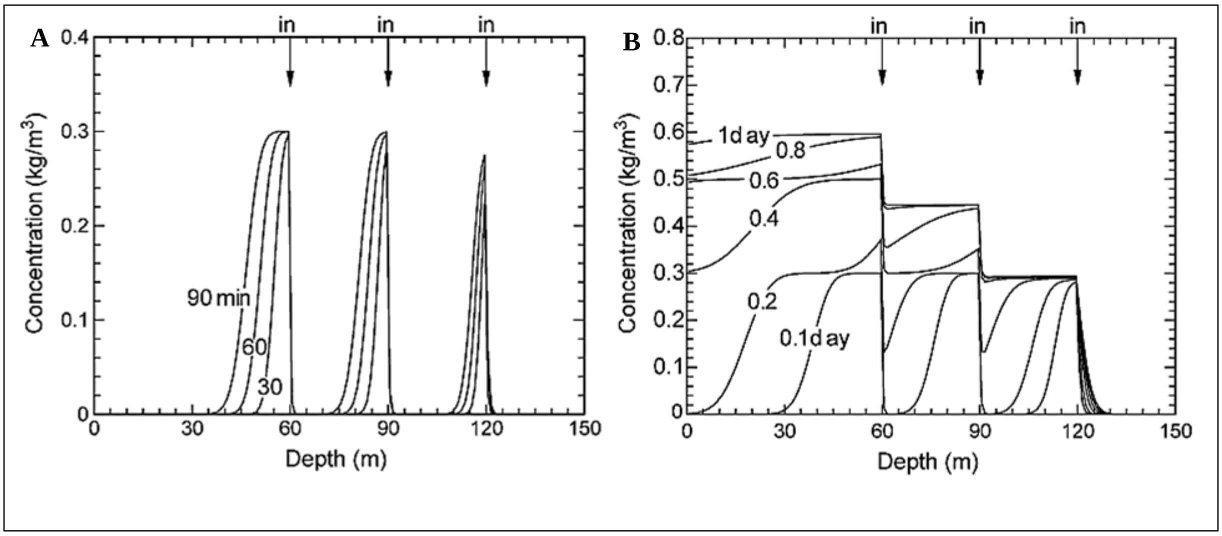

Figure 2-8 Concentration profiles generated using BORE II for three inflow points at different times: (A) early time before peaks interfere and (B) at later times.
Source: Doughty and Tsang (2005).

The matching of FEC profiles recorded in the field to the ones calculated using BORE II involves choosing concentration (C) and inflow rate (q_i) values for each peak by trial and error, until an acceptable match is obtained. The vertical dispersion parameter is also adjusted in order to obtain the best fit.

The transmissivity (T_i*) values of inflow zones are calculated by using the hydraulic head in the borehole (h_{bh}) and q_i in the Thiem (1906) equation. So, for each inflow zone intercepted by the borehole:

$$q_i = \frac{2\pi \mathrm{T}_i^*}{\ln\left(\frac{r_i}{r}\right)} = (h_i + h_{bh}) \qquad \textit{Equation 2-7}$$

Where:

q_i = Inflow rate [LT^{-1}];
T_i^* = Transmissivity [L^2T^{-1}];
h_i = Ambient hydraulic head [L];
h_{bh} = Hydraulic head in the borehole [L];
r_i = Assumed outer radius where the pressure response to pumping drops to zero [L]; and
r = Borehole radius [L].

If the hydraulic heads of all the flow zones are assumed to be equal, then they will be equivalent to the initial hydraulic head in the borehole, and $h_i = 0$. Therefore, under these conditions Figure

2-8 can be used to determine T_i^*. However, if the FEC profiling method was applied under various pumping rates, the Multi-rate Analysis is used to help determine T_i^*.

2.3.1.3.3 Multi-rate Analysis

When the FEC profiling method is conducted under different pumping rates (Q), the Multi-rate Analysis yields ambient hydraulic heads of the flow zones at different depths (Tsang and Doughty, 2003).

The multi-rate profiling method shows that by simultaneously analysing multiple sets of FEC logs with varying Q-values, not only can ambient hydraulic heads of each inflow point (h_i) be obtained, but T_i^* and C_i can also be determined with confidence. Although two sets of profiles with varying Q-values are enough, three sets at three varying Q-values are recommended for additional internal checking of results.

If a borehole containing N inflow points is considered, the strength of the i^{th} feed point is q_i and $\sum q_i = Q$. Conventionally, the q_i of inflow points is positive and negative for outflow points. Up-flow from below the studied interval can either be absent or shown by an additional feed point at the lower end. For each feed point, q_i and concentration C_i are assumed to be under a steady state (i.e. constant in time). Furthermore, it can be assumed that the flow towards the borehole is described by Darcy's law and the flow geometry is radial. However, the general approach would still be valid for a non-radial flow geometry, but the glow geometries must be the same for all flow zones.

Under these assumptions, the inflow rate (q_i) is related to its transmissivity (T^*_i), the ambient "far-field" hydraulic head (h_i) at a distance (r_i) away from the borehole, and the hydraulic head (h_{bh}) at the borehole radius (r), through the Darcy law as:

$$q_i = \frac{2\pi T_i^*{}_{(h_i - h_{bh})}}{\ln\left({}^{r_i}/_{r}\right)} = T_i(h_i - h_{bh}) \qquad \textit{Equation 2-8}$$

Where:

q_i = Inflow rate [LT^{-1}];

T_i^* = Transmissivity [L^2T^{-1}];

T_i = Effective transmissivity [L^2T^{-1}];

h_i = Ambient hydraulic head [LT^{-1}];

h_{bh} = Hydraulic head in the borehole [LT^{-1}];

r_i = Assumed outer radius where the pressure response to pumping drops to zero [L]; and
r = Borehole radius [L].

The effective transmissivity comprises of constant factors involving radial distances. *Equation 2-8* describes a scenario of a horizontal flow zone tapped by a vertical borehole. In a case where there is no density-driven flow present, the equation would also apply to the more general case of non-horizontal flow zones tapped by a non-vertical borehole, in which case the distances r and r_i are interpreted as distances measured in the plane of the flow zone.

Normally the transmissivity within the borehole itself is greater than any inflow zone, thus h_{bh} is constant over the interval of the studied borehole. Since $\sum q_i = Q$, we can write:

$$Q = \sum T_i \left(h_i - h_{bh}\right) \quad \text{Equation 2-9}$$

If the pumping rate is altered from Q to Q', T_i and h_i stay unchanged, however h_{bh} changes to h'_{bh}, and

$$q'_i = T_i(h_i - h'_{bh}) \quad \text{Equation 2-10}$$

$$Q' = \sum T_i \left(h_i - h'_{bh}\right) \quad \text{Equation 2-11}$$

Considering the difference between *Equation 2-8* and *Equation 2-10* and between *Equation 2-9* and *Equation 2-11*, it respectively results in:

$$\Delta q_i = T_i(h_{bh} - h'_{bh}) \quad \text{Equation 2-12}$$

$$\Delta Q = T_{tot}(h_{bh} - h'_{bh}) \quad \text{Equation 2-13}$$

Where:
Δq_i = $q'_i - q_i$;
ΔQ = $Q' - Q$; *and*
T_{tot} = $\sum T_i$.

When combined, Equation 2-12 and Equation 2-13 yield:

$$\frac{T_i}{T_{tot}} = \frac{\Delta q_i}{\Delta Q} \quad \text{Equation 2-14}$$

Equation 2-14 is the fundamental relationship between the change in feed-point strength (Δq_i) and the change in pumping rate (ΔQ). Since Δq_i is directly proportional to T_i, the feed points with larger hydraulic transmissivity show greater changes in strength when Q is modified.

When two sets of FEC profiles obtained with Q and $Q + \Delta Q$ are available, and we apply the BORE II code to each set to obtain the C_i and q_i values, then *Equation 2-14* can be employed to determine T_i / T_{tot}. Furthermore, *Equation 2-9* can be rewritten as:

$$Q = \sum T_i (h_i - h_{wb}) = T_{tot}(h_{avg} - h_{wb}) \qquad \textit{Equation 2-15}$$

Where h_{avg}, expressed as $h_{avg} = \sum(T_i h_i)/T_{tot}$, is defined as the hydraulic-transmissivity weighted average of the ambient hydraulic heads. It can be measured by a pressure probe in a borehole. Using the ratio of *Equation 2-8* and *Equation 2-15*, then rearranging, it yields:

$$\frac{(h_i - h_{avg})}{(h_{avg} - h_{wb})} = \frac{q_i/Q}{T_i/T_{tot}} - 1 \qquad \textit{Equation 2-16}$$

Using Equation 2-14 to eliminate T_i/T_{tot} results in a convenient measure of feed point ambient hydraulic head:

$$\frac{(h_i - h_{avg})}{(h_{avg} - h_{wb})} = \frac{q_i/Q}{\Delta q_i/\Delta Q} - 1 \qquad \textit{Equation 2-17}$$

The left side of *Equation 2-17* provides a dimensionless measure of the departure of feed point ambient hydraulic head from h_{avg}, whereas the terms on the right can be acquired from a BORE II analysis, and the denominator on the left is the hydraulic head drawdown in the borehole when it is pumped at rate Q, which can be directly measured. If three sets of FEC profiles at three pumping rates (Q_1, Q_2 *and* Q_3) is available, then three sets of results can be obtained by analysing three combinations of data (Q_1, Q_2), (Q_2, Q_3), and (Q_3 and Q_1).

The Multi-rate Analysis shows that by analysing multiple sets of FEC profiles with varying Q-values, not only can ambient hydraulic head (h_i) of each inflow point be obtained, but inflow concentration and transmissivity can also be determined with confidence. Although two sets of profiles with varying Q-values are enough, three sets at three varying Q-values are recommended as this enables internal checking and reduces the impact of measurement errors.

2.3.2 Advantages and limitations of borehole profiling methods

Borehole profiling methods can promptly produce data over long periods of time. The comparability and repeatability of the information obtained assists in providing baseline aquifer properties, which help determine changes in water quality over time and assists in monitoring the migration of the contaminant plume through a network of observation boreholes. According to Keys (1996), borehole profiles offer a unique advantage over groundwater sampling in that they offer continuous measurements (throughout the entire borehole depth) that can be interpreted on site in real time. Whereas in groundwater sampling data is only available from the sampled depth intervals after laboratory analysis has been conducted.

It is important to highlight that borehole profiling cannot completely replace groundwater sampling, especially in assessments where the objective is to obtain a complete geo-chemical and microbial composition of the groundwater. However, in such cases borehole profiles can still be used and analysed to provide in-field information which could help determine the location and frequency of sampling, consequently reducing the number of unnecessary samples and associated processing costs (Wonik and Hinsby, 2006).

Although useful and versatile, borehole profiles cannot be accurately interpreted without prior knowledge of the local hydrological and geological conditions of the study area. Therefore, to reduce inaccuracies during data interpretation and effectively utilise the obtained data, it is recommended that at least one core hole is drilled at the study site. Furthermore, a comprehensive understanding of the operating principles of the employed borehole profiling method is required.

2.4 Physical characteristics of a porous and weathered basement aquifer system

The different aquifer systems have been extensively documented throughout the study of hydrogeology (i.e. Gillham and O'Hannesin, 1984; Jiao and Zhang, 2014; Nadiri et al., 2018; Perina and Lee, 2006). This study mainly focused on the unconfined porous and weathered basement aquifer systems.

Unconfined aquifers are also commonly referred to as phreatic aquifers or water table aquifers, this is due to their upper boundary being the water table or a phreatic surface, as opposed to a confining layer. In most areas of the world, shallower aquifers are related to unconfined aquifers. This type of aquifer system generally indicates the absence of a confining layer. On the contrary, the confined aquifer system is recognised by the presence of an impermeable formation above the aquifer. Figure 2-9 is a schematic illustration of an unconfined porous aquifer system.

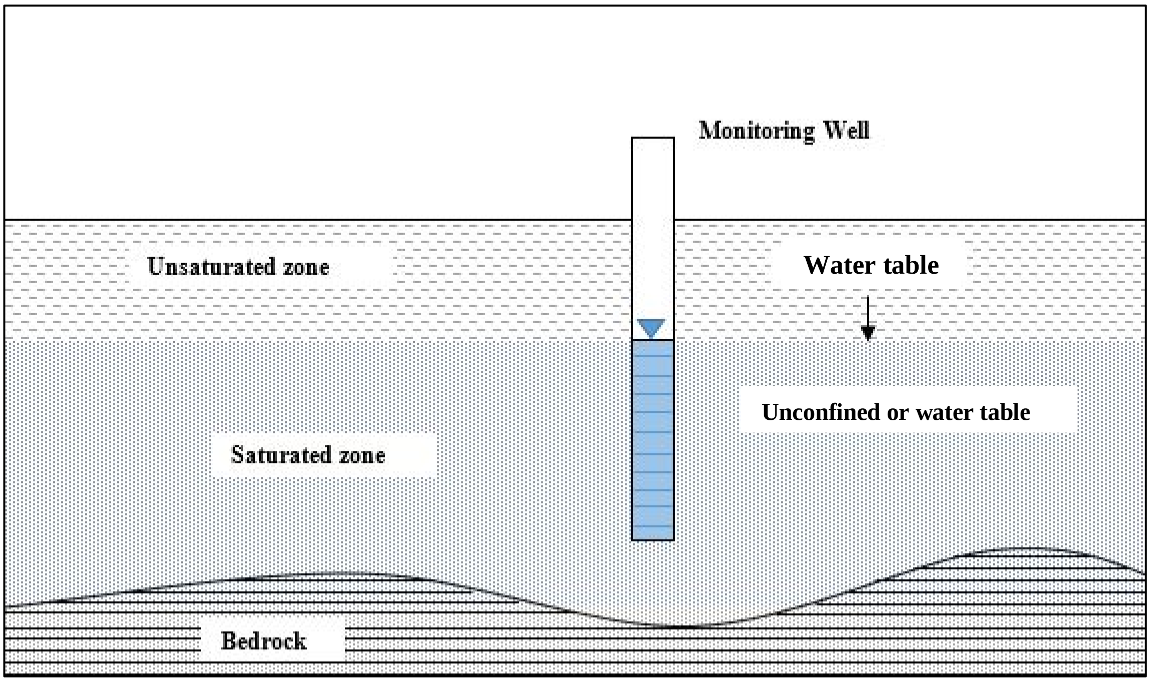

Figure 2-9 Schematic illustration of an unconfined porous aquifer system.

Based on the structure and arrangement of a geological formation, aquifers can be classified as either porous media or fractured. Typically, a porous aquifer system consists of aggregates of individual grain particles such as sand, gravel or silt. When these aggregates are cemented together, the system is referred to as a consolidated porous media, whereas unconsolidated porous media refers to where the individual grains within the system are not connected to each other, and as a result water may migrate easily through the openings between the individual grains, for example an alluvial aquifer.

The weathered basement aquifer system is slightly more complex. Typically, the upper part of the bedrock is often mechanically and chemically weathered, thus resulting in a variably, permeable, fractured, and porous rock mass (Jones, 1985). The extent of the weathered zone is dependent on the parent rock type and the physiochemical conditions of the site.

From the basic schematic illustration of crystalline basement aquifer systems presented in Figure 2-10, conceptually the system may consist of two possible aquifer systems:

1. The unconfined weathered aquifer layer overlying a fractured bedrock. In this system, both layers are permeable and are effectively interconnected aquifers.

2. The unconfined weathered aquifer layer overlying an impermeable bedrock unit. In this system, the weathered upper layer is the only permeable formation, thus forming an unconfined aquifer.

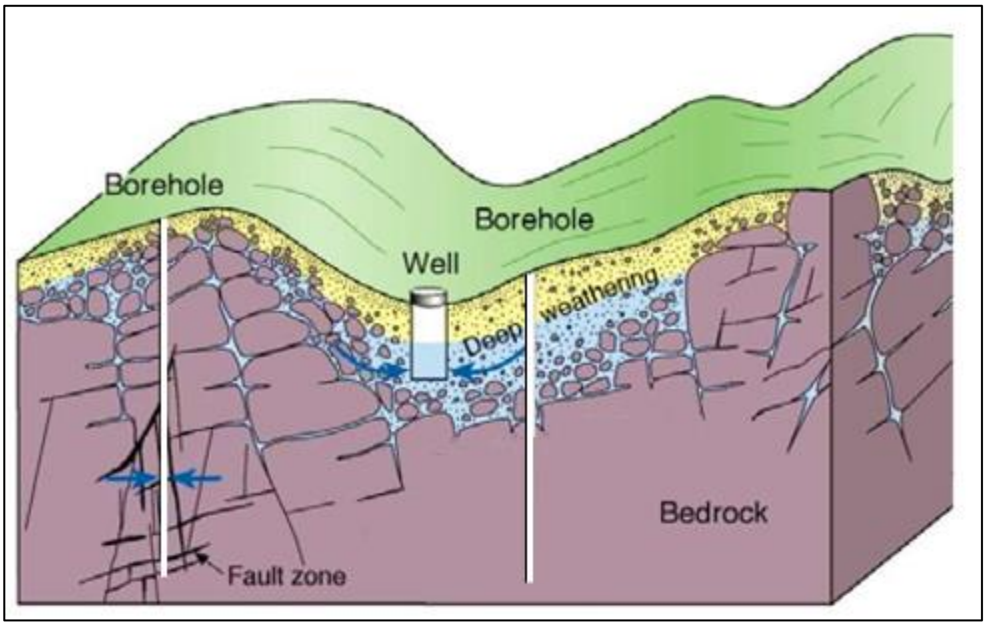

Figure 2-10 Crystalline basement aquifer systems, with a weathered overburden and regolith on top of the underlying, lower-yielding fractured bedrock aquifer.
Modified from: MacDonald et al., 2012.

The focus of this study is based on the second aquifer system, where the unconfined weathered overburden aquifer overlies the impermeable bedrock. From an exploration point of view, it is only after the analysis of lithological logs from the drilling that one can distinguish if the bedrock is fresh and impermeable or fractured and permeable. In other words, boreholes in typical crystalline basement aquifer systems will penetrate both the weathered overburden and part of the bedrock, irrespective of whether the bedrock is permeable or impermeable. It is therefore not uncommon to have boreholes drilled through the weathered and impermeable bedrock but effectively only tapping from the weathered layer.

2.5 Mass transport characteristics in porous media

Mass transport and hydraulic properties are largely related and are therefore often studied together. Hydraulic properties largely influence the behaviour of flow under both natural and stressed conditions, and transport characters generally influence the movement of mass and are critical in vulnerability and risk assessment studies of aquifer systems (Freeze and Cherry, 1979; McCarty et al., 1981; National Research Council, 1984; Pacome, 2010). Contaminant transport predictions that disregard mass transport characters and only consider hydraulic properties are prone to numerous mistakes (Van Wyk, 1998).

The primary processes that influence solute transport behaviour in groundwater are mainly (1) advection, (2) dispersion and (3) sorption (Freeze and Cherry, 1979; National Research Council, 1984). Advection and dispersion define the role of hydrodynamics in influencing the rate of migration and the dilution of a solute (MacKay et al., 1986). Sorption results in the attenuation of liquid-phase concentrations without changing the total mass of the compound, as well as the retardation of its movement relative to groundwater flow (Freeze and Cherry, 1979).

The mathematical relationship between these processes can be expressed as:

$$\frac{\partial}{\partial_{x_i}}\left[D_{ij}\frac{\partial C}{\partial_{x_i}}\right]-\frac{\partial}{\partial_{x_i}}(Cv_i)-\frac{C'W'}{n}=\mathrm{R}\frac{\partial C}{\partial t} \qquad \ldots\ldots(1)$$

$$V_i=\frac{-K_{ij}}{n}\frac{\partial h}{\partial_{x_j}} \qquad \ldots\ldots(2)$$

Equation 2-18

$$\mathrm{R}=\left[1+\frac{\rho_b K_d}{n}\right] \qquad \ldots\ldots(3)$$

Where:

C = Solute concentration [ML^{-3}];

V_i = Mean pore (solute) velocity in the x_i direction (i = 1, 2, 3) and equals q_i/n [LT^{-1}];

D_{ij} = Dispersion coefficient, (i, j = 1, 2, 3) [L^2T^{-1}];

K_{ij} = Hydraulic conductivity, (i, j = 1, 2, 3) [LT^{-1}];

C’ = Solute concentration in the source [$M\ L^{-3}$];

W’ = Volume flow rate per unit volume of the source [L^3T^{-1}];

n = Effective porosity [-];

h = Hydraulic head [-];

R = Retardation factor [-]; and

x_i = Cartesian coordinate [-].

Bear (1972) described three-dimensional transport of a nonreactive solute in a saturated porous media using a differential equation. However, the discussion below uses a simplified two-dimensional representation to represent solute migration in groundwater in a homogeneous, isotropic medium having a unidirectional steady state flow with velocity *V*:

$$D_L \frac{\partial^2 C}{\partial_{x^2}} + D_T \frac{\partial^2 C}{\partial_{y^2}} - V \frac{\partial C}{\partial x} = R \frac{\partial C}{\partial t}$$ *Equation 2-19*

Where:

C = Contaminant concentration [ML^{-3}];

V = Average pore velocity (seepage) [LT^{-1}];

D_L = Longitudinal dispersion coefficient [L^2T^{-1}];

D_T = Transversal dispersion coefficient [L^2T^{-1}]; and

R = Retardation factor [-].

2.5.1.1 Advection

Advection describes the transport of solute pulse or dissolved contaminant along a mean direction of fluid flow at an equal rate to the average interstitial fluid velocity or linear pore fluid velocity (Kinzelbach, 1992; MacKay et al., 1986; Mau, 1992). Advection and dispersion are primary physical properties that govern solute transport. Advection is controlled by Darcy's law because it is the transport of solute with respect to flowing groundwater.

Darcy's law expresses that the flow rate of fluid through a porous media from one point to another is directly proportional to the head loss and inversely proportional to the flow path length:

$$\mathrm{Q} = -\mathrm{K}.\mathrm{A} \frac{h_2 - h_1}{L}$$ *Equation 2-20*

Where:

Q = Groundwater flow rate [L^3T^{-1}];

A = Cross sectional area of flow [L^2];

$h_2 - h_1$ = Head loss between point 2 and point 1 [-];

L = Distance between the two points [L]; and

K = Hydraulic conductivity [LT^{-1}].

The average pore water velocity (seepage) can be calculated as:

$$\mathrm{V} = \frac{Q}{n.A} - \frac{K}{n} \frac{h_2 - h_1}{L}$$ *Equation 2-21*

Where *n* is the percentage of interconnected pore spaces that actually contributes to flow (effective porosity).

The mean pore velocity (V_i) represented in *Equation 2-18*, is a conservative estimate of the migration velocity of the contaminant transport. When only the advective process is considered, a contaminant migrates at the same rate as the groundwater flow; however, in reality, other processes such as dispersion and retardation affect the movement of the contaminant.

2.5.1.2 Dispersion

The mixing and spreading of solutes along and transverse to the direction of flow due to local variations in interstitial fluid velocities is referred to as dispersion. It is primarily a result of two processes: mechanical mixing and molecular diffusion (Bear, 1972). Mechanical dispersion (mixing) takes place when uncontaminated water comes into contact with contaminated water, which results in dilution. Figure 2-11 is a schematic illustration of the dispersive process in a homogeneous, granular medium on (A) a macro and (B) a micro-scale.

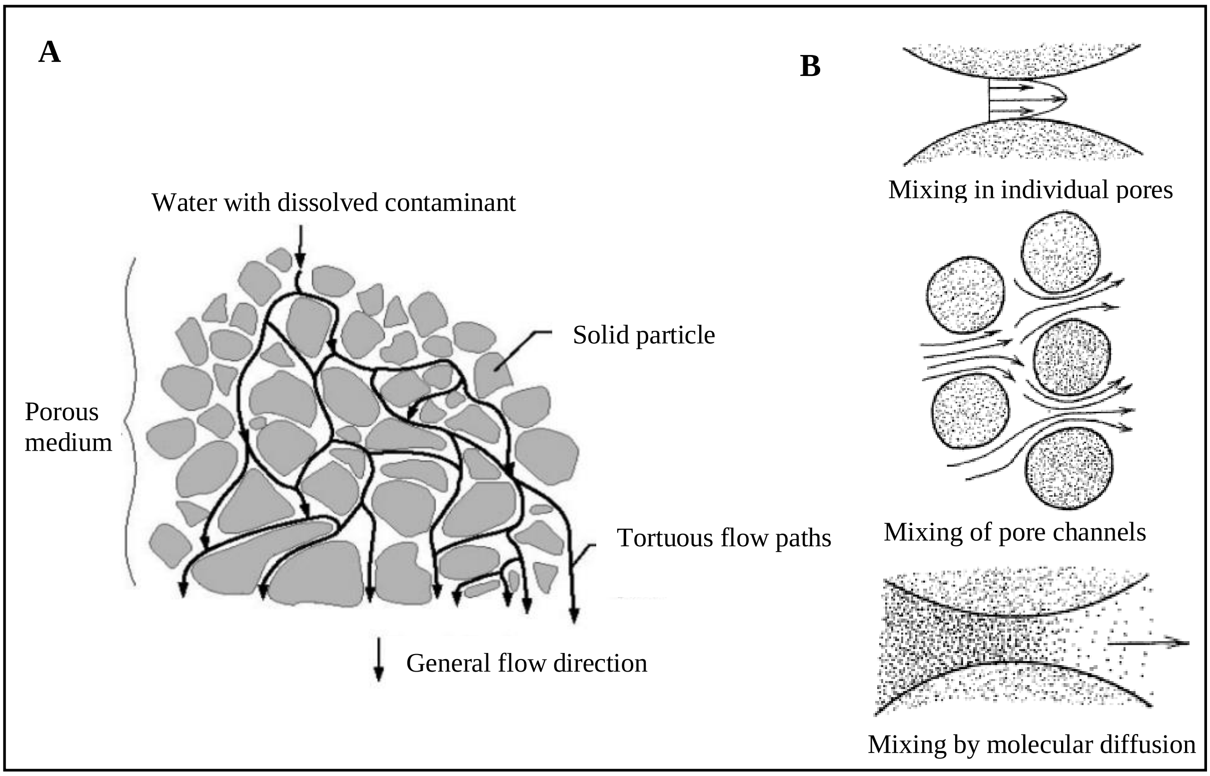

Figure 2-11 Schematic illustration of the dispersive process on (A) macro and (B) microscopic scale.
Source*:* Patil and Chore (2014), and Freeze and Cherry (1979), respectively.

The molecular diffusion is a dispersive process whereby ionic or molecular constituents move from regions of higher concentrations to lower concentrations. This process can be defined by Fick's law as:

$$\mathrm{F} = -D_f \frac{dC}{dx} \qquad \textit{Equation 2-22}$$

Where:

F = Mass flux per unit area, per unit time [M $L^{-2}T^{-1}$];

D_f = Diffusion coefficient [L^2T^{-1}];

dC = Solute concentration [M L^{-3}]; and

dx = Concentration gradient [-].

Fick's law was derived for chemicals in unobstructed water solution. Therefore, when it is applied to porous media, the diffusion coefficient should be smaller because the ions follow longer paths due to the presence of solid particles in the solid matrix and adsorption of solids (Freeze and Cherry, 1979). Thus, yielding an apparent diffusion coefficient D^* defined as:

$$D^* = w.\, D_f \qquad \textit{Equation 2-23}$$

Where w is an empirical coefficient of less than 1, which accounts for the effect of the solid phase of the porous media on the diffusion. This value has been suggested to be between 0.5 and 0.01 to account for tortuosity of the flow path (Freeze and Cherry, 1979). These two processes cannot be separated in groundwater flow, therefore the coefficient of hydrodynamic dispersion is usually taken into account and represented as:

$$D_L = \propto_L . V + D^* \qquad \textit{Equation 2-24}$$

$$D_T = \propto_T . V + D^* \qquad \textit{Equation 2-25}$$

Where:

D_L = Longitudinal mechanical mixing component of dispersion [L^2T^{-1}];

D_T = Transverse mechanical mixing component of dispersion [L^2T^{-1}];

α_L = Longitudinal dispersivity [L]; and

α_T = Transverse dispersivity [L].

Gelhar et al. (1992) roughly estimated the α_L as 0.1 L, where L is the flow path length. The α_T was estimated to be 1/10 to 1/100 of the α_L.

2.5.1.3 Sorption

The exchange of ions and molecules between the liquid and solid phase is termed as sorption. This includes desorption and adsorption. Desorption is the release of ions or molecules from the solid phase to the solute, whereas adsorption is the attachment of ions or molecules from the solute phase to the solid phase, thus causing a decrease in the concentration of the contaminant. This is called retardation.

According to Freeze and Cherry (1979), the retardation coefficient can be determined from the desorption coefficient of the contaminant plume as well as the properties of the porous medium as:

$$R = \left[1 + K_d \frac{\rho_d}{n}\right] \qquad \textit{Equation 2-26}$$

Where:

K_d = Adsorption coefficient [L^3M^{-1}];

ρ_d = Bulk density of the soil [ML^{-3}]; and

n = Porosity of the soil [-].

The velocity of the contaminant in groundwater can be determined by:

$$V_c = \frac{V}{R} \qquad \textit{Equation 2-27}$$

Where:

V_c = Velocity of the contaminant movement in groundwater [LT^{-1}];

V = Groundwater velocity [LT^{-1}]; and

R = Retardation factor [-].

A high retardation factor notably decreases the migration of the contaminant plume in groundwater. This has been extensively discussed in Back and Cherry (1976) and Bear (1972).

2.6 Methods for estimating hydraulic and transport parameters

In hydrogeological investigations the estimation of chemical transport and groundwater flow parameters is done by conducting field tests, these tests include hydraulic tests and artificial tracer breakthrough tests. Recent studies have shown efficiency in conducting these two tests simultaneously (Riemann, 2002; van Tonder et al., 2001).

The analysis of the resulting data from these tests usually entails (1) conceptually modelling the transport and fluid flow in the rock mass using the common knowledge of the rock mass in conjunction with the behaviour of the test response, and (2) estimating parameters by matching field data with the model data. These steps often require repetition for better matching between model computed responses and field responses (Gorokhovski, 2014).

2.6.1 Hydraulic tests

Hydraulic tests have been found useful in determining physical and hydraulic parameters which aid in the understanding and improved conceptualization of aquifer systems. These tests often involve inducing groundwater flow through pumping and monitoring the response of the aquifer system. The most commonly used hydraulic test methods are constant head tests, constant discharge tests, slug tests and multi-rate tests, these have been extensively described in many hydrogeological textbooks including Kruseman and de Ridder (1994) and van Tonder et al. (2001). Depending on the objective of the study different set-ups can be used, and these tests can be conducted on either a single borehole or multiple boreholes.

2.6.1.1 Single borehole hydraulic tests

Single borehole hydraulic tests are the most popularly used field tests for site characterisation due to their ability to offer basic aquifer parameters at a relatively low cost. They are commonly conducted in an open borehole or using packers. When the open borehole approach is used, the entire uncased borehole section is tested, and the hydraulic head response of the aquifer-borehole system is primarily controlled by the most conductive zone. Although valuable information such as the hydraulic properties of the formation can be obtained, this approach can be quite problematic in fracture characterisation assessments where the contribution of each (minor) fracture intercepted by the borehole needs to be determined. Additionally, according to Kruseman and de Ridder (1994), in a low transmissive formation, open borehole hydraulic tests may be influenced by borehole storage effects.

When the straddle packer test approach is employed, two or more packers are used to isolate a section(s) of the borehole for testing. This makes it possible to measure the hydraulic properties of individual permeable zones (or fractures) and essentially determine their individual contribution (Botha et al., 1998; Haimson and Lee, 1984; Stewart, 2000). Figure 2-12 is a schematic illustration showing a typical straddle packer test set up.

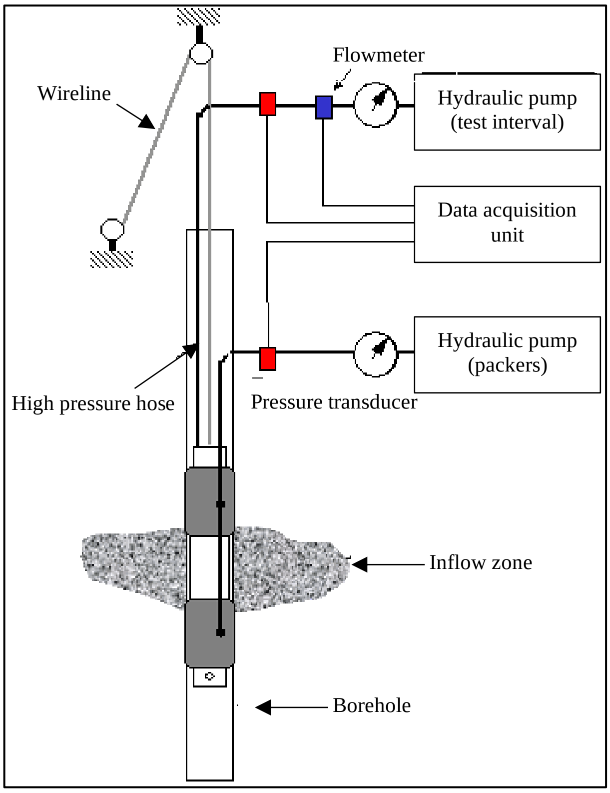

Figure 2-12 Schematic illustration of a typical straddle packer test system set up.
Source: Haimson and Lee, 1984.

When analysing packer test data, borehole storage can usually be neglected since the change in hydraulic head is not associated with a change in water level. However according to Botha et al. (1998) equipment compliance could induce the borehole storage effect that needs to be taken into consideration, particularly in very low transmissive environments.

2.6.1.2 Multiple borehole hydraulic tests

Multiple borehole hydraulic tests generally entail the use of one pumping borehole and at least two observation boreholes to monitor the response of the aquifer system. The tests entail groundwater being pumped from one borehole and aquifer responses being monitored in one or more observation boreholes. Unlike single borehole test, multiple borehole tests allow a larger scale of the aquifer to be tested and monitored thus leaving less uncertainty on the inferred hydraulic parameters.

Multiple borehole tests offer valuable information on the connectivity of flow zones as well as aquifer anisotropy. Additionally, depending on the design and set-up, information on the spatial variability of the flow zones can also be acquired (Pretorius, 2007). A detailed discussion on various multiple borehole set-ups for the most commonly encountered conditions and environments has been discussed by the National Research Council (1996), Botha et al. (1998) and van Tonder et al. (2001).

2.6.2 Artificial tracer breakthrough tests

Hydrological tracer breakthrough tests are generally performed to either estimate the degree of hydraulic interconnection between different locations, to determine a solute-matrix interaction parameters, to approximate physical transport parameters and hydraulic characteristics involved in solute migration, and or to calibrate and validate a flow or transport model (Malloszweski and Zuber, 1992).

These tests may be conducted under either natural gradient or forced gradient conditions. The test principally entails introducing a tracer into the groundwater system and monitoring the movement of the spreading tracer. Natural gradient tracer tests are most effective in highly porous aquifer systems such as weathered aquifer systems (as seen in Gomo, 2011 and LeBlanc et al., 1991). Under these conditions particularly when using a single borehole, the tracer dilution in the test section is assumed to be due to horizontal influx of fresh groundwater into the borehole, thus Darcy velocity (groundwater flux) is computable from the dilution test (Drost et al., 1968; Drost and Neumaier, 1974).

Natural gradient tests are rarely used in fractured aquifer systems because the large-scale heterogeneity associated with secondary aquifers makes it difficult to effectively apply them. Additionally, since the tracer usually travels along channels that occupy small portions of the fracture planes (Abelin et al., 1991; Tsang and Tsang, 1989), the grid of the of the sampling boreholes may not be adequately designed to sample the full extent of the plume, thus making the natural gradient tracer testing approach an undesirable technique for accurately determining mass transport parameters in fractured aquifer systems. It is for this reason, that forced gradient conditions are generally preferred in fractured aquifer systems. Forced gradient tests generally involve creating a flow field with injection and or withdrawal, introducing a tracer in one borehole (injection borehole) and monitoring the arrival of the tracer at the second borehole (observation borehole). An example of this approach using different set ups can be found in numerous studies including Carleton et al. (1999), van Wyk (1998), and Welty and Gelhar (1989).

A range of tracers generally exists but sodium chloride (NaCl) is often the most preferred option since it is readily available at a low cost and can easily be monitored using an EC probe

(Gomo, 2011). However, in areas where the natural groundwater already has a relatively high EC, alternative tracers should be considered.

2.7 Hydrogeological test models

Hydrogeological modelling is the characterization of real systems and hydrogeological features using computer simulations, mathematical analogues, and small-scale physical models (Allaby and Allaby, 1999). These models are predominantly used to aid in the understanding of various hydrological processes and predicting the behaviour of a system. Although each model has its own unique characteristics, a good model is considered one which gives results closest to the real system, with the least use of input parameters and model complexity (Singh, 2018).

The outputs of a real system can never be forecasted with absolute certainty, this is mainly because of the heterogeneities that exist across space and time scales. These heterogeneities are important because they may have an effect on flow velocity, flow path, residence time and can create response thresholds that depend on velocity and flow path (Ogden, 2021). Therefore, hydrogeological models are at best approximations of reality. Furthermore, understanding the limitations of a model is essential for the correct interpretation and understanding of the outputs.

Hydrogeological models have a wide range of applications, these include but are not limited to, water resources planning and management, flood design and forecasting, and coupled systems modelling such as hydro-ecology, water quality evaluation and climate. There exist several publications on hydrogeological modelling, these include Singh and Woolhiser (2002); Wagener et al. (2004), and Wheater et al. (1993).

2.7.1 Classification of hydrogeological models

Various publications have outlined ways to classify hydrogeological models (i.e. Singh, 1995; Singh and Frevert, 2006; and Wheater et.al., 1993;). Hydrogeological models are either based on the aspect of randomness or process description.

2.7.1.1 Hydrogeological models based on randomness

Models that are based on randomness can be classified into two groups as shown in Figure 2-13; stochastic models or deterministic models. In a stochastic model different values of output can be produced for a single set of input values, these models can be categorised as time correlated, time independent, space correlated, and space independent (Singh, 2018).

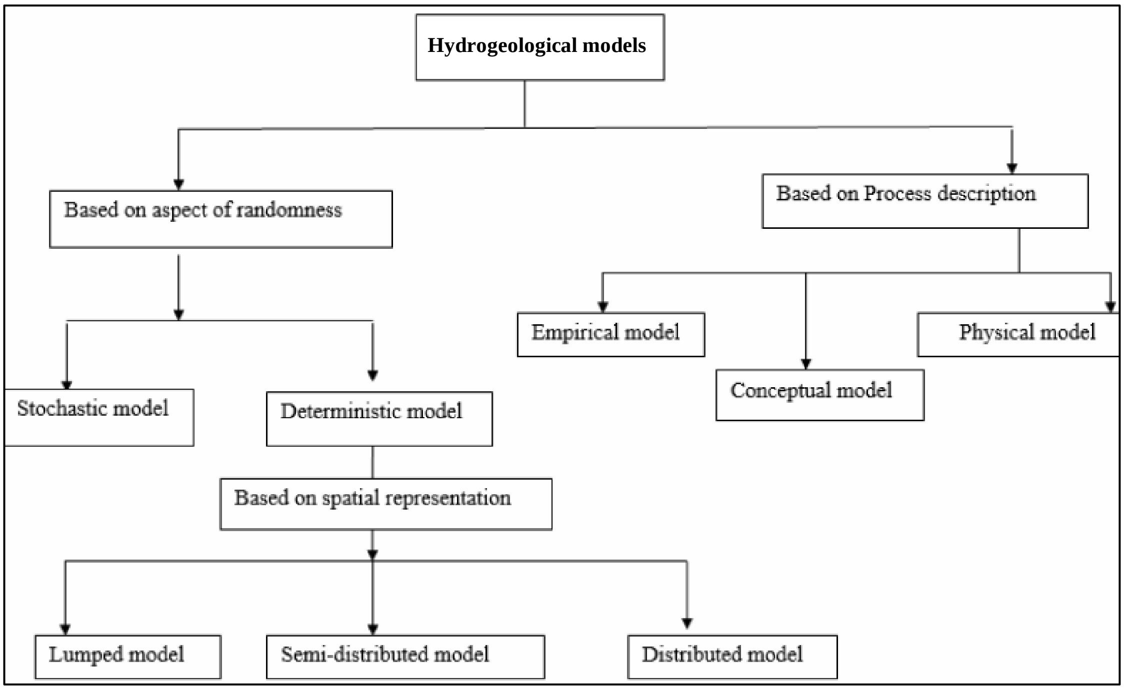

Figure 2-13 Classification of hydrogeological models.
Source: Singh, 2018.

A deterministic model gives the same output for a single set of input values, the model makes forecasts and is further divided into unsteady state flow and steady state flow hydrogeological model. Deterministic hydrogeological models that are based on spatial representation can be further divided into lumped, semi-distributed, and distributed model.

2.7.1.2 Hydrogeological models based on process description

The hydrogeological models that are based on process description are divided into empirical, conceptual, and physical models.

2.7.1.2.1 Empirical models

Empirical models, also referred to as metric models are primarily observation orientated and characterises the system's response from existing data, with little or no consideration for the processes and features of the hydrological system (Wheater et al., 1993; Pechlivanidis et al., 2011). Thus, the models are also described as "data driven models". They involve mathematical equations derived from concurrent input and output time series and not from physical processes, and the models are only valid within boundaries (Singh, 2018).

An early-time example of an empirical model is a Unit Hydrograph (UH) for event-based catchment-scale simulation, developed by Sherman (1932). The simplicity of these models enables them to be easily applied to ungauged catchments by regional analysis, relating model properties (such as percentage runoff, unit hydrograph time to peak etc.) to climatic and physical descriptors of the catchment (Pechlivanidis et al., 2011).

Although empirical models have been used to extrapolate in ungauged catchments and extreme events, since they depend on existing data, results acquired from them are usually lacking in formal specification of confidence limits (Wheater, 2002). Other examples of empirical modelling can be found in Dawson et al., 2006; Jain et al., 2004; Lekkas, 2008; Ratto et al., 2007; and Young et al., 1997.

2.7.1.2.2 Conceptual models

Conceptual models, also referred to parametric models in other studies, represents components of a hydrological process deemed to be important (Singh, 2018; Wheater, 2002). In these models the structure of the models is specified before undertaking any modelling. Additionally, not all of the model parameters are independently measurable (Wheater et al., 1993), thus at least one or more parameters has to be estimated through calibration against observed data. The first major conceptual model is the Stanford Watershed Model IV (SWM), developed in 1966 by Crawford and Linsley. The model had 16 to 20 parameters.

The complexity of conceptual models differs depending on the objective of the study, model complexity can be appropriately reduced through sensitivity analysis (van Werkhoven et al., 2009), identification statistics (Dunn et al., 2008), and by either formally restructuring the model or keeping insensitive parameters constant (MsIntyre and Al-Qurashi, 2009).

2.7.1.2.3 Physical models

A physical model, also known as a mechanistic model, is an idealised representation of a real phenomenon and includes principles of physical processes (Singh, 1998). These models use measurable state variables which are functions of both time and space. Although for their calibration these models do not require extensive meteorological and hydrological data, the evaluation of a large number of data sets descriptive of physical characteristics are required (Abbott et al., 1986).

Physical models can overcome limitations observed in empirical and conceptual models due to the use of parameters that have physical interpretation. These models can provide valuable information even outside of the boundary and can be used in a wide range of situations (Abbott et al., 1986). In hydrogeology, physical models have been employed to represent components of hydrological process such as overflow, evapotranspiration, infiltration, unsaturated and saturated zone flow using governing equations of motions based on continuum mechanics (Pechlivanidis et al., 2011).

Theoretically, physical models can provide continuous simulations without calibration since they are defined by wholly measurable parameters (Beven, 2001). Although these models are a great compilation of important idealised processes, they raise several issues that need to be taken into consideration, the physics behind the model structure is commonly based on either a small-scale in-situ field experiments or laboratory experiments, therefore they are affected by the nature of the experiments themselves.

Extrapolating the outputs of these experiments to larger scales assumes that the physical properties and hydrological processes are independent of scale, this raises uncertainty about their applicability (Beven, 2004) and increases their need to be validated.

2.7.2 Scale issues in hydrogeological modelling

In modelling, the term scale refers to the length (or time) of an observation, process, or model. Over the years the issues associated with scale in hydrogeology have been extensively reviewed (i.e. Bloschl et al., 1995; Dooge, 1982 and 1986; Dozier, 1992; Klemes, 1983; Mackay and Riley, 1991; and Zlotnik et al., 2000).

Usually, processes are commonly modelled and observed at short-time scales, but the outputs are needed for long-term scales such as the lifetime of a dam. Similarly, the outputs of models designed in small space-scale laboratory experiments are expected to be applicable in a large-scale field setting. Contrarily, often times large-scale data and model outputs are used for small-scale predictions (Bloschl et al.,1995). This extrapolation or transfer of information across varying scales is referred to as scaling, and there are a lot of scale issues associated with it. One of the main issues is that scaling disregards the nature of heterogeneity and variability in space and time.

The term heterogeneity is used for media properties such as hydraulic conductivity, that differs in space. And variability is used for state variable (i.e. soil moisture) or fluxes (i.e. runoff) that differs in time and space (Beven, 1981). Variability and heterogeneity are prominent at a range of scales. At a local scale micropores such as root holes, wormholes, or microfractures that occur in soil can transport the bulk of the flow, with minimum contribution from the soil matrix

(Germann, 1990). According to Chapell and Ternan (1992) the difference in hydraulic conductivity of lithology and the presence of fractures can affect flow at a regional scale.

According to the NRC (1991), adequately addressing the issue of integration and the linkage of formulations at different scales remains one of the biggest challenges in hydrogeological modelling. However, scale issues are not only unique to the field of hydrogeology but also poses a range of challenges in other disciplines such as oceanography (Stommel, 1963), meteorology and climatology (Raupach and Finnigan, 1995), biology (Haury et al., 1977), soil science (Hillel and Elrick, 1990), and social sciences (Dovers, 1995).

2.8 Summary

Chapter 2 provides a literature review of basic methods and concepts which are important for the comprehensive understanding of FEC profiling in porous and weathered basement aquifer systems. Various hydrogeological profiling methods are reviewed to bring insight to which methods can be used based on the information required, borehole conditions, and objectives of the study. Among the various borehole profiling methods described, the FEC profiling method has proven to be the easiest to use, most efficient and cost effective.

Borehole profiling methods can produce data over long periods of time, and the information obtained can assists in providing baseline aquifer properties, which help determine changes in water quality over time and assists in monitoring the migration of the contaminant plume through a network of observation boreholes. However, they cannot completely replace groundwater sampling, especially in assessments where the objective is to obtain the complete geo-chemical and microbial composition of the groundwater.

This study mainly focused on the unconfined porous and weathered basement aquifer systems; thus, it was important that the physical structure, the mass, and transport processes in typical porous media are reviewed because it is these processes, together with the hydraulic properties of the formation, that influence the shape of FEC profiles. Mass transport and hydraulic properties are largely related and are therefore often studied together. Hydraulic properties largely influence the behaviour of flow under both natural and stressed conditions, and transport characters generally influence the movement of mass and are critical in vulnerability and risk assessment studies of aquifer systems. The primary processes that influence solute transport behaviour in groundwater are mainly advection, dispersion, and sorption.

Physical models are used in this study to simulate the unconfined porous and weathered basement aquifer systems and to monitor these transport processes under controlled laboratory conditions. Hydrogeological models are predominantly used to aid in the understanding of various hydrological processes and prediction of the behaviour of a system. However, since the outputs of a real system can never be forecasted with absolute certainty mainly because of the heterogeneities that exist across space and time scales, hydrogeological models are at best approximations of reality.

Chapter 3
LABORATORY EXPERIMENT

3.1 Introduction

The first part of this section focuses on methods and materials used during the laboratory assessment of the porous and weathered aquifer systems. This includes a description of the design and construction of the two physical models, the tests that were conducted to assess their ability to simulate a real system, and a description of how the FEC profiling tests were undertaken within these models under laboratory conditions. Thereafter, this section discusses the results obtained from the experiments.

3.2 Methods and material

3.2.1 Design and construction of the physical models

Two physical models were developed under controlled conditions to represent (1) an unconfined porous aquifer system and (2) a weathered basement aquifer system. As mentioned in Section 2.3.1.2 the FEC profiling method is traditionally conducted under induced groundwater flow, however, as part of its outcomes this study aimed to explore the efficiency of a non-invasive approach of obtaining FEC profiles under natural gradient conditions, thus flow was not induced.

3.2.1.1 Porous aquifer system

An acrylic clear Perspex material was used to build and construct the outline of the physical model. Poly-vinyl chloride (PVC) pipes perforated throughout their entire length were used to represent boreholes (BH1 and BH2), which were placed 18.5 cm apart from each other. A 25-liter container was used to supply water at a constant rate into the model via the inflow section. To simulate the unconfined porous aquifer system, a single-layered, homogeneous, coarse-grained sand of 2 mm diameter was used to represent the permeable porous layer. Figure 3-1 shows a picture of the physical model which was used to simulate the porous aquifer system.

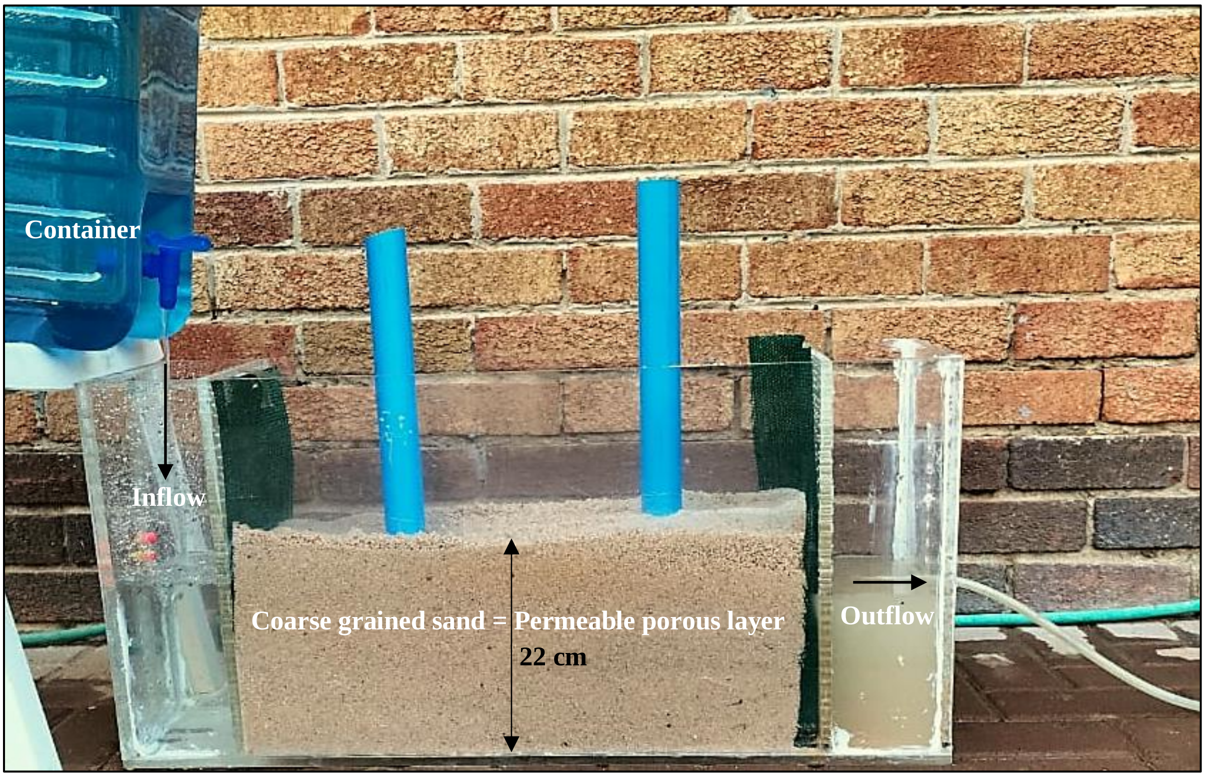

Figure 3-1 A picture showing the physical model of the porous aquifer system.
Note: A single-layered, homogeneous, coarse-grained sand of 2 mm diameter was used to represent the permeable porous layer.

The dimensions of the physical model were 75 cm in length, 40 cm in height, 20 cm in width, and the flow length was 55.5 cm long. The aquifer itself was 22 cm thick. Since no form of pumping was used throughout this study, groundwater flow was driven by the hydraulic gradient due to the difference in hydraulic heads between the inflow and the outflow points. To ensure constant flow rate and discharge throughout the duration of the test, hydraulic heads of 19 cm at H_1 and 14 cm at H_2 above the base of the model were maintained. A schematic illustration of the simulated unconfined porous aquifer system with its dimensions is shown below in Figure 3-2.

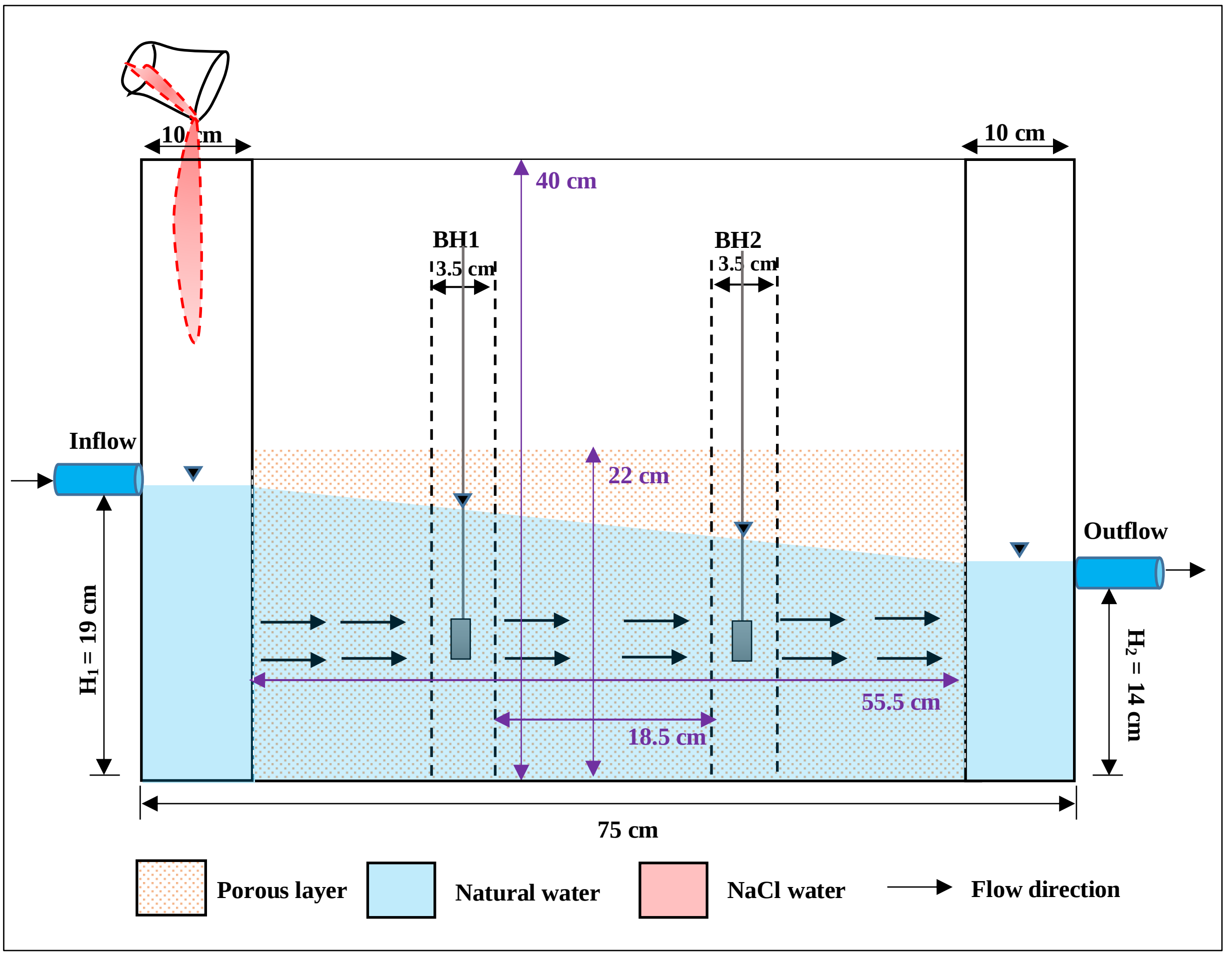

Figure 3-2 Schematic illustration of the dimensions of the unconfined porous aquifer model.

Note: The dashed lines indicate the perforated parts of the model. The solid arrows within the permeable layer illustrate the flow direction. All dimensions are presented in centimetres.

3.2.1.2 Weathered basement aquifer system

The physical model representing the weathered basement aquifer system consisted of a two-layered system where the permeable weathered layer was placed on top of an impermeable bedrock, as shown in Figure 3-3. To construct the model, homogenous sieved coarse-grained sand of 2 mm diameter was used to simulate the permeable weathered layer. It was assumed that the basement was uniformly weathered, thus approximating a homogeneous system. The impermeable bedrock was represented by a silty-clay layer with a thickness of 18 cm.

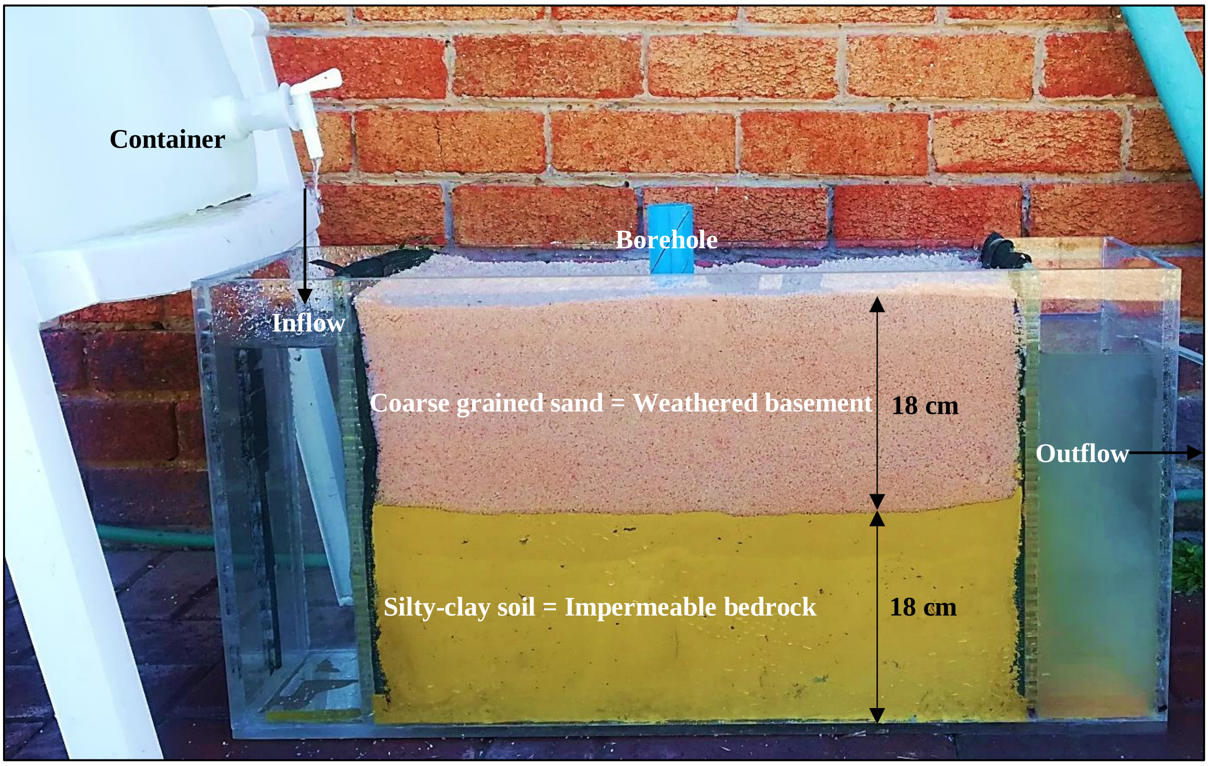

Figure 3-3 A picture showing the physical model of the weathered basement aquifer system.
Note: Silty-clay was used to represent the impermeable bedrock, and coarse-grained sand was used to simulate the weathered zone.

An acrylic clear Perspex material was used to build the physical model. A perforated PVC pipe was used to represent a screened observation borehole and was placed at the centre of the physical model. A 25-litre container provided water into the model via the inflow section at a constant rate. The groundwater flow was driven by the natural hydraulic gradient caused by the difference in hydraulic heads between the inflow and outflow points. The hydraulic heads were maintained at 32 cm at H_1 and 28 cm at H_2 above the base of the model throughout the duration of the tests. Figure 3-4 is a schematic illustration of the weathered basement aquifer model, the diameters of the aquifer, outflow, inflow, flow length as well as the hydraulic heads are indicated on the diagram.

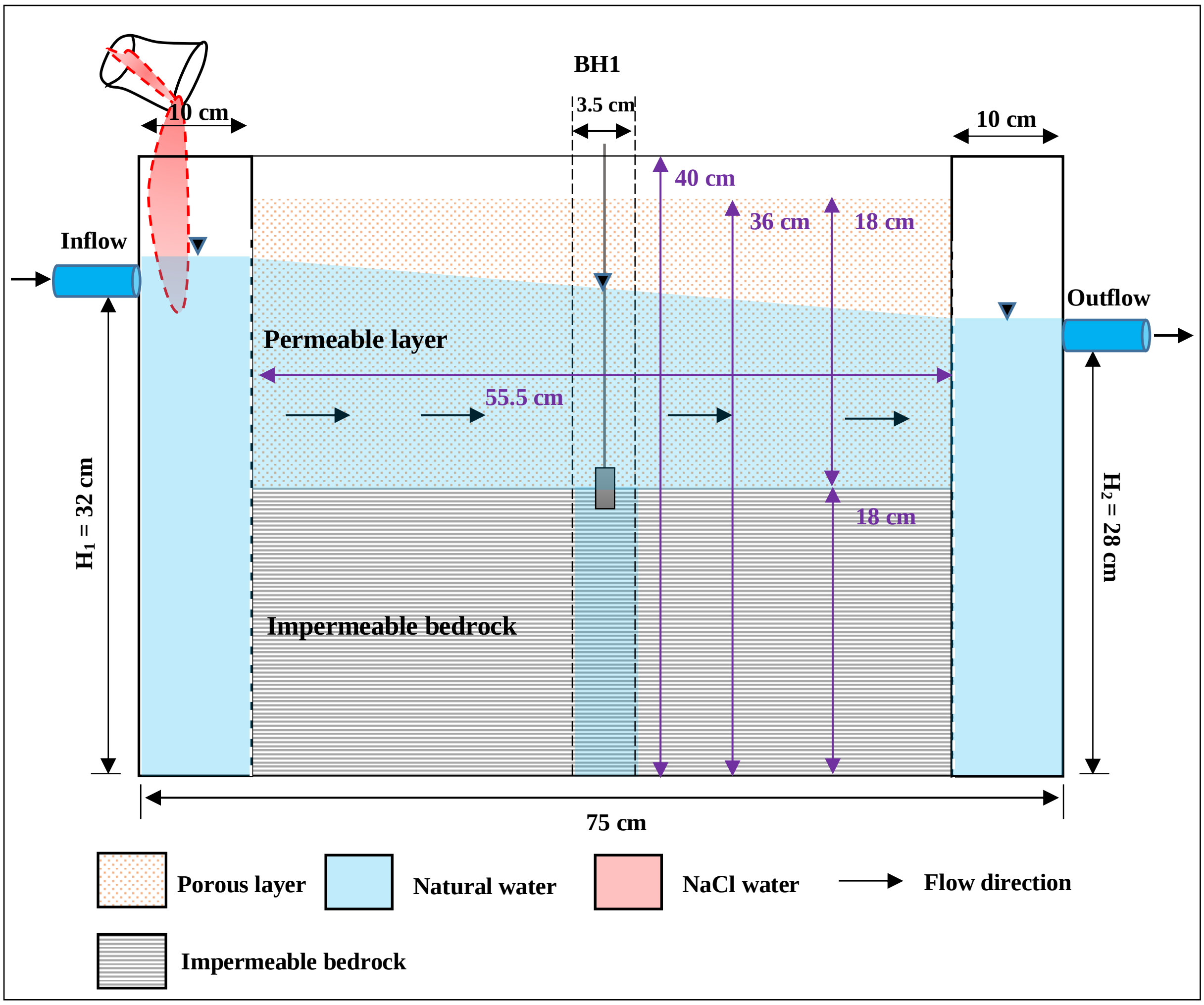

Figure 3-4 Schematic diagram of the physical model of the weathered aquifer system.
Note: The dashed lines indicate the perforated parts of the model. The solid arrows within the permeable layer illustrate the flow direction. All dimensions are presented in centimetre.

3.2.2 Testing the performance of the physical models

Hydrological tracer testing has been applied to obtain information on the sub-surface structure such as contaminant preferential flow pathways, structural anisotropy, the connectivity of different aquifer layers, and to verify hydrogeological models (Käss, 1998, and Ptak et al., 2004). It is also the most reliable method commonly used to identify and quantify hydro-dispersive transport processes and establish flow trajectories in order to understand solute-transport processes in aquifer systems (Field, 2003). Thus, as part of quality control it was important to assess whether the mass-transport characteristics of the physical model conformed to that of theoretical models.

The performance of the physical model was validated by conducting tracer breakthrough tests and comparing the obtained breakthrough curves to the ones of typical porous and weathered-basement aquifer systems observed in literature. This was done to confirm the capability of the models to simulate mass-transport characteristics of a real or typical system. The test was repeated three times using varying mass concentrations (10, 15, and 20 g of salt) to assess repeatability. To avoid cross contamination a model of the same dimensions, aquifer thickness, and soil material was constructed for each test.

Additionally, the tracer breakthrough tests were used as a tool to aid in determining the time of the first arrival, the peak arrival, and dilution stage of the plume. This was crucial as it would assist with profiling at the right intervals and to ensure that the above-mentioned stages were captured. The movement of the tracer within the system was monitored by using a temperature-level-conductivity (TLC) probe to measure the FEC and head values within the borehole column; it was set to take a reading per minute. The probe was attached to a string and positioned inside the borehole with the sensor placed at the centre of the aquifer system. Since the porous aquifer system had two monitoring points, a TLC probe was placed in each borehole.

Natural water flowed through the system for six minutes, within this time the TLC probe recorded background FEC measurements. Subsequently 10, 15, and 20 g, respectively, of NaCl was diluted within a 500 ml jar of water and introduced into the system as a pulse source through the inflow side. NaCl was selected as a tracer for this study as it has low toxicity, it is readily available, cost-effective, and easily measurable in real time with a hand-held probe.

3.2.3 Fluid electrical conductivity profiling

Once the hydrological tracer tests confirmed the usability of the models and intervals to capture the relevant stages were established, the models were used to assess the progression of FEC profiles related to a contaminant plume. To assess whether the results obtained from this test were repeatable, the test was conducted three times using different salt concentrations (10, 15, and 20 g). It was important to reconstruct the models for each test to avoid cross-contamination and ensure the accuracy of the trends obtained.

The FEC profiling method was employed using two different water quality scenarios: natural water quality and saline contaminated water. To clarify, the term *natural water* mentioned throughout this study refers to regular tap water continually flowing through the system; *contaminant plume* refers to the saltwater mixture which was injected into the system; and the term *profiling* is also referred to as logging in other studies.

Regular tap water with an EC of 130 μS/cm during the porous aquifer tests and 112 μS/cm during the weathered basement aquifer tests was used to simulate natural groundwater quality flow, and 10, 15, and 20 g respectively, of NaCl was added into 500 ml tap water to raise the EC in order to simulate contaminated groundwater conditions. The tap water maintained an average EC value of 130 μS/cm and 112 μS/cm throughout the respective tests. FEC profiling was conducted by slowly lowering a TLC probe into the borehole and subsequently raising it back up, negligible mixing is suspected while moving the probe down and up the borehole.

Under natural groundwater quality flow, background FEC profiles were recorded within the borehole and were used as indicators to identify and monitor changes within the simulated borehole column. Subsequently, the contaminant was introduced into the system as a four-second pulse injection through the inflow side. Thereafter, continuous FEC profiling was conducted.

Within the porous aquifer system there was a waiting period of one minute, which was the expected time for the first arrival of the plume as determined by the performance tests of the physical model. Thereafter, continuous FEC profiling was conducted every two minutes until the arrival of the plume peak at eight minutes. Afterwards, the borehole was profiled after 16, 18, 27, 33, 47, 62, 82, 111 and 116 minutes.

In the weathered basement aquifer system, continuous FEC profiling was also conducted every minute. The first arrival of the plume was observed after two minutes, which aligned with observations from the tracer breakthrough tests, and the plume peak was recorded after 12 minutes. Once the plume had passed the borehole and natural water continued to flow, replenishment took place, the EC started decreasing at a constant rate and the sampling interval was increased to three minutes.

3.3 Results and Discussion

The first subsection shows the results obtained from testing the performance of the physical model. This is followed by findings obtained from measurements recorded while assessing the progression of FEC profiles in the two aquifer systems studied, starting with the porous aquifer system and thereafter the weathered basement aquifer system. These findings include the background profiles that were obtained under natural water conditions, and the FEC profiles associated with various stages of the contaminant plume migration; namely the arrival of the plume, plume peak, residual plume, and the near-background FEC profile. All the recorded data that was used to make the graphs shown in this section can be found in Appendices A, B and C located at the end of this document.

3.3.1 Validating the performance of the physical models

Testing the performance of the physical models included estimating the models' hydraulic properties, and then performing tracer breakthrough tests to determine the extent to which the simulated physical models represented real systems.

3.3.1.1 Estimation of the hydraulic properties of the models

The hydraulic conductivity of the porous layer in both models was obtained by conducting Darcy's experiment and the K-value was calculated using Darcy's equation for flow in porous media (Darcy, 1856):

$$K = \frac{Q}{Ai} \qquad \textit{Equation 3-1}$$

Where:

Q = Specific discharge [L^3T^{-1}];

K = Hydraulic conductivity [LT^{-1}];

A = Cross-sectional area to flow [L^2]; and

i = Hydraulic gradient [-].

The test was conducted four times in each model and an average hydraulic conductivity value of 51.69 m/day was acquired in the porous aquifer model, and 47.70 m/day in the weathered basement aquifer model as shown in Table 3-1.

Table 3-1 The hydraulic conductivity of the porous layer in the porous aquifer model and the weathered basement aquifer model.

Test no.	Porous aquifer model				Weathered aquifer model			
	Q (m^3/day)	A (m^2)	i	K (m/day)	Q (m^3/day)	A (m^2)	i	K (m/day)
Test 1	0.279	0.061	0.090	50.69	0.169	0.050	0.072	46.85
Test 2	0.284	0.061	0.090	51.68	0.174	0.050	0.072	48.21
Test 3	0.290	0.061	0.090	52.70	0.172	0.050	0.072	47.87
Test 4	0.279	0.061	0.090	50.69	0.172	0.050	0.072	47.87
Average	**0.284**	**0.061**	**0.090**	**51.69**	**0.172**	**0.050**	**0.072**	**47.70**

3.3.1.2 Assessing the performance of the models

Testing the performance of the physical models was not only important in order to determine the extent to which the simulated models represented real systems but it also aided in establishing the travelling time of the plume; namely the initial time the plume arrived at the monitoring point, the plume's breakthrough time, the time dilution started taking place within the system, and the time it took for the system to return to background conditions.

Figure 3-5 (A-C) shows tracer breakthrough curves obtained from the simulated boreholes, BH1 and BH2, in the porous aquifer system over a period of 120 minutes. It is important to note that since the plume had completely passed the monitoring points and the system had reached background conditions by this time, it was not necessary to continue or extend the monitoring period to longer than 120 minutes. The test was repeated three times using varying salt concentrations, Figure 3-5 (A) represents results obtained from Model 1 where 10 g of salt was used, (B) are results from Model 2 where 15 g of salt was used, and (C) are results obtained from Model 3 where 20 g of salt was used. T1 represents the first test conducted, T2 the second test, and T3 the third test conducted in each borehole.

It can be noted from the graphs of the three models that the first arrival of the plume at BH1 was observed after one minute. In Model 1 there was a slight increase in FEC from 141 µS/cm to an average value of 153 µS/cm during the respective tests (T1, T2, and T3), however, this increase became more evident after two minutes where the FEC increased to an average value of 827 µS/cm. The FEC concentration in Models 2 and 3 were evident after one minute, where average FEC values increased from 141 µS/cm to 505 µS/cm in Model 2, and 898 µS/cm in Model 3, this notable increase was due to the increased initial contaminant concentration in these two models.

At BH2 the first arrival of the plume was noted after two minutes whereby the FEC values increased from 141 µS/cm to average values of 145, 353, and 577 µS/cm, in the respective models. The progression of the plume at this monitoring point was not as rapid as at BH1, this is because BH2 was located slightly further from the source.

The plume peak at BH1 was observed eight minutes later, where the FEC concentrations reached average values of 1 215 µS/cm in Model 1, 3 474 µS/cm in Model 2, and 5 091 µS/cm in Model 3. The plume peak concentration represents the highest recorded FEC throughout the tracer test experiment. Thereafter, the FEC values declined continuously until they were the same as those of the background FEC.

The plume peak at BH2 was observed 14 minutes later and had an average FEC value of 1 049 µS/cm, 2 893 µS/cm, and 4 730 µS/cm, in the respective models, which was lower than those recorded at BH1. Since BH2 was located further from the source, the migrating plume was subjected to dispersion and diffusive effects which resulted in reduced contaminant concentrations at that monitoring point.

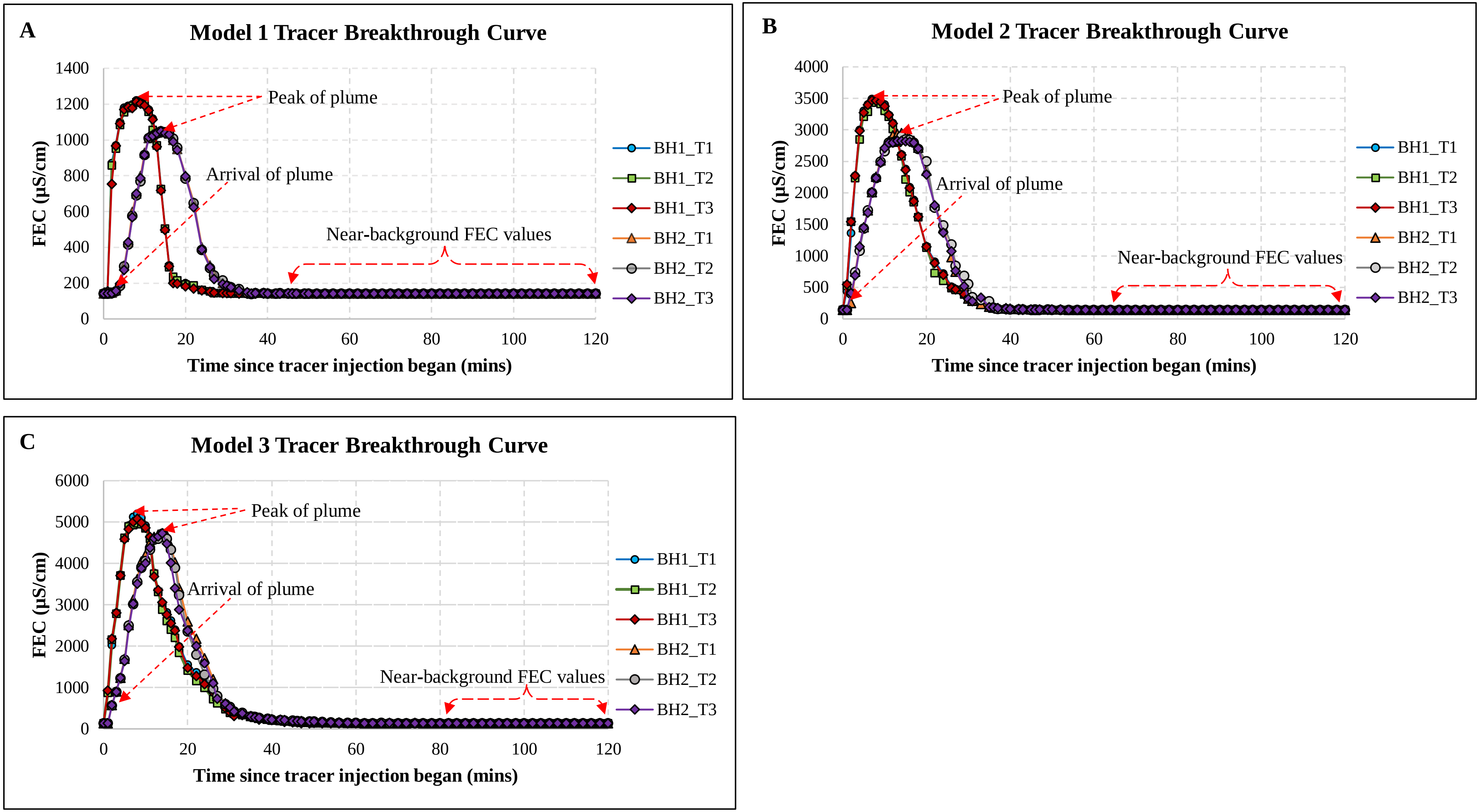

Figure 3-5 Tracer breakthrough curves recorded in BH1 and BH2 in the simulated porous aquifer system model. The test was conducted three times in each borehole.

Note: (A) represents results obtained from Model 1 where 10 g of salt was used, (B) are results from Model 2 where 15 g of salt was used, and (C) are results obtained from Model 3 where 20 g of salt was used. BH1_T1 are results obtained in BH1 during the first test, BH1_T2 are results obtained in BH1 during the second test, and BH1_T3 are the test obtained during the third test.

The general characteristics noted from the tracer breakthrough curves shown in Figure 3-5 were that they were relatively bell-shaped with the peak symmetrically aligned and prolonged (instead of sharp), and had a short tail. According to Field (2003) this is typical of a porous homogeneous aquifer system. The FEC values in both BH1 and BH2 had already reached background values after 47 minutes in Model 1, 62 minutes in Model 2 and 82 minutes in Model 3, thus showing a short tail unlike in a fractured aquifer system as discussed by Haggerty et al. (2000) and Moleme and Gomo (2018).

The tracer breakthrough test was also conducted three times using varying salt concentrations in the weathered basement aquifer model and the obtained results are illustrated in Figure 3-6 (A-C). The first arrival of the plume was observed after two minutes, this was reflected by an average increase in FEC values from 123 µS/cm to 131 µS/cm, 419 µS/cm, and 741 µS/cm, in the respective models. The peak of the plume reached the borehole after 12 minutes, reaching maximum average FEC values of 1 176 µS/cm, 3 228 µS/cm, and 4 828 µS/cm, respectively. Once the centre of the contaminant plume passed the borehole, dilution took place, this was represented by decreasing FEC values. The higher the initial salt concentration, the longer it took for the system to reach near-background FEC values.

The breakthrough curves obtained in the weathered basement aquifer models were similar to those observed in the porous aquifer models in terms of shape, as shown in Figure 3-5. This was because the upper transmissive layer of the weathered basement aquifer model was also porous and homogeneous.

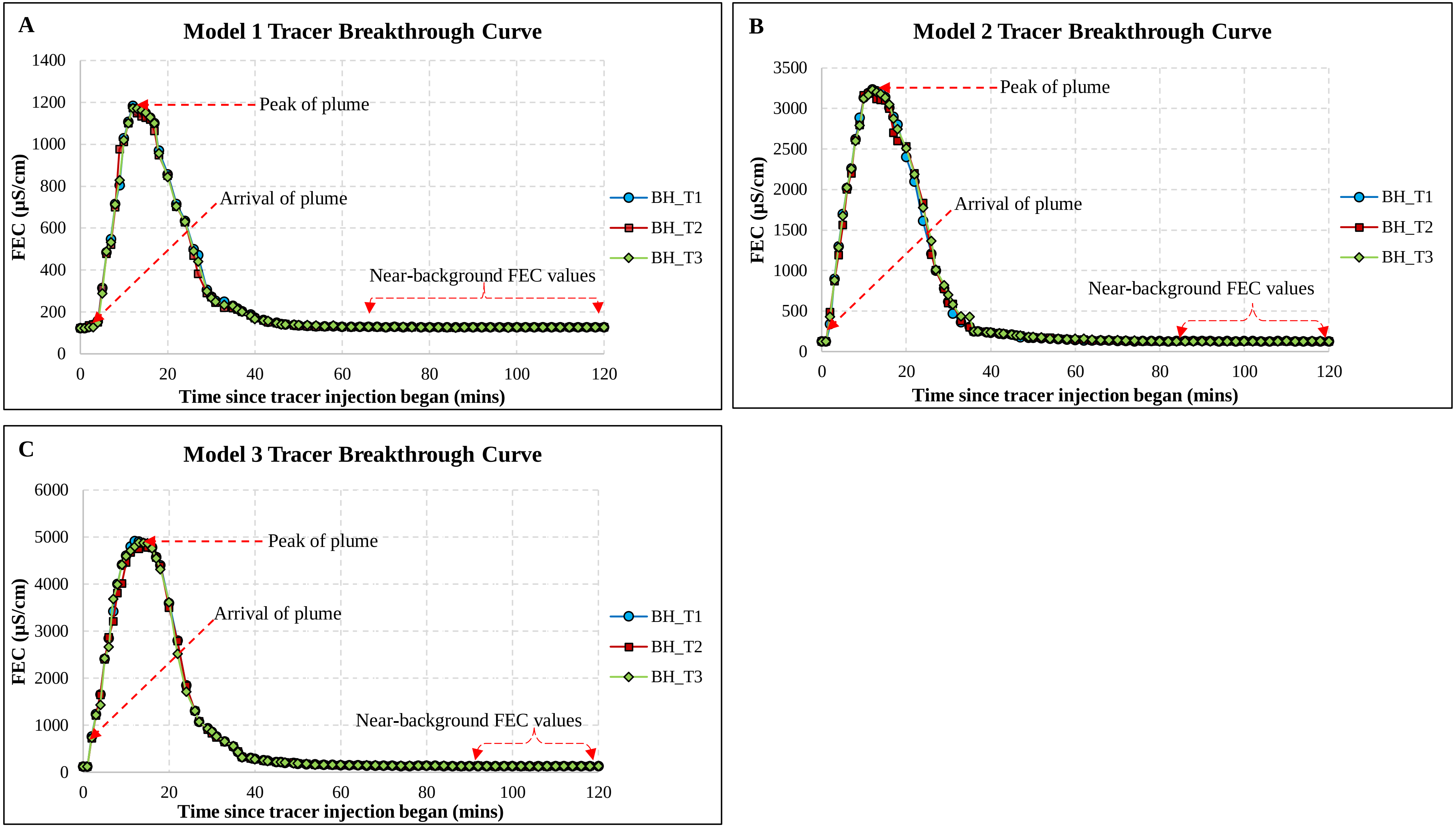

Figure 3-6 Tracer breakthrough curves recorded in the simulated weathered basement aquifer system model.

Note: (A) represents results obtained from Model 1 where 10 g of salt was used, (B) are results from Model 2 where 15 g of salt was used, and (C) are results obtained from Model 3 where 20 g of salt was used. BH_T1 are results obtained in BH during the first test, BH_T2 are results obtained in BH during the second test, and BH_T3 are the test obtained during the third test.

Different aquifer systems produce their own distinct tracer breakthrough curves irrespective of concentration. The fractured aquifer system produces a breakthrough curve that is sharp, positively skewed with the peak time lying behind the mean transit time, and has a long tail (Haggerty et al., 2000, Moleme and Gomo, 2018). Whereas the tracer breakthrough curve of a porous and weathered basement aquifer system is relatively bell-shaped with the peak symmetrically aligned and prolonged (instead of sharp), and a short tail (Field, 2003). The tracer breakthrough curves obtained in this study (Figure 3-7 A and B) were compared to typical homogeneous, unconfined, porous and weathered basement breakthrough curves observed in literature (Figure 3-7 C, D, E and F). This was done to compare the extent of their similarities.

The curves were comparable in terms of their shape, symmetrical peak, and short tails. This confirmed that the physical structure of the simulated aquifer systems in terms of flow characteristics and the interaction between the weathered and the impermeable bedrock was similar to field conditions for such aquifer systems. Therefore, the general characteristics of FEC profiles obtained in these respective laboratory aquifer models should be representative of the ones which would be obtained in the field. This deemed the performance of the physical models satisfactory to be used to study FEC responses in these simulated aquifer systems. However, it is worth mentioning that the laboratory experiments provide FEC profiles under ideal, homogeneous conditions which can then be used for the interpretation of field data, minor deviations from these profiles may be observed under heterogeneous field conditions.

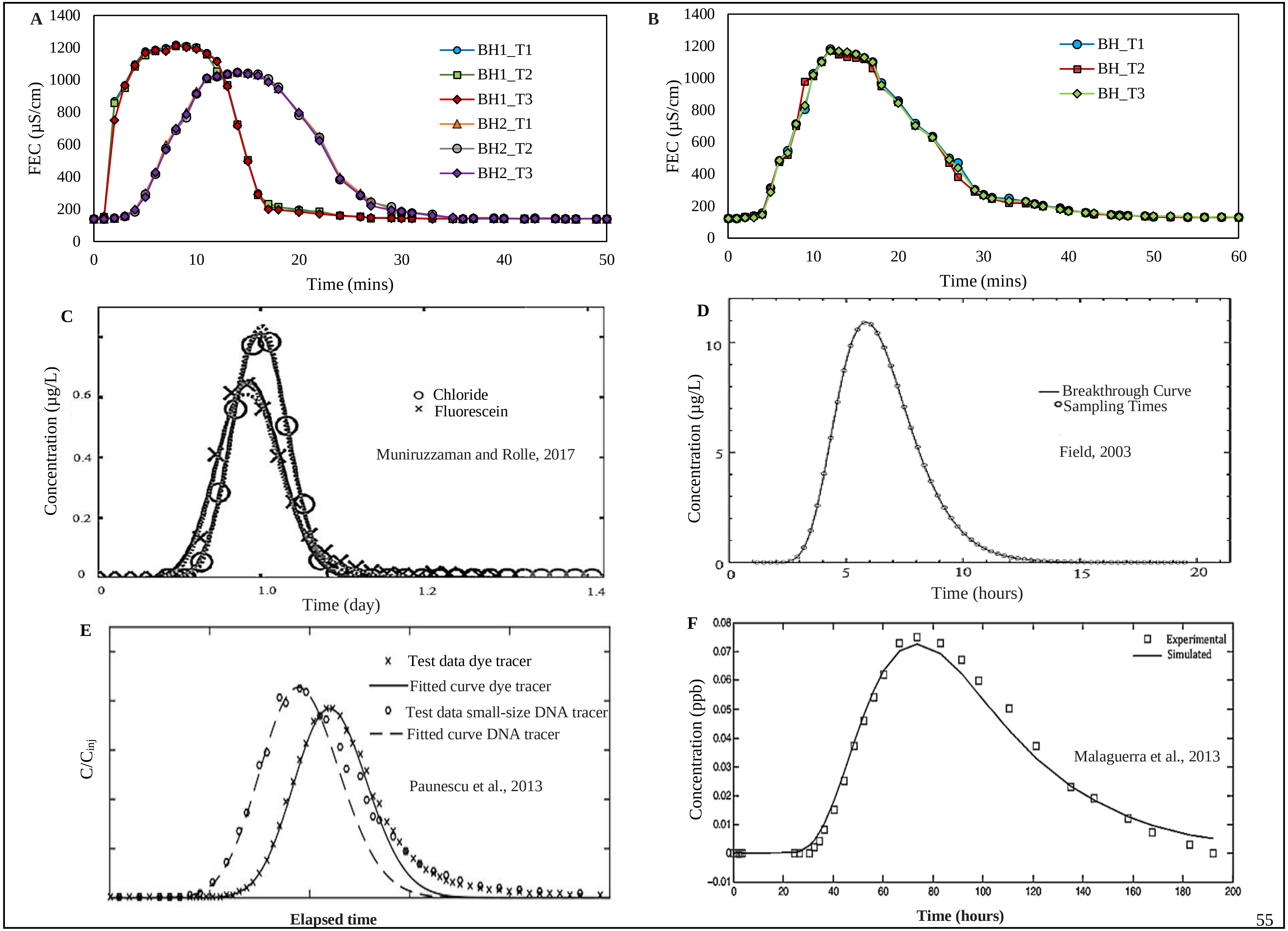

Figure 3-7 Tracer breakthrough curve graphs (A and B) obtained in this study compared to ones observed in literature (C, D, E and F).
Source: Muniruzzaman and Rolle (2017), Field (2003), Paunescu et al. (2013), and Malaguerra et al. (2013).

3.3.2 Fluid electrical conductivity profiles

This section discusses the results obtained during the investigation of the progression of FEC profiles in both the porous and weathered basement aquifer systems. The FEC profiles obtained from the porous aquifer system are presented first; this includes the background FEC profile which was observed before the saline contaminant was introduced into the system, and the FEC profiles associated with various stages of the contaminant plume evolution (i.e. arrival of the plume, plume peak, residual plume profile, and near-background FEC profile). Thereafter, following the same sequence, results obtained from the weathered basement aquifer system are presented and discussed.

The tests were conducted in three models with varying salt concentrations (10, 15, and 20g), and were repeated three times in each model in order to confirm repeatability. Throughout the duration of the FEC profiling tests, tap water maintained an average EC value of 130 µS/cm within the porous aquifer system, and 112 µS/cm within the weathered basement aquifer system.

3.3.2.1 FEC profiles in the porous aquifer system

3.3.2.1.1 Background FEC profile

Before any profiles were recorded natural water was allowed to flow through the porous aquifer system for two minutes. Thereafter, the background FEC profiles were recorded. Figure 3-8 shows the FEC measurements obtained from a borehole installed within the simulated porous aquifer system, in the three models. The first profiles were recorded two minutes after natural water entered the system, a slightly unstable trend was observed due to natural water mixing with salts from the soil material.

As natural water continued to flow through the system, profiles were recorder after four and eight minutes, the profiles obtained were vertically straight in shape and had a constant FEC value of 141 µS/cm, which meant that the quality of water throughout the entire system was the same. This vertically straight signature in the porous aquifer system is referred to as the background FEC profile.

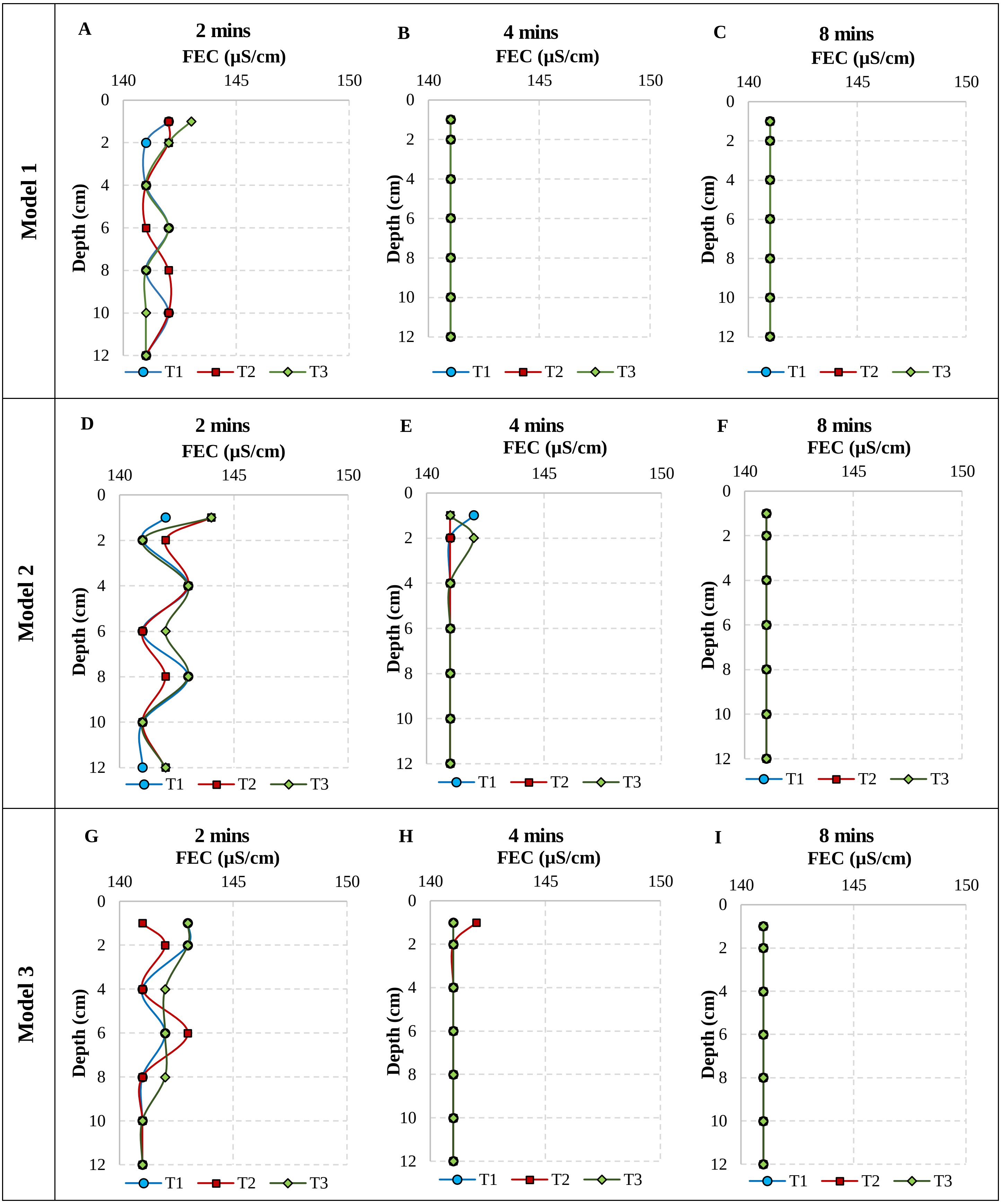

Figure 3-8 FEC profiles obtained under natural water flow conditions.

Note: The graphs indicate repeated measurements taken at different times in three porous aquifer models. The background profiles obtained in both BH1 and BH2 were the same.

It can be noted that although there was no contamination in the system yet, the background FEC values were slightly higher than the FEC of the natural water, this was due to salts naturally found in the soil material. Even in a real system, the natural salts present in the formation would slightly increase the FEC of the formation water. However, this had no effect on the ability to effectively observe various profiles associated with the evolution of the contaminant plume since the FEC of the contaminant plume was significantly higher than that of the background.

3.3.2.1.2 Plume arrival FEC profile

The plume reached BH1 one minute after it was injected into the system (Figure 3-9) as informed by the tracer breakthrough test (Figure 3-5). This led to a profile with increasing FEC values towards the bottom of the borehole.

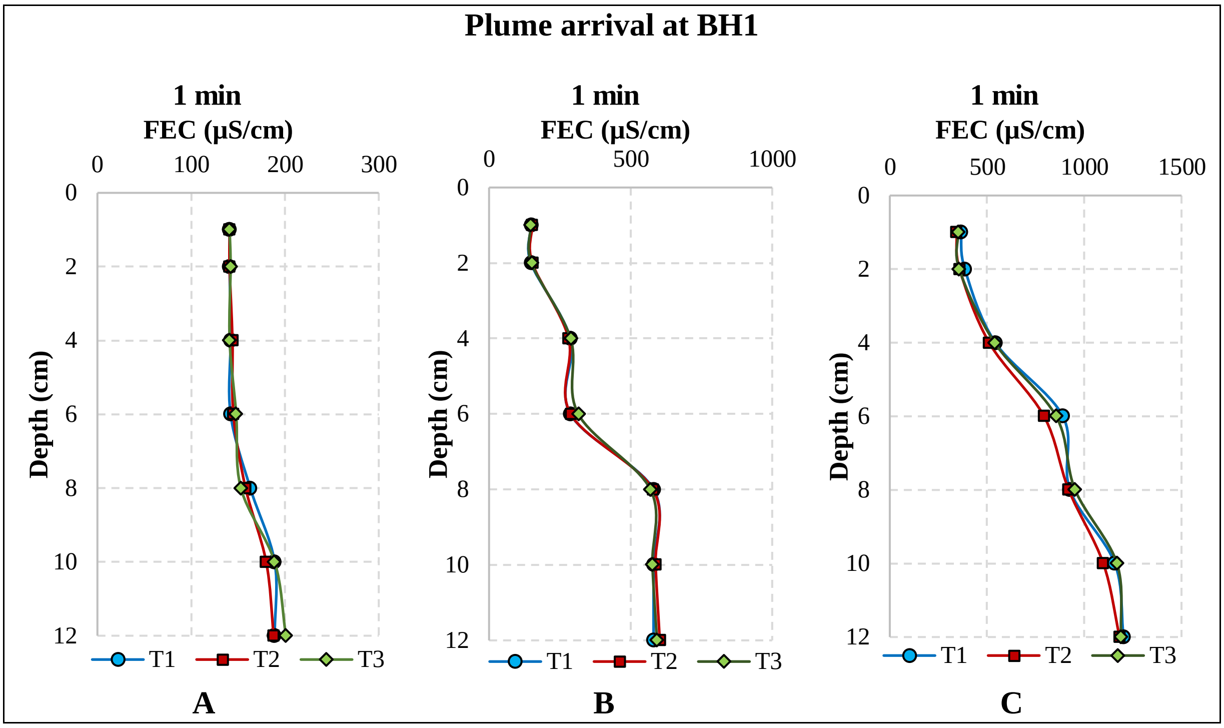

Figure 3-9 FEC profiles showing the arrival of the plume at BH1 one minute after injection.

Note: (A) represents results obtained from Model 1 where 10 g of salt was used, (B) are results from Model 2 where 15 g of salt was used, and (C) are results obtained from Model 3 where 20 g of salt was used. The tests were repeated three times in each model.

The significantly high density of the plume compared to the system's natural water caused the plume to migrate downwards instead of moving laterally. This density effect represents the dominance of the gravitational force over the advection force at this point. The effects of density have been of interest in groundwater studies (Diersch and Kolditz, 2002; Simmons et al., 2001), and higher initial concentrations of tracer solutes in the test section have often been associated with greater density effects (Gomo, 2011; Shakhane, 2011).

The first arrival of the plume at the second monitoring point (BH2) was observed after two minutes as shown in Figure 3-10. Unlike the first arrival FEC profile at BH1 which was characterised by an increasing trend towards the bottom, the resulting first arrival FEC profile at BH2 was characterised by an anomaly towards the centre of the aquifer system.

At this point it was apparent that the distance of the monitoring point from the source (injection point) had an influence on the FEC profile produced. BH2 was located further away from the injection point compared to BH1, therefore, mass transport effects such as dilution played a bigger role in reducing the concentration (and density) of the plume reaching it. Additionally, the distance from the monitoring point also allowed the plume to align with the flow lines of the system and move laterally.

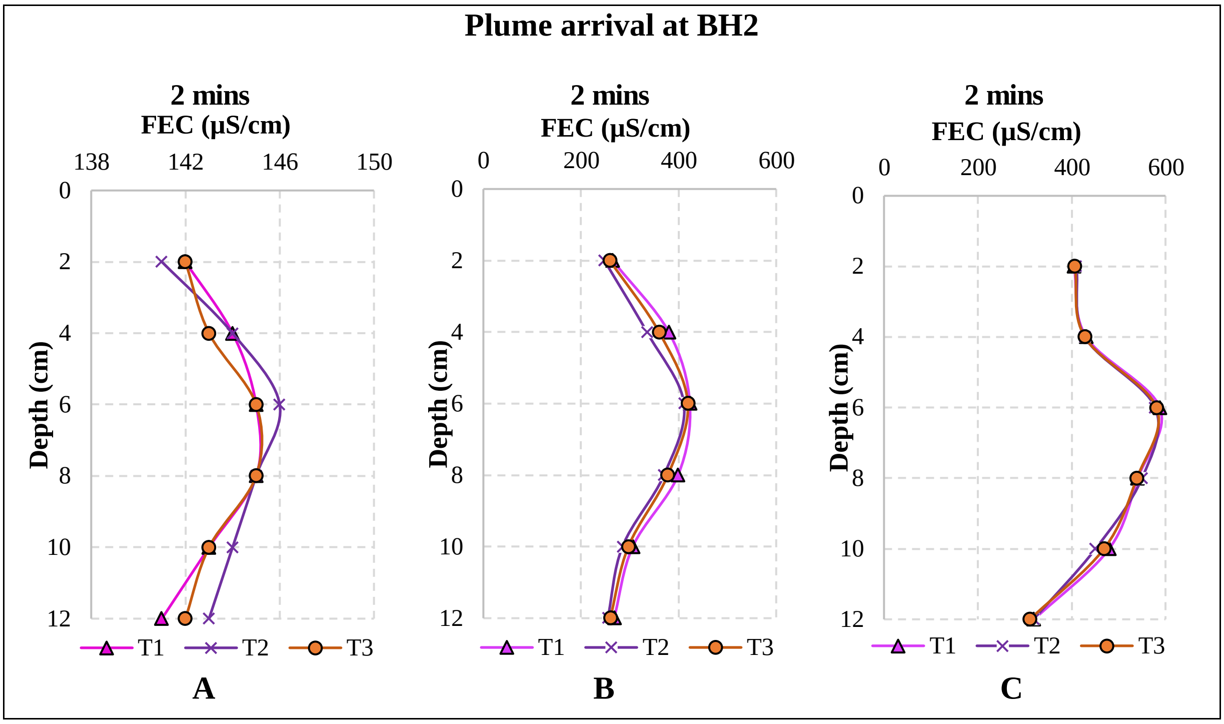

Figure 3-10 FEC profiles showing the first arrival of the tracer at BH2 two minutes after injection.
Note: (A) represents results obtained from Model 1 where 10 g of salt was used, (B) are results from Model 2 where 15 g of salt was used, and (C) are results obtained from Model 3 where 20 g of salt was used.

3.3.2.1.3 Plume peak FEC profile

After eight minutes the FEC within BH1 reached maximum values as shown in Figure 3-11. The increase in FEC was observed throughout the entire system with the highest average value recorded being 1 216 µS/cm (in Model 1), 3 470 µS/cm (in Model 2) and 5 092 µS/cm (in Model 3). Typically, fluid closer to the walls of the aquifer system will flow slower than the fluid in the centre, also referred to as the centreline in natural attenuation studies (Bockelmann et al., 2003). The centreline is the area with the least friction and thus the highest transporting velocity.

In the unconfined porous aquifer system, the friction created as water flowed against the bottom of the system, and the friction due to the atmosphere towards the top of the aquifer decreased the transporting velocity at these areas, and the centre of the permeable zone was the place with the least friction and highest transporting velocity.

However, in the case of BH1 the plume was migrating more downwards than forward, proving that although the effects of advection had increased, the effects of density (and the gravitational force) were still relatively greater at this monitoring point. Furthermore, due to the close distance of BH1 to the injection point (source), there was not enough time for the plume to align with the flow lines of the system. It was observed that the higher the concentration, the more the profile displayed a sinking effect as seen in Figure 3-11 C.

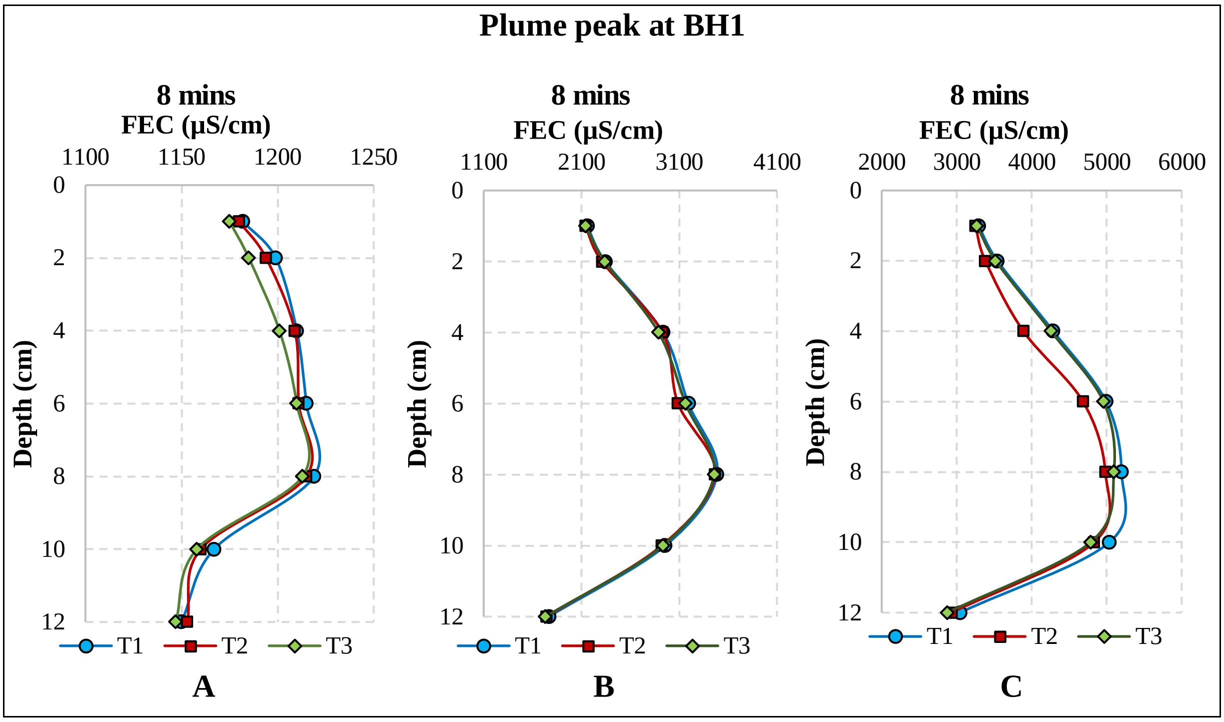

Figure 3-11 FEC profiles showing the plume peak which was observed after eight minutes at BH1.
Note: (A) represents results obtained from Model 1 where 10 g of salt was used, (B) are results from Model 2 where 15 g of salt was used, and (C) are results obtained from Model 3 where 20 g of salt was used.

The plume peak at BH2 was observed 14 minutes after the contaminant plume was introduced into the system as shown in Figure 3-12 . Unlike in BH1, the plume did not display a sinking effect, even in Model 2 and 3 where mass concentration was increased. Instead, the central axis of the plume remained at the centre of the aquifer system where the least friction and the highest transporting velocity was expected. This is because BH2 was located further away from the source, which gave the plume enough time to be aligned with the flow lines of the system.

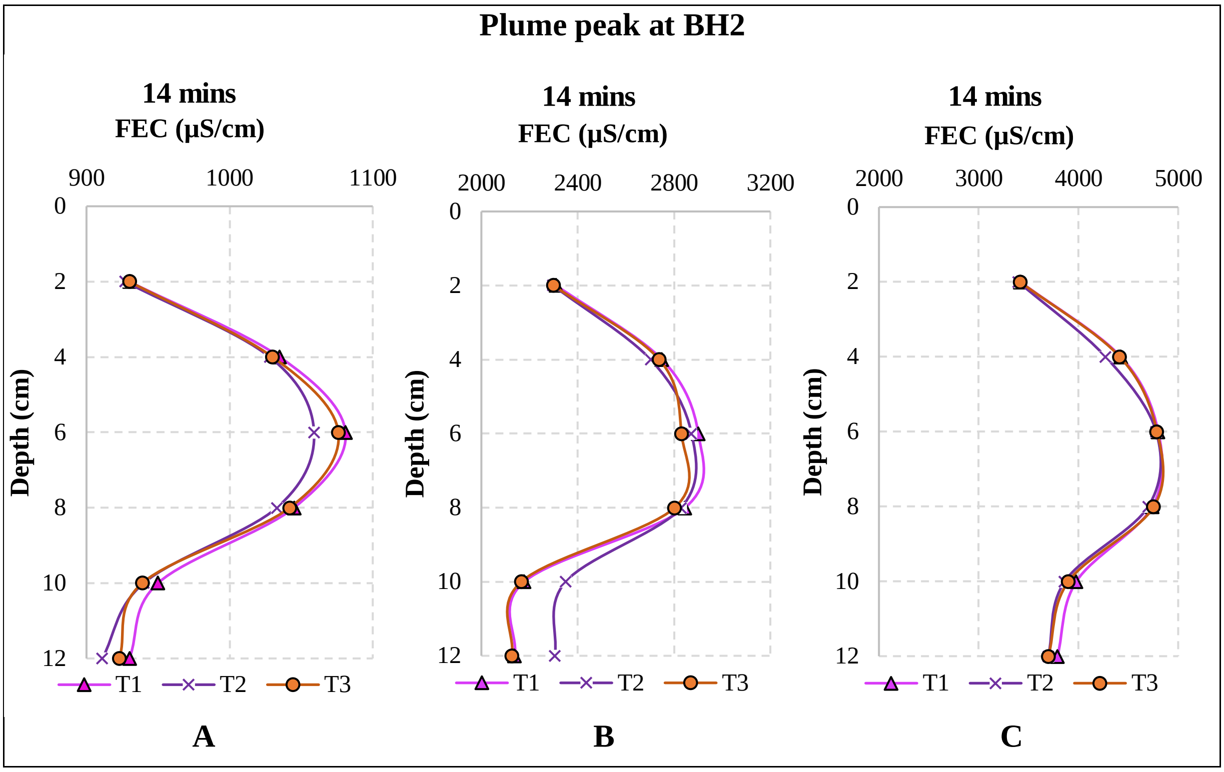

Figure 3-12 Arrival of the plume peak at BH2 observed after 14 minutes.

3.3.2.1.4 Residual plume FEC profile

After most of the contaminant plume had passed the boreholes, natural water continued flowing through the system, and dilution continued taking place thus resulting in a decrease in FEC values. Figure 3-13 shows the FEC profiles associated with the residual plume at BH1 and BH2 observed at 16 and 18 minutes, respectively, in the three models. The residual plume FEC profile measured at BH1 displayed a diagonal shape with decreasing FEC values towards the bottom of the aquifer system (Figure 3-13A, C, E).

Whereas the shape of the residual plume FEC profile observed at BH2 (Figure 3-13B, D, F). remained similar to the one seen in Figure 3-12, with the central axis of the plume still located at the centre of the aquifer system. However, due to continuous dilution taking place within the system, the thickness and amplitude of the plume peak anomaly decreased. The anomaly was expected to continue decreasing with time as replenishment continued until it became a vertically straight-line once background values were reached.

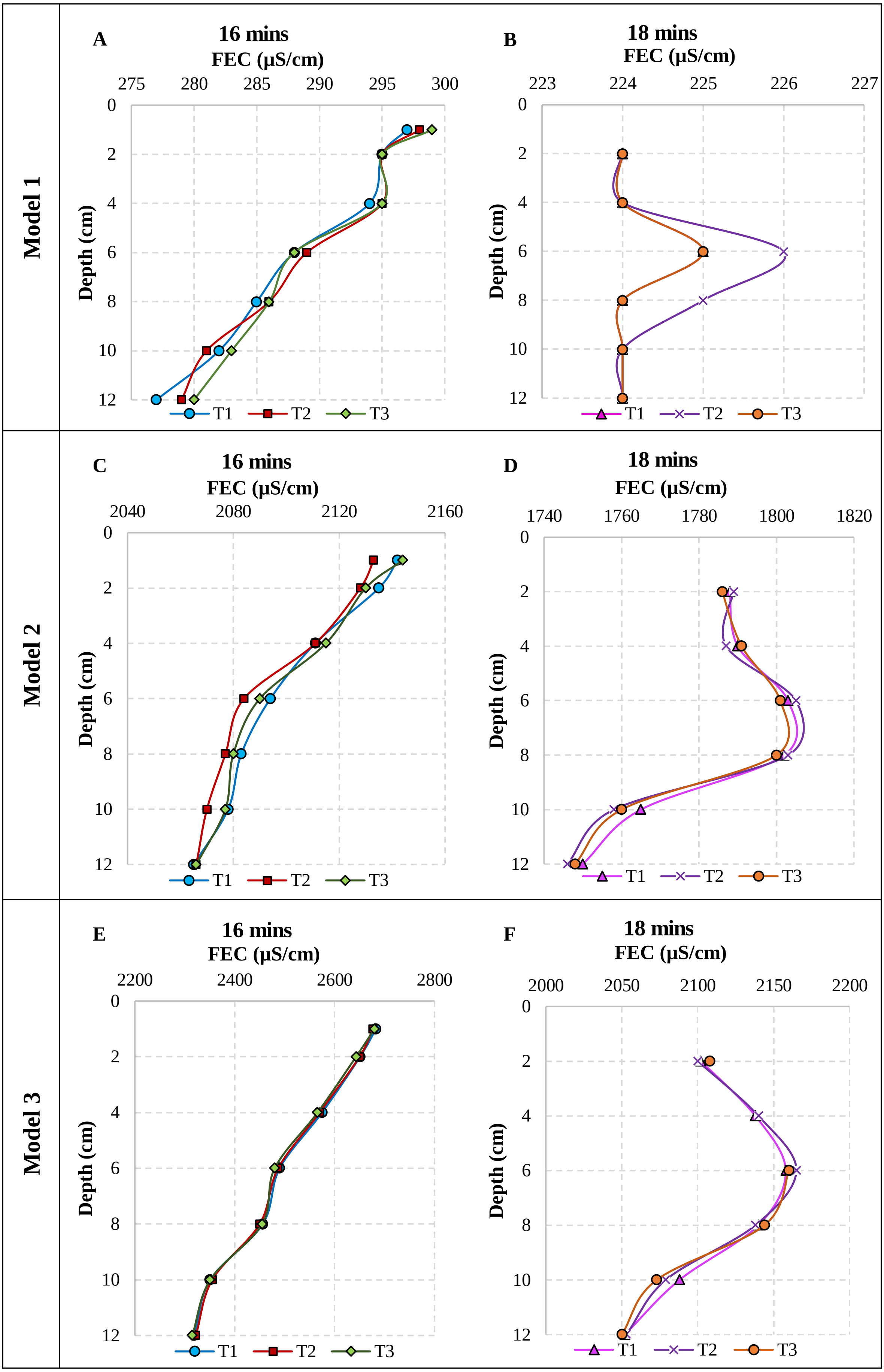

Figure 3-13 FEC profiles associated with the residual plume at BH1 (A, C, E) and BH2 (B, D, F).

3.3.2.1.5 Near-background FEC profile

Once the contaminant plume had migrated past the boreholes and natural water had replenished the system, the FEC values continued to decrease until they reached near-background values as illustrated in Figure 3-14. Since the system was porous and homogeneous dilution took place throughout the entire system, the system reached initial FEC values of 141 µS/cm after 33 minutes in Model 1, 47 minutes in Model 2, and 62 minutes in Model 3. At that point in time, it was evident that the contaminant plume had completely passed the monitoring points and only natural water was present.

The system took longer to reach near-background values in the third model due to the high initial contaminant concentration in the system compared to the first model. However, the near-background profile in all three models was represented by a vertically straight profile.

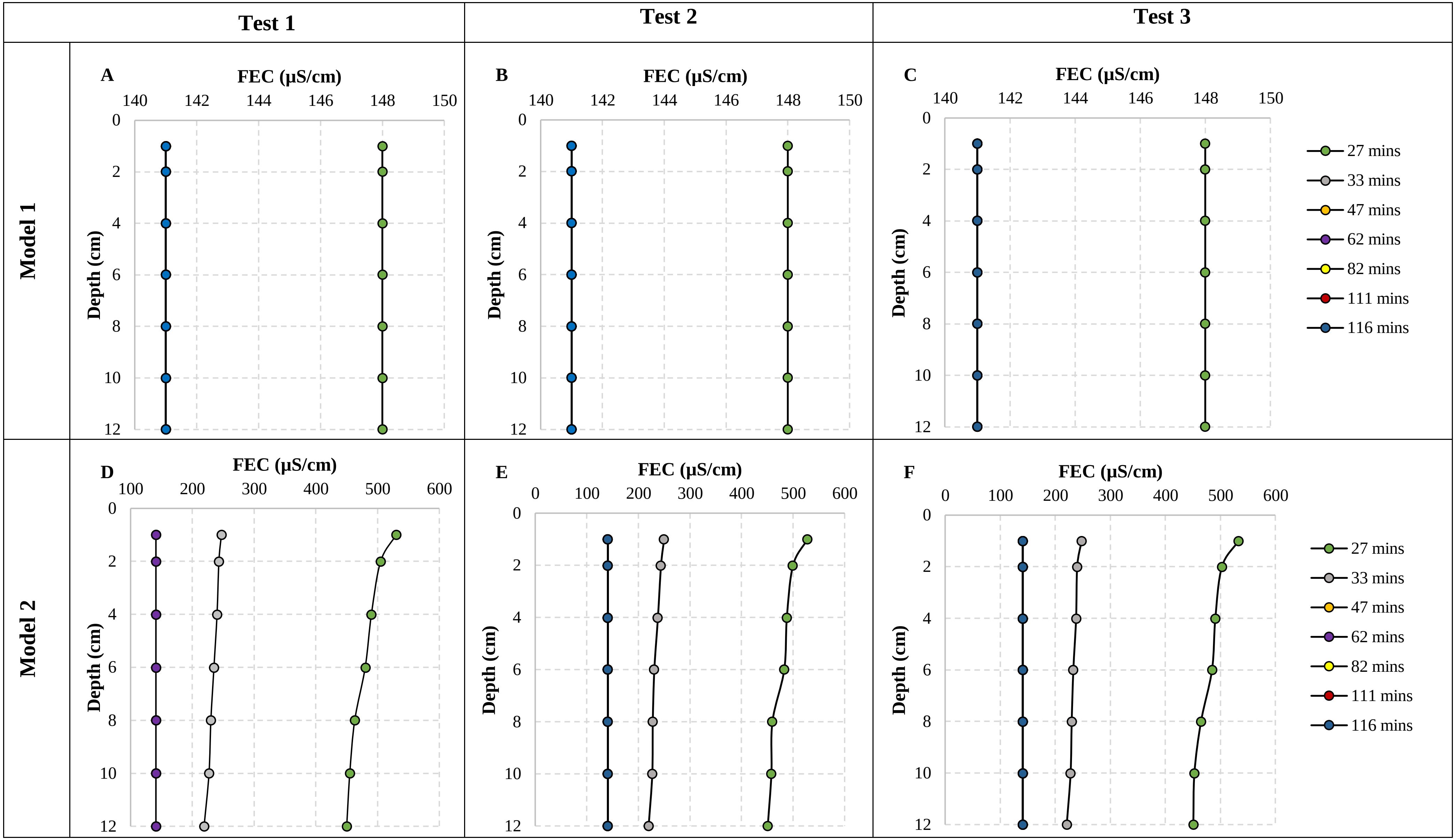
Test 1
Test 2
Test 3
Model 1
Model 2
A
B
C
D
E
F
FEC (µS/cm)
Depth (cm)
140
142
144
146
148
150
0
100
200
300
400
500
600
2
4
6
8
10
12
27 mins
33 mins
47 mins
62 mins
82 mins
111 mins
116 mins

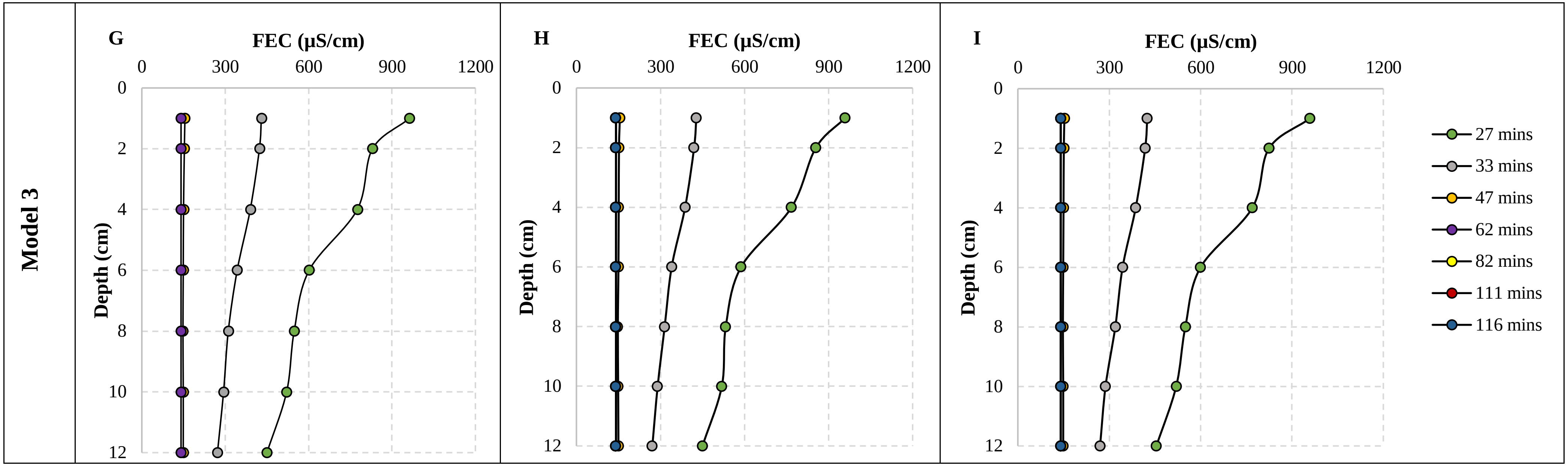

Figure 3-14 FEC profiles showing near-background values within the unconfined porous aquifer system.

Note: Since the system was porous and homogeneous, dilution took place throughout the entire system.

3.3.2.1.6 Plume orientation phenomenon

Initially the FEC profiles obtained at BH1 and BH2 were expected to be similar throughout all stages since they were recorded in the same aquifer system. However, this was not the case. Based on observations made during the analysis of FEC profiles obtained in the porous aquifer system, it became evident that the contaminant plume undergoes an orientation evolution as it migrated through the aquifer system. The orientation evolution of the plume was due to the magnitude of forces acting upon it, which primarily were the gravitational (F_G) and advection force (F_A). The dominance of each force was largely influenced by the distance of the borehole from the source (injection point). Figure 3-15 is a schematic illustration which explains the phenomenon of the evolution of the contaminant plume orientation through the porous aquifer system.

When the contaminant plume is introduced into the system (point O), the magnitude of the gravitational force is at its maximum and the advection force is zero, hence the plume initially migrates downward at a vertical inclination ($\theta = 90^o$). As the plume migrates through the system, dilution continuously occurs, thereby reducing the plume density, and consequently the magnitude of the gravitational force decreases. The decrease in the gravitational force leads to the transition in the orientation of the migrating plume from a vertical ($\theta = 90^o$) to a sub-vertical orientation ($\theta < 90^o$).

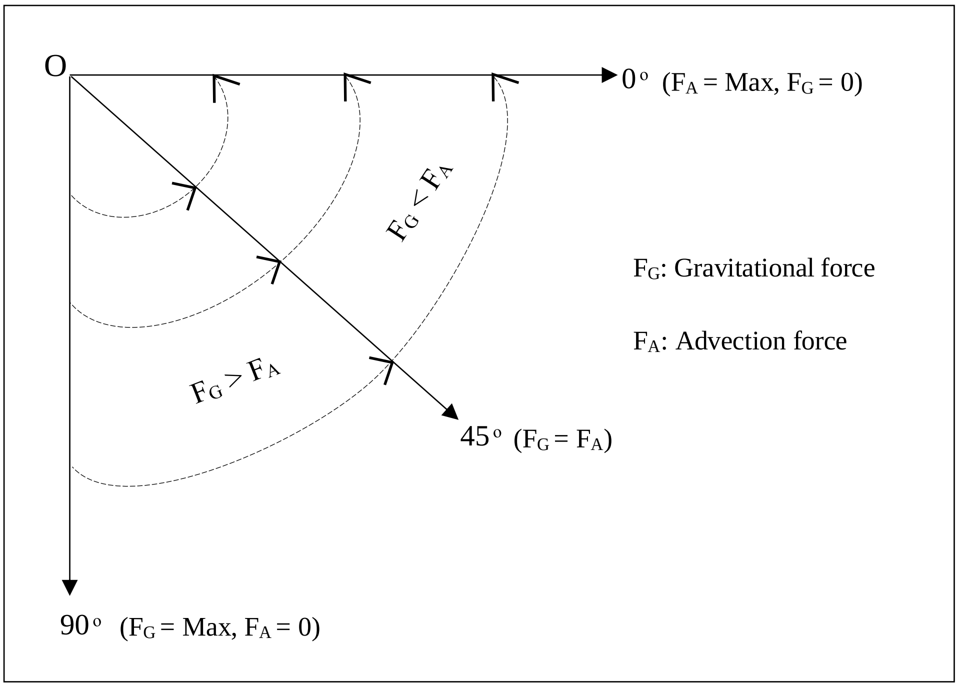

Figure 3-15 Schematic illustration showing the evolution of the contaminant plume orientation as it migrates through a porous aquifer system.

Once the plume has a sub-vertical orientation, the plume is subjected to both the gravitational and advection force. When the plume orientation is between 89^o and 46^o as shown in Figure 3-15, the plume is subjected to a gravitational force greater than the advection force ($F_G > F_A$). At a 45^o plume orientation, the plume is subjected to gravitational and advection forces of equal magnitude ($F_G = F_A$). The plume is subjected to an advection force that is greater than the gravitational force ($F_A > F_G$) when it is orientated at an angle between 44^o and 1^o, it is at this point that the orientation of the plume starts aligning with the flow lines of the system. At (θ = 0^o) the advection force approaches a maximum magnitude with no gravitational force, which results in a horizontal plume orientation parallel to the groundwater flow direction.

The horizontal plume orientation is what is typically illustrated in the available literature. However, based on this study it is apparent that the plume orientation of the plume may vary depending on the location of the monitoring point from the source. This therefore makes the evolution of the plume orientation concept proposed in this thesis a novel and important contribution. This phenomenon was observed throughout the profiling of the porous aquifer system and was well supported by the profiles.

3.3.2.2 FEC profiles in the weathered basement aquifer system

This sub-section discusses FEC profiles associated with various stages of the contaminant plume within the weathered basement aquifer system.

3.3.2.2.1 Background FEC profile

Recording the background FEC profile was important as it provided a baseline which could be used to monitor the changes taking place within the aquifer system as the contaminant plume progressed, and aided in determining how this affected the shape of the FEC profiles obtained over time. Natural water was allowed to flow through the system for two minutes before any profiles were recorded. Thereafter the background FEC profile was recorded under natural groundwater flow at different times in three models as shown in Figure 3-16 (A-I).

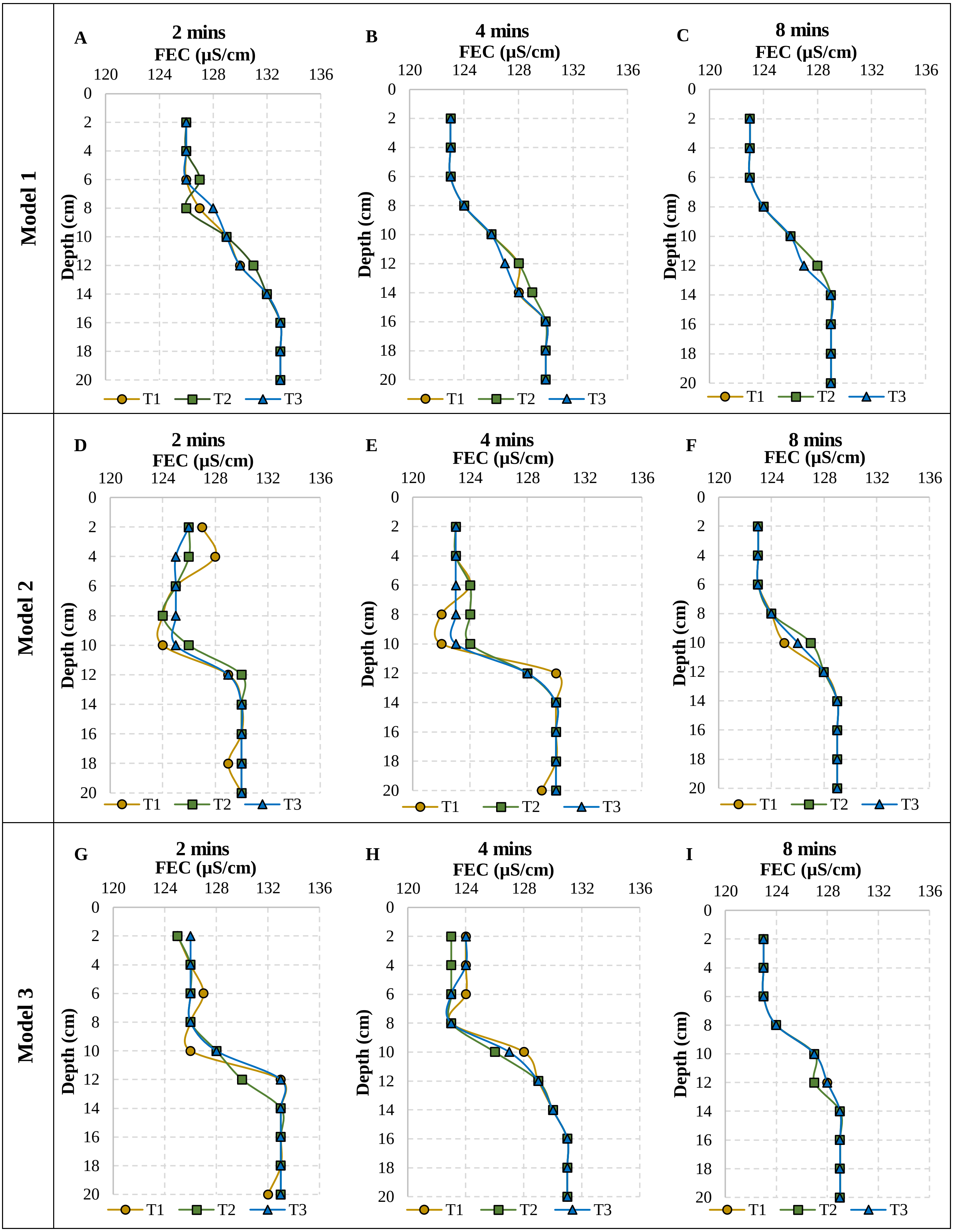

Figure 3-16 Background FEC profiles observed under natural water flow conditions.
Note: The graphs indicate repeated measurements taken at different times in three weathered basement aquifer models.

The background FEC profiles displayed an increasing trend towards the bottom of the aquifer system; lower FEC values were observed on the upper section and higher FEC values were present towards the lower section of the system. Since at this point the contaminant plume was not yet introduced into the system, the observed FEC values were entirely a result of incoming natural water coupled with the soil material. Both the weathered material and the impermeable bedrock had natural salts, but the high transmissivity and permeability of the weathered material allowed for effective replenishment to take place, thus decreasing the salinity naturally found in the soil material over time. This process was significantly limited within the impermeable bedrock.

The background profiles recorded between two and four minutes were not as distinct as the ones recorded after eight minutes. This was due to the mixing of incoming natural water coupled with the natural salts found in the soil which led to unstable trends. However, once adequate replenishment had taken place the FEC recorded in the system became stable. Although replenishment was continuously taking place - especially within the permeable zone, it is worth noting that due to the presence of natural salts in the soil material, the FEC of 123 µS/cm recorded in the permeable zone was slightly higher than the one of natural water which was recorded to be 112 µS/cm.

The background profile was measured more than once in three models at different times to confirm repeatability. The shape of the profiles consistently showed lower FEC values in the upper permeable zone and higher FEC values in the lower impermeable zone due to limited replenishment.

3.3.2.2.2 Plume arrival FEC profile

The plume reached the borehole (BH) two minutes after it was injected into the system, this was also informed by the tracer breakthrough test results shown in Figure 3-6. The highest FEC values were detected near the centre of the permeable zone as illustrated in Figure 3-17, this was the position of the maximum transporting velocity. The friction created as the water flowed against the surface of the impermeable layer, and the friction due to the atmosphere towards the top of the aquifer decreased the transporting velocity. Hence, the centre of the permeable zone was the place with the least friction and thus the highest transporting velocity. Although the lower segment of the aquifer system (impermeable bedrock) also increased in FEC, this was due to the density contrast, the sinking of denser saline water towards the bottom of the borehole rather than the migration of the contaminant through the impermeable bedrock.

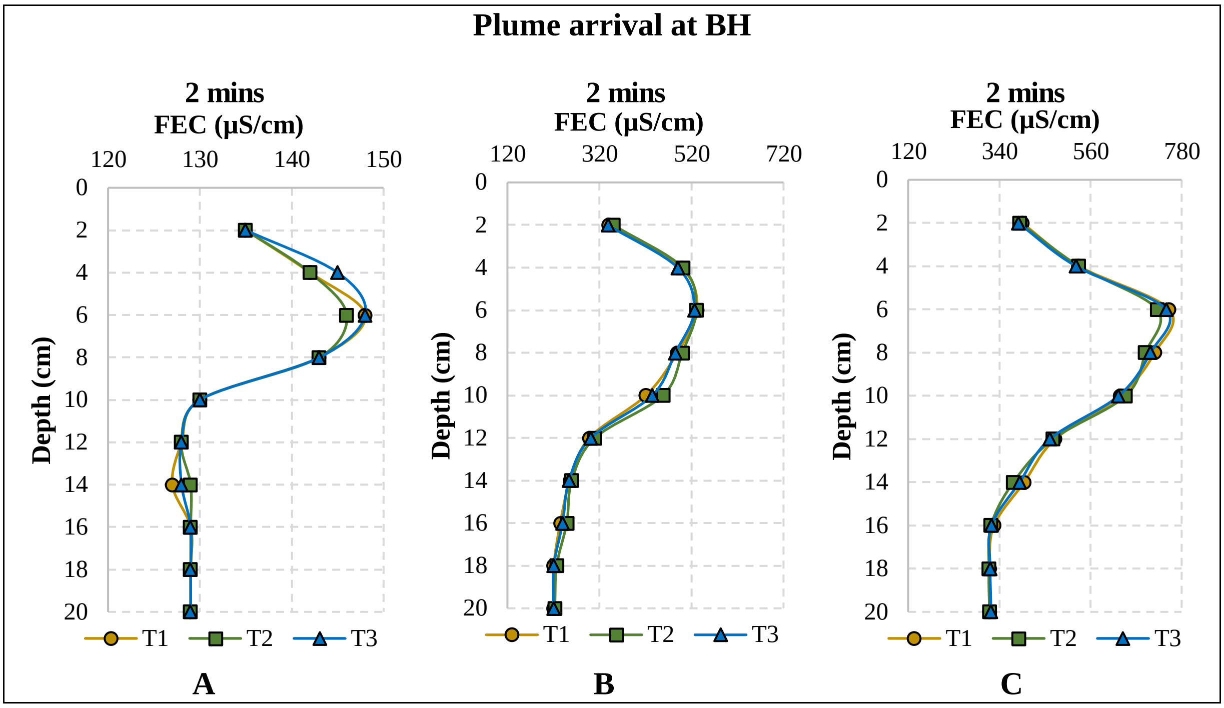

Figure 3-17 FEC profiles observed two minutes after the injection of a saline contaminant into the weathered basement aquifer system.

Note: (A) represents results obtained from Model 1 where 10 g of salt was used, (B) are results from Model 2 where 15 g of salt was used, and (C) are results obtained from Model 3 where 20 g of salt was used. A noticeably high increase in FEC values was observed at the highly permeable weathered upper segment.

3.3.2.2.3 Plume peak FEC profile

After 12 minutes of monitoring, the centre of the contaminant plume reached the borehole which resulted in elevated FEC values as shown Figure 3-18. The profile observed is referred to as the plume peak FEC profile, it represents the maximum FEC values recorded during the profiling duration. Similar to Figure 3-17 the profile displayed an increase in FEC values throughout its entire length with a maximum FEC value recorded near the centre of the high permeability weathered material, where the maximum transporting velocity was expected.

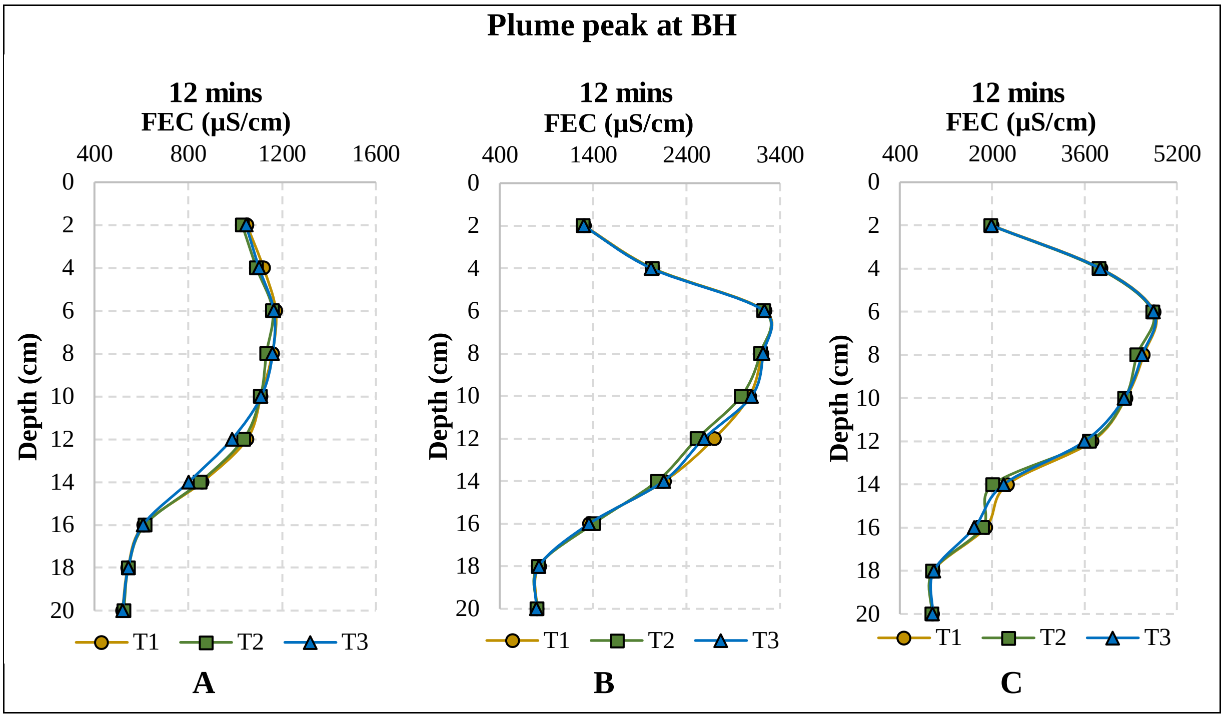

Figure 3-18 The arrival of the plume peak FEC profile in the weathered aquifer system was observed after 12 minutes. Note: (A) represents results obtained from Model 1 where 10 g of salt was used, (B) are results from Model 2 where 15 g of salt was used, and (C) are results obtained from Model 3 where 20 g of salt was used. An elevated FEC peak average value of 1 166 µS/cm was observed in Model 1, 3 232 µS/cm in Model 2, and 4 798 µS/cm in Model 3.

3.3.2.2.4 Residual plume FEC profile

Once the centre of the plume had passed the borehole FEC values started decreasing as shown in Figure 3-19. Most of the dilution took place within the permeable weathered zone (upper segment) due to continuous replenishment by natural water. The extent of dilution taking place within the lower segment was highly limited since natural water could not flow through the impermeable bedrock. The only process which facilitated dilution within this segment was diffusion, which is generally a much slower process compared to advection and dispersion. It is worth noting that this process of diffusion was mostly taking place within the borehole column rather than within the impermeable bedrock itself.

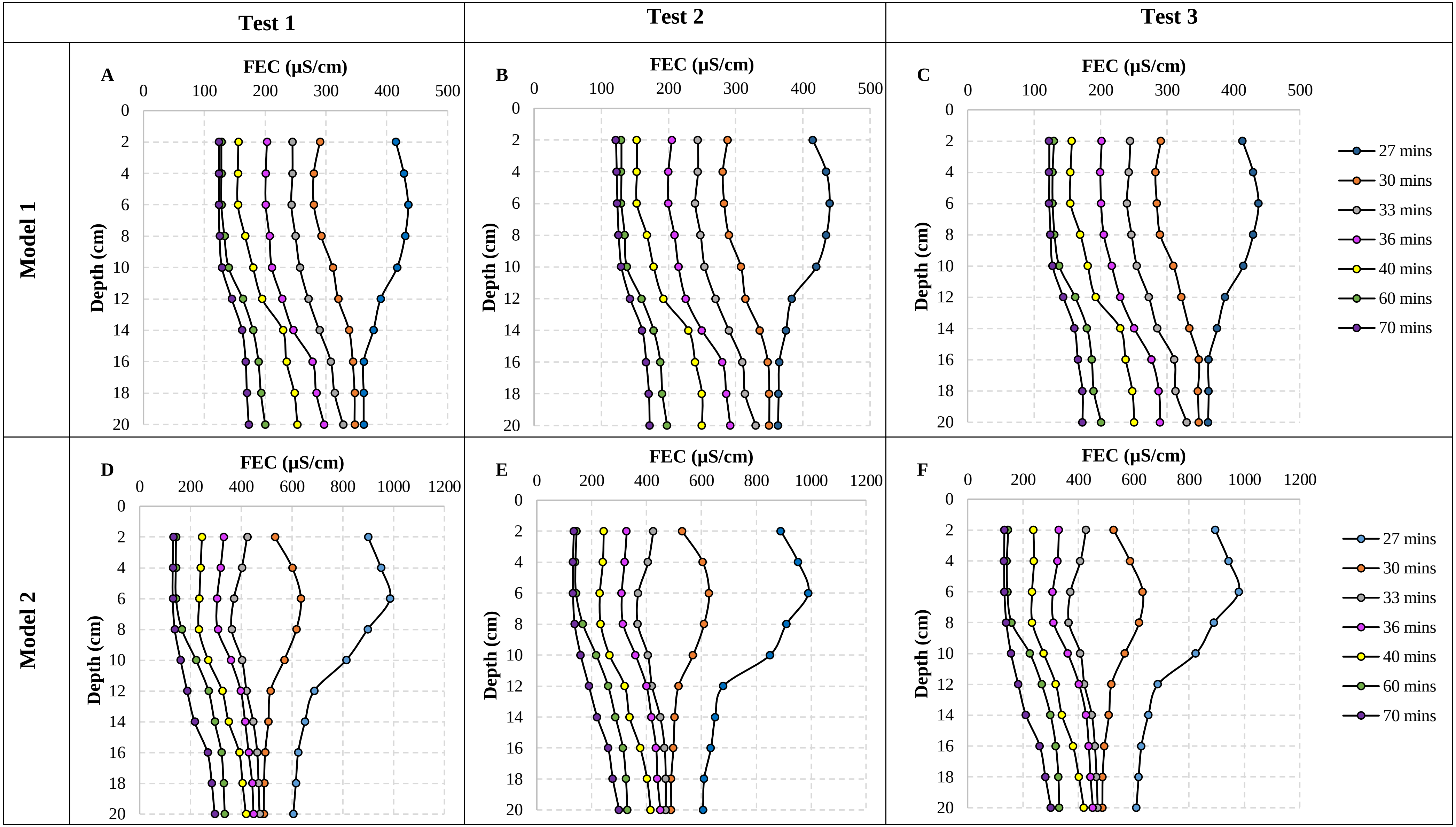
Test 1
Test 2
Test 3
Model 1
Model 2
A
B
C
D
E
F
FEC (µS/cm)
Depth (cm)
0
100
200
300
400
500
600
800
1000
1200
2
4
6
8
10
12
14
16
18
20
27 mins
30 mins
33 mins
36 mins
40 mins
60 mins
70 mins

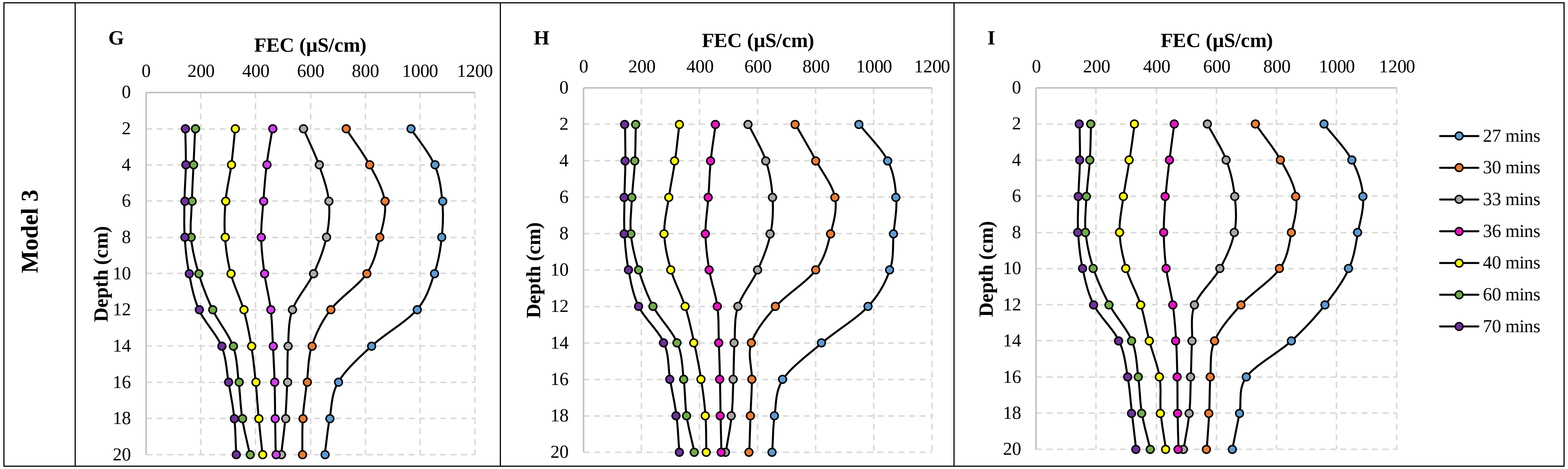

Figure 3-19 FEC profiles associated with the residual plume.

Note: Once the plume peak had passed BH, natural water continued entering the system thus decreasing the FEC values of water within the aquifer system.

3.3.2.2.5 Near-background FEC profile

The constant inflow of natural water within the aquifer system caused continuous dilution to take place throughout the system until near-background values were reached. However, the FEC values of the lower segment did not decrease as rapidly as the ones of the upper segment due to the permeability and transmissivity differences between the two layers. Figure 3-20 illustrates that by 130 minutes the FEC values of the system were similar to those initially recorded (on the background profile), these values were referred to as near- background FEC values. The near-background FEC profile represents conditions where the contaminant plume has passed, and initial conditions are reinstated within the aquifer system. The near-background values were reached faster in Model 1 due to the lower initial contaminant concentration, however the shape of near-background profiles was similar in all three models.

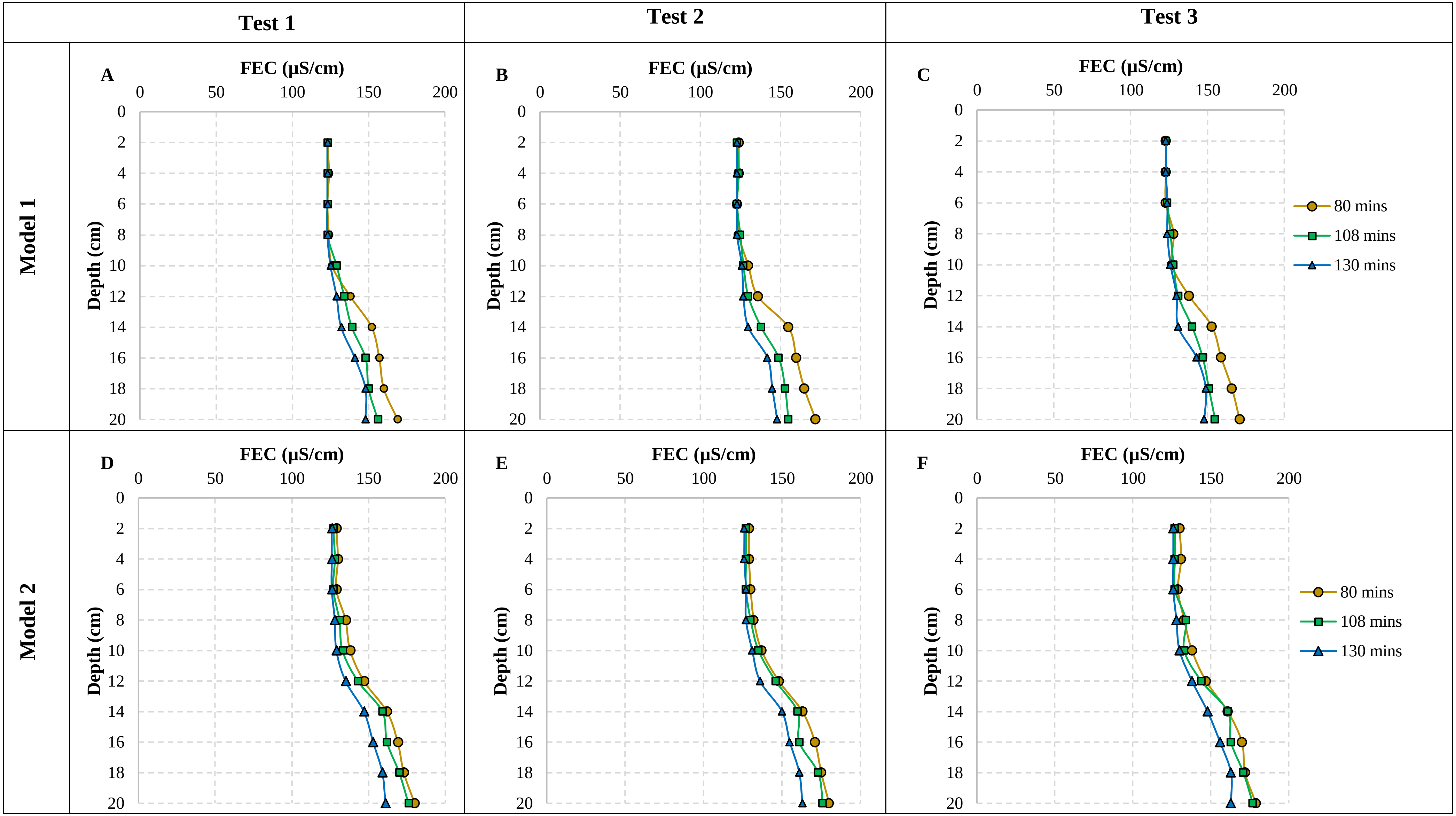
Test 1
Test 2
Test 3
Model 1
Model 2
A
B
C
D
E
F
FEC (µS/cm)
0
50
100
150
200
Depth (cm)
0
2
4
6
8
10
12
14
16
18
20
80 mins
108 mins
130 mins

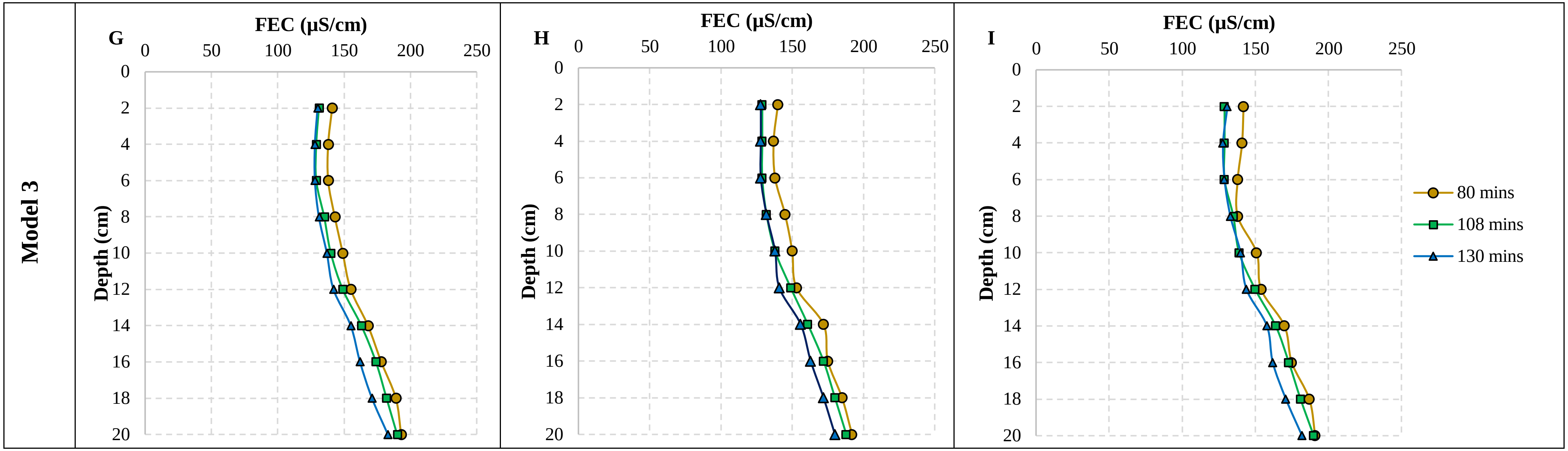

Figure 3-20 FEC profiles showing dilution within the aquifer system until near-background values were reached.

To determine the extent to which the system had gone back to its initial conditions, the background FEC profile was plotted on the same axis as the final profile as shown in Figure 3-21. The two profiles were highly comparable especially towards the permeable zone, therefore confirming that the contaminant plume had passed, and the initial aquifer conditions were re-established. It is worth noting that the FEC values towards the lower segment of the near-background profile took longer to be comparable to the background profile due to no replenishment taking place in this segment (only diffusion). However, given more time, the near-background and the background profiles are expected to overlay.

<table>
<tr><th></th><th>Test 1</th><th>Test 2</th><th>Test 3</th></tr>
<tr><td>Model 1</td><td>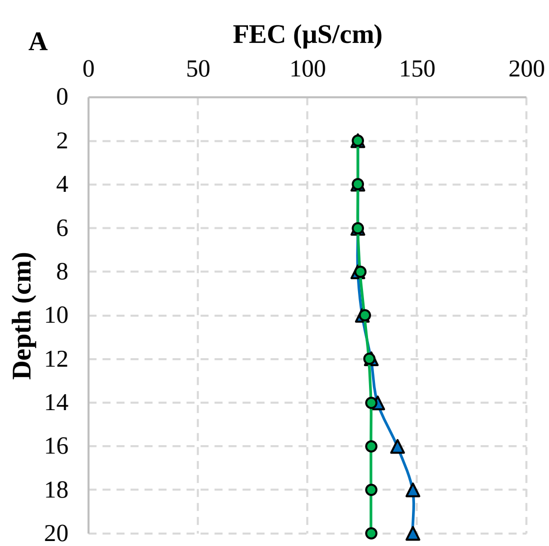</td><td>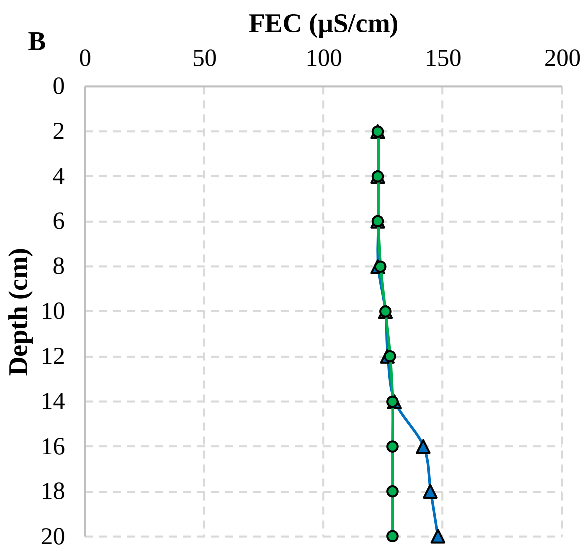</td><td>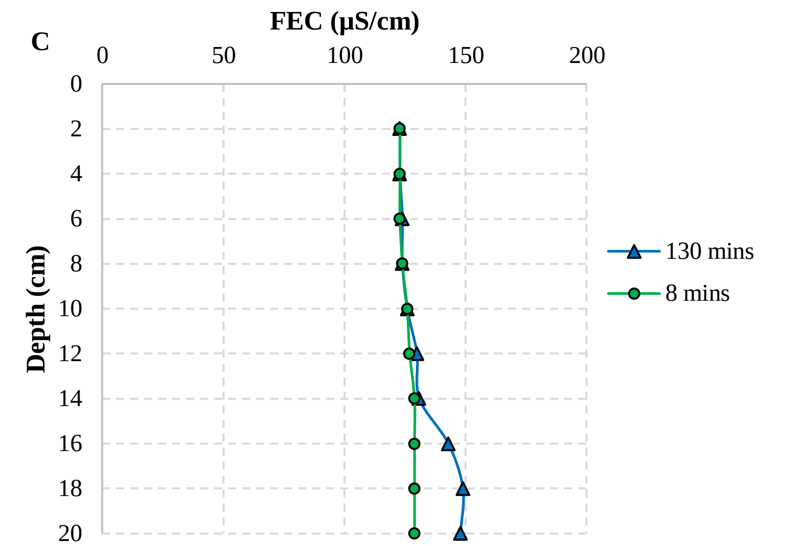</td></tr>
<tr><td>Model 2</td><td>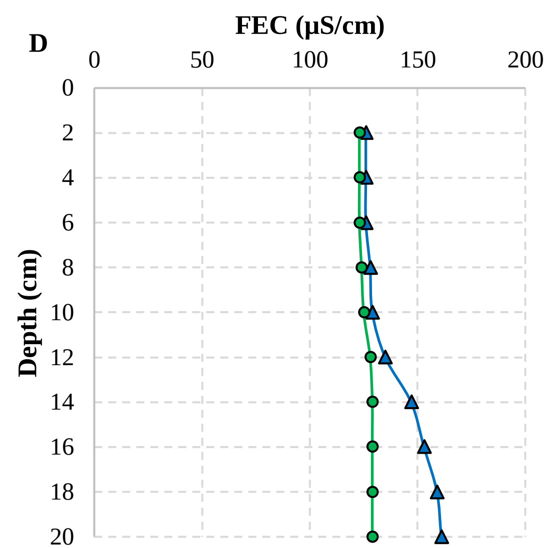</td><td>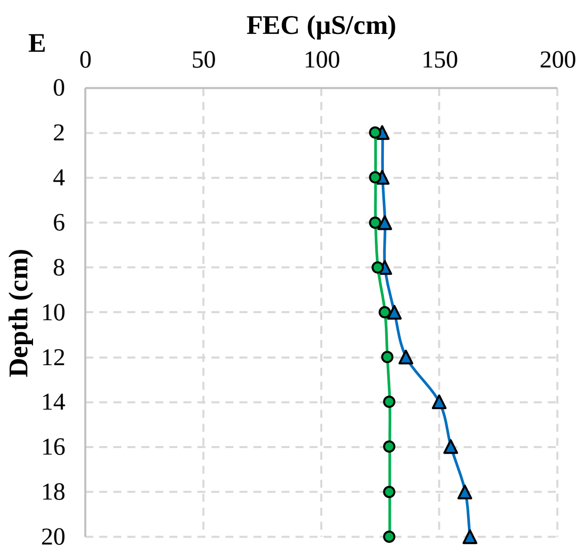</td><td>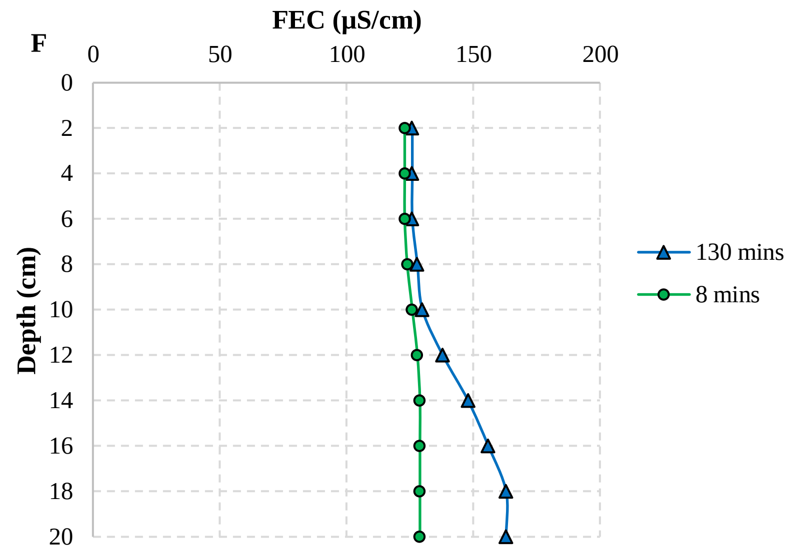</td></tr>
</table>

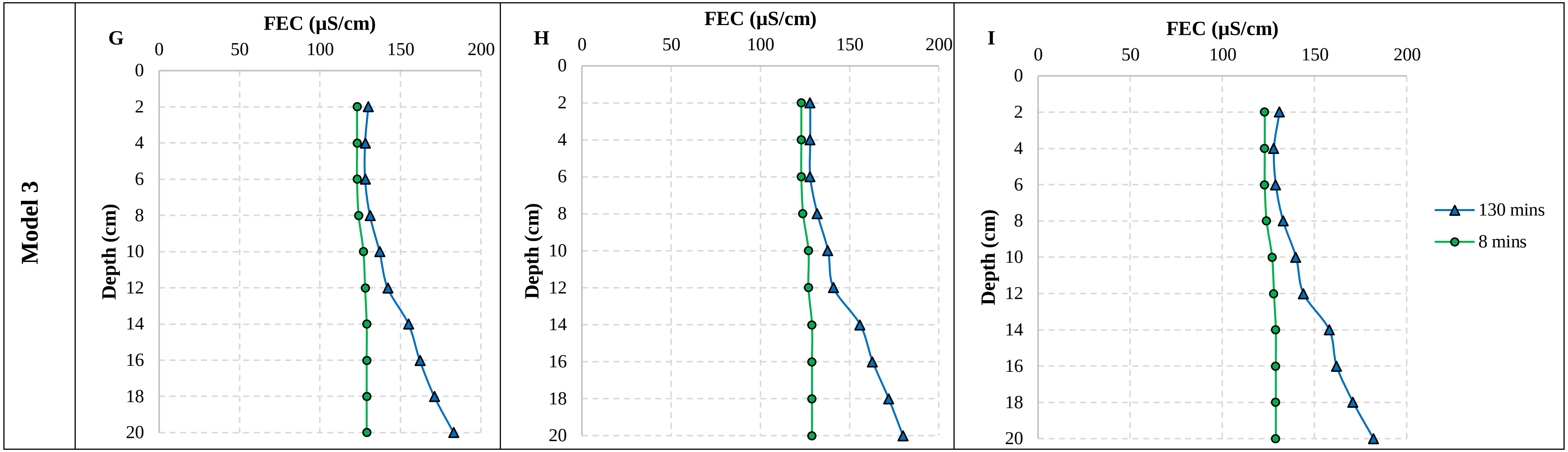

Figure 3-21 A comparison between the initial background FEC values taken at 8 mins and the final near-background FEC values recorded at 130 mins.

Chapter 4 FIELD EXPERIMENT

4.1 Introduction

Once the tests were conducted in the laboratory it was important to repeat them in the field for further validation. A forced gradient test was conducted at a site representative of porous aquifer system conditions, located in Plettenberg Bay, Western Cape Province, South Africa. The second test was conducted at a site representative of weathered basement aquifer conditions, located in Giyani, Limpopo Province, South Africa.

The purpose of the tests was to assess the comparability between the results obtained in the laboratory with the ones obtained in the field. The forced gradient was achieved through low flow pumping, this was done to reduce the duration it would take for the saline contaminant to migrate through the system. Unlike the laboratory tests, varying concentrations could not be used in the field as this would have resulted in cross-contamination.

This section discusses the FEC profiling field experiments undertaken in porous and weathered basement aquifer systems, respectively. A description of the two sites is provided first, followed by the methods and materials used, thereafter the results obtained are shown and discussed.

4.2 Description of the sites

4.2.1 Porous aquifer system

The porous aquifer system test site was located in Plettenberg Bay, Western Cape, South Africa. It lies at an elevation of approximately 420 meters above mean sea level (m amsl). According to the 1:250 000 scale Geological map of the area (3322 Oudtshoorn), the regional geology of the site consists of highly weathered sandstone of the Peninsula Formation, Table Mountain Group. This is overlain by a thin layer of sandy transported sediments of Quaternary age.

The lithology comprises of mature, greyish sandstone which weathers to whitish/grey sand. Thin layers of conglomerate occur discretely throughout the formation, usually at its base (Toerien, 1979). Figure 4-1 illustrates a lithological log of PMB which was drilled at the site, it shows that the local geology comprises of loose, fine grained, residual sand, and medium grained sandy-clay towards the bottom of the borehole.

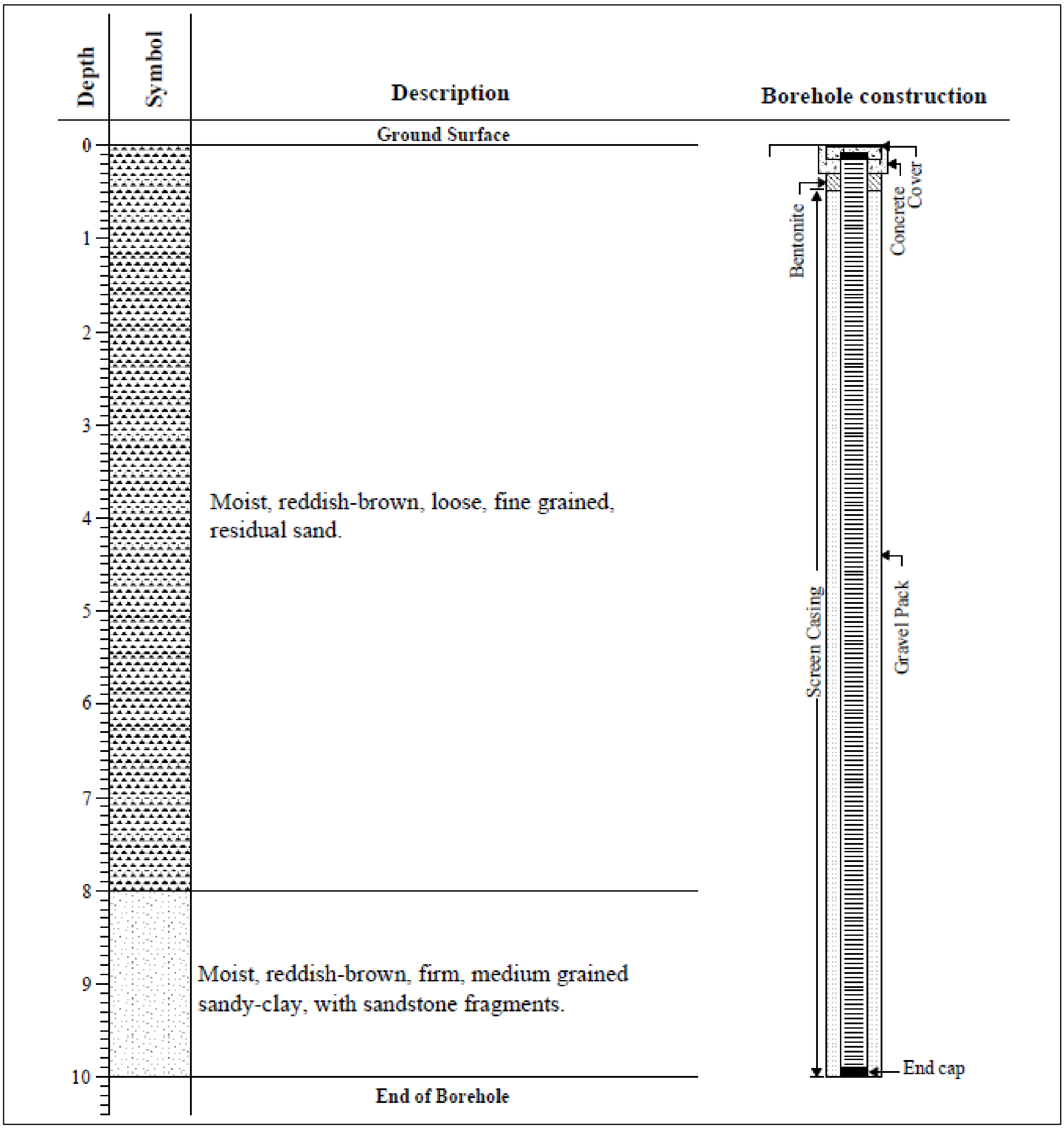

Figure 4-1 Lithological log obtained from the monitoring borehole (PMB).

According to the 1:500 000 Hydrogeological map of Oudtshoorn (3321), the site is underlain by granular aquifers with typical yield of between 0.0 and 0.1 litres per second (l/s). The groundwater quality is reportedly good with electrical conductivities ranging between 700 and 3 000 µS/cm. According to the Aquifer Classification Map of South Africa (Department of Water Affairs and Forestry, 2012), the aquifer underlying the area is classified as a minor aquifer with moderate vulnerability and medium susceptibility to contamination.

4.2.2 Weathered basement aquifer system

The weathered basement aquifer system test site was located in Giyani, Limpopo Province, South Africa. It lies at an elevation of approximately 458 meters above mean sea level (m amsl) and the topography of the surrounding area is relatively flat.

According to the 1:250 000 Geological map of Tzaneen (2330), the regional geology comprises of gneiss and migmatite of the Goudplaats Gneiss. Figure 4-2 displays a lithological log obtained from a monitoring borehole drilled at the site. It shows that the local geology comprises of an upper layer of dry, light brown to reddish, fine grained, slightly compacted, residual, sandy clay from 0.0 to approximately 2.0 m bgl. This is underlaid by moist, light brown, medium grained, loose, highly weathered sandstone, and followed by competent bedrock gneiss.

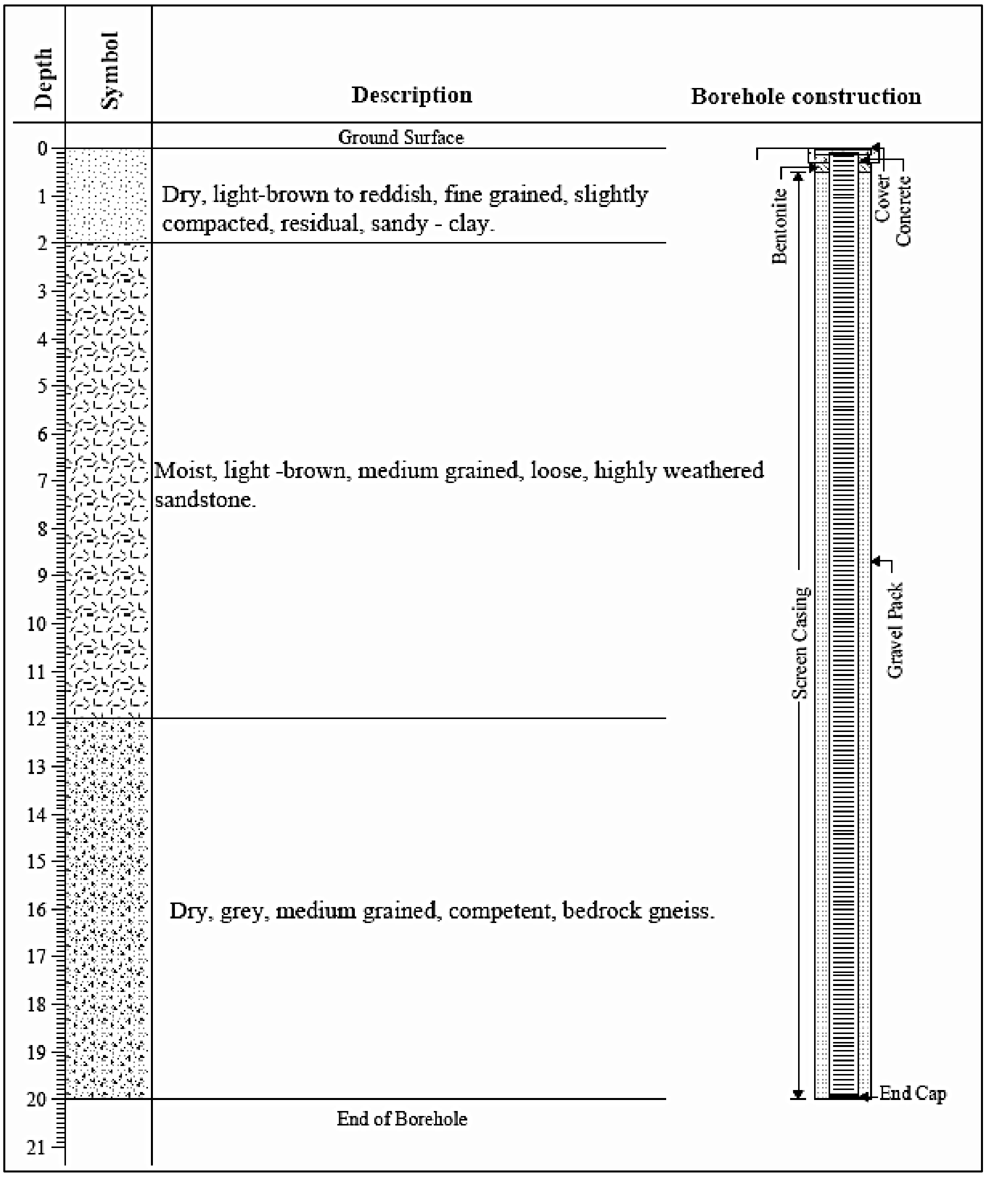

Figure 4-2 Lithological log obtained from the monitoring borehole (WMB).

According to the 1:500 000 Hydrogeological map series of Phalaborwa (2330), borehole yields of 2.0 to 5.0 l/sec could be expected for the area. The groundwater quality is good with the expected electrical conductivity ranging between 700 and 3 000 µS/cm. According to the Aquifer Classification map of South Africa, the aquifer underlying the area is classified as a minor aquifer with moderate vulnerability and medium susceptibility to groundwater impact via anthropogenic activities (Department of Water Affairs and Forestry, 2012).

4.3 Methods and material

The test set-up in both the porous and weathered field tests comprised of three boreholes placed at varying distances from each other. In the porous aquifer system field set-up, the pumping borehole (PPB) was 53 m from the injection borehole (PIB) and 20 m from the monitoring borehole (PMB). The static water level at PIB and PMB was 2.32 and 2.12 m bgl, respectively.

In the weathered basement aquifer system field set up, the monitoring borehole (WMB) was located 18.34 m from the pumping borehole (WPB), and the injection borehole (WIB) was located 31.64 m from the pumping borehole. The static water level of WMB and WIB was 6.032 and 5.289 m bgl, respectively, and 5.078 m bgl at the WPB. Similar to the laboratory tests, NaCl was used to simulate the contaminant, and the pumping boreholes (i.e. PPB and WPB) were pumped at a constant rate of 2 l/s.

The FEC profiling test was only started once pseudo-state conditions were reached, particularly between the monitoring and injection borehole. Once this was achieved, a TLC probe was used to obtain the system's background FEC conditions. Thereafter, the saline contaminant was introduced into the system through the injection borehole using an injection sock which was tied to a rope. The sock was slowly lowered down and up the borehole to ensure that a change in salinity of the groundwater throughout the entire borehole profile was created. The probe was set to record readings every five seconds. To eliminate data mismatch, the FEC and head values were both recorded by the probe simultaneously. Once the sock was pulled out of the borehole, contaminant concentration was monitored using the TLC probe.

4.4 Results and Discussion

The results presented in this sub-section were obtained from the field tests conducted at the test sites. The results from the porous aquifer system are shown first, followed by the ones obtained in the weathered basement aquifer system. The section first presents the background FEC profile which was obtained under natural groundwater quality conditions - in the absence of the salt contaminant plume, thereafter the FEC profiles captured after the saline contaminant was introduced into the system are shown and discussed.

4.4.1 FEC profiles in the porous aquifer system

4.4.1.1 Background FEC profile

The background FEC profile was captured before introducing the contaminant into the system. The main purpose of the background profile was to assist in assessing the changes in groundwater quality that have taken place once the contaminant was introduced into the system. Figure 4-3A shows the background FEC profile that was captured in the field porous aquifer system. The profile displayed FEC values that ranged from 698 µS/cm to 731 µS/cm.

It was evident that the field background profile was not as straight as one captured in the laboratory (Figure 4-3B). This indicated that the field aquifer system was not completely homogenous and isotropic. The changes in FEC at different depths could be accounted for by various chemical reactions that were taking place at those specific depths or stratification. Additionally, the sandy-clay material present at 8 m bgl could account for the increased FEC values observed towards the bottom of the borehole.

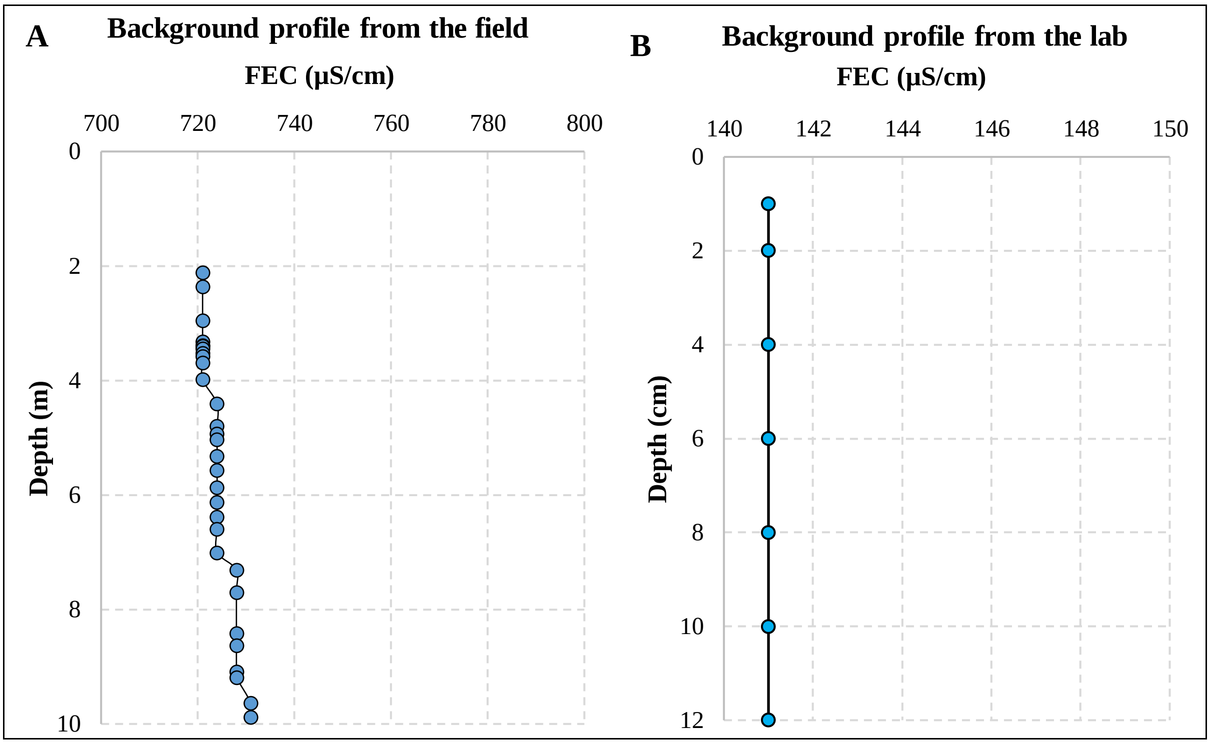

Figure 4-3 The porous aquifer system background FEC profile captured in the field (A) and in the laboratory (B).

4.4.1.2 First arrival of plume FEC profile

Once the contaminant was introduced into the system, 16 minutes later the plume had already reached PMB. The FEC values increased from an average of 722 µS/cm to 1 160 µS/cm, with most of the increase occurring towards the middle of the aquifer (Figure 4-4A), this is expected as it is the area with the least friction and thus the highest transporting velocity. Figure 4-4B and C shows the first arrival plumes captured during the laboratory tests. The field test profile was more comparable to the laboratory profile obtained in BH2 (Figure 4-4C) than BH1. This was because similar to BH2, PMB was situated at a distance from the source.

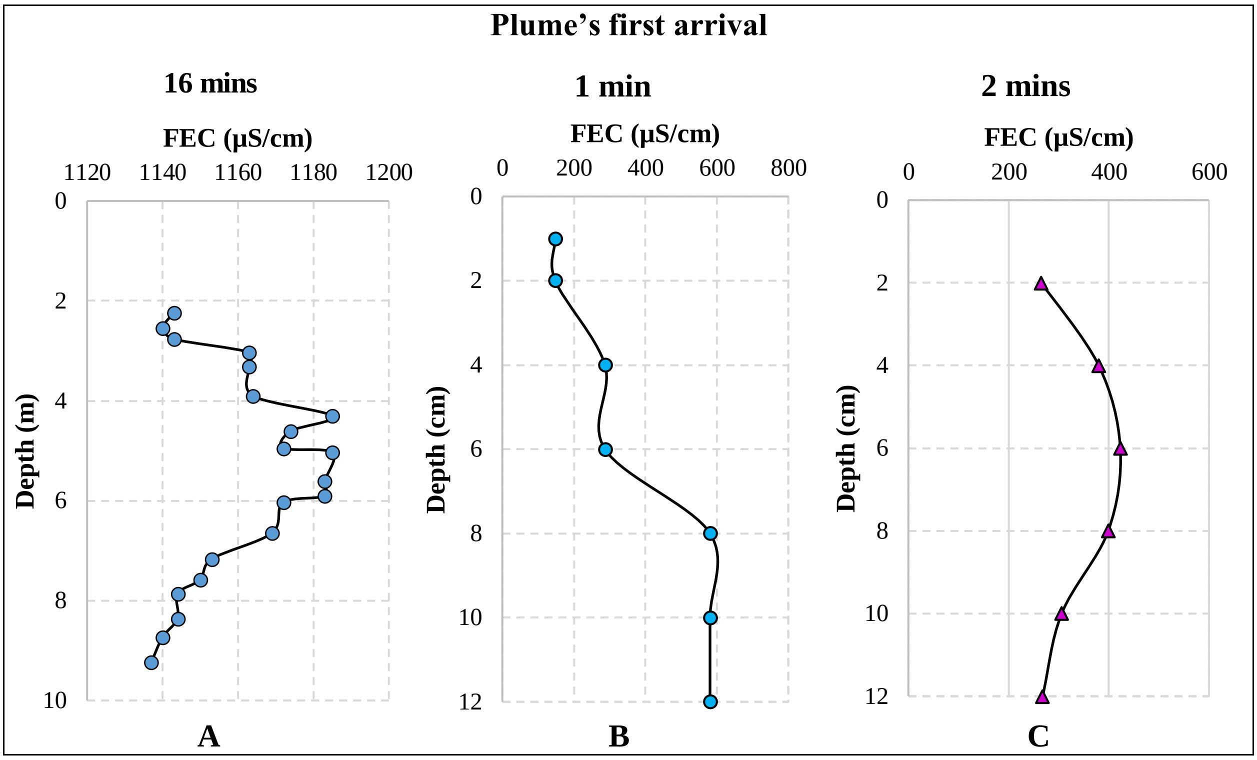

Figure 4-4 The plume's first arrival at (A) field PMB, and laboratory (B) BH1 and (C) BH2.

4.4.1.3 Plume peak FEC profile

As the centre of the contaminant plume continued approaching the monitoring point the FEC values also increased. Once the centre of the plume reached the monitoring point maximum FEC values were recorded within the system. The highest FEC value recorded was 1 469 µS/cm as shown in Figure 4-5A.

The effects of density were notably reduced in the field compared to the laboratory (Figure 4-5B). This could be due to (1) the injection method used; in the field the sock was used to introduce the contaminant into the system, this technique changed the salinity of the groundwater slowly instead of abruptly like in the laboratory, which in turn limited the effects of density, (2) the scale factor; the aquifer thickness in the field was large, which resulted in a higher dilution rate compared to the laboratory aquifer model.

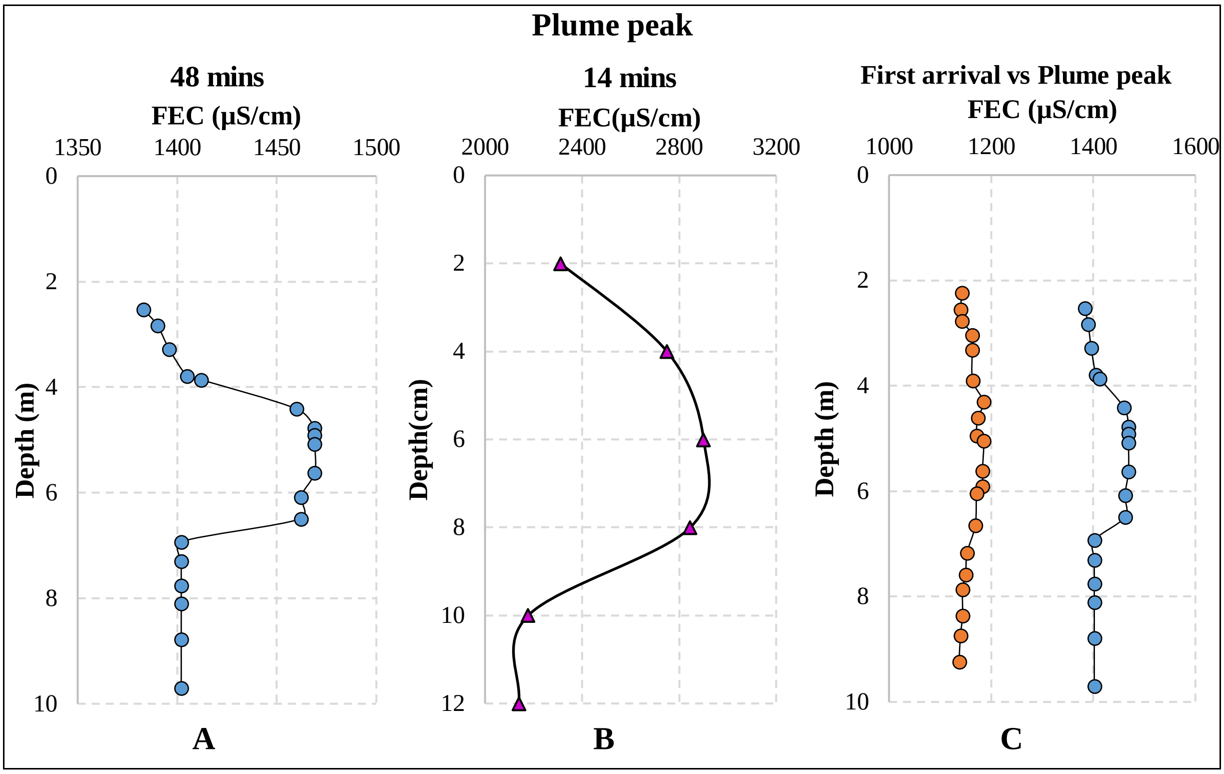

Figure 4-5 The plume peak obtained in the field (A) and in the laboratory (B). C is a comparison between the field's first arrival FEC profile (in orange) and the plume peak profile (in blue).

When comparing the field's first arrival FEC profile to the plume peak FEC profile (Figure 4-5C) anomalies were evident towards the middle, indicating that the central axis of the plume remained at the centre regardless of the increase in mass concentration. This demonstrated that the aquifer's highest transporting velocity was located towards the centre of the system, and that the distance between the source and the monitoring point sufficiently gave the plume enough time to align with the flowlines of the system. This was also observed in the laboratory profile obtained in BH2. Even though most of the FEC increase took place towards the centre, an increase in FEC values was evident throughout the entire profile.

4.4.1.4 Residual plume FEC profile

Once the centre of the contaminant plume had passed the monitoring borehole and the process of dilution continued taking place, the concentration of the contaminant plume decreased noticeably. This was reflected by the reduced FEC values shown in Figure 4-6A. As the system continued to be diluted by the incoming formation water, the amplitude of the anomaly was also expected to decrease until it became a vertically straight line which reflected conditions similar to the those of the background. The process of dilution was observed to be more rapid in the laboratory (Figure 4-6B) compared to the field, this was expected due to the large-scale differences between the two.

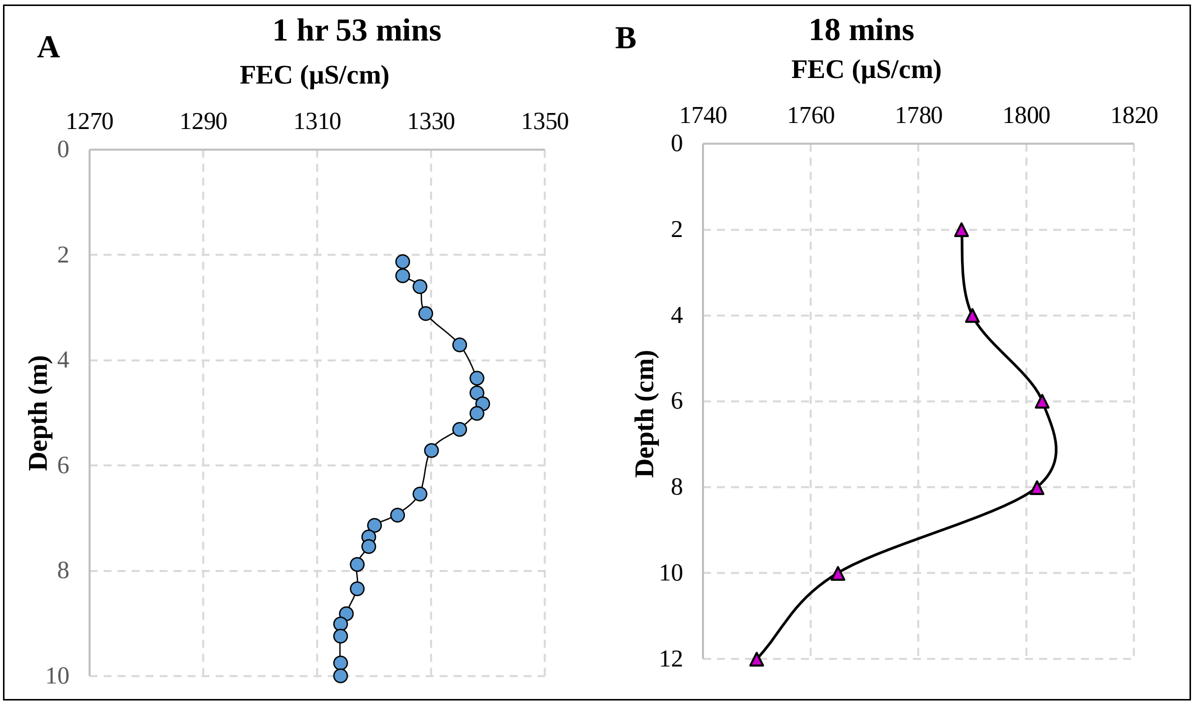

Figure 4-6 Residual plume profile obtained in the field porous aquifer system (A) compared to the one obtained in the laboratory (B). The process of dilution was more rapid in the laboratory compared to the field. This can be accounted for by the scale factor, the field experiment was conducted on a larger scale.

4.4.1.5 Near background FEC profile

Formation water continued to replenish the system until the FEC values were similar to the ones of the background profile, represented in blue (Figure 4-7). It is expected that with an extended monitoring period, the near-background FEC profiles (shown in green on the field profile, and grey on the laboratory profile) would continue to decrease until they overlap the background profile. It is worth noting that the profiles observed in the laboratory (Figure 4-7B) were more vertically straight compared to the ones in the field (Figure 4-7A), this is because the field system was not as perfectly homogeneous and isotropic as the laboratory system.

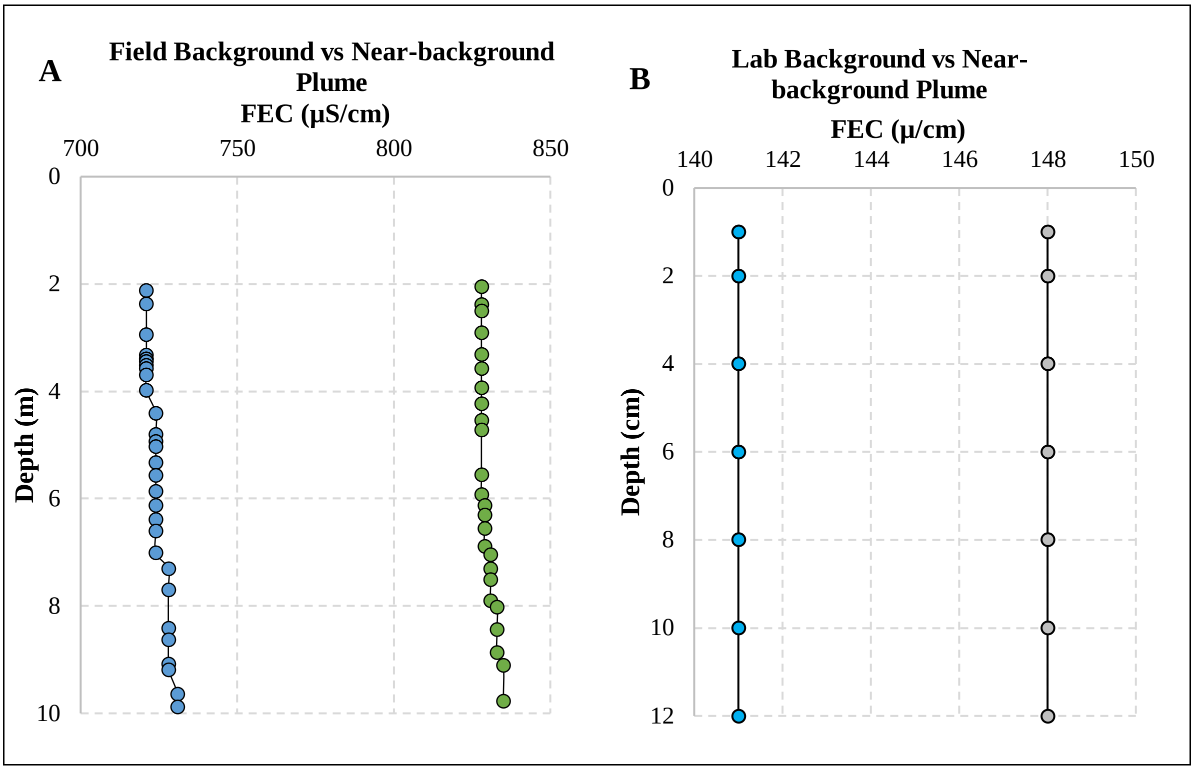

Figure 4-7 Near-background profile in the field (A) and in the laboratory (B) compared to the background profile. It is expected that with an extended monitoring period, the near-background FEC profiles would continue to decrease until they overlap the background profiles.

4.4.2 FEC profiles in the weathered basement aquifer system

This sub-section discusses the FEC profiles associated with various stages of the contaminant plume within the field weathered basement aquifer system.

4.4.2.1 Background FEC profile

The background FEC profile was obtained under formation groundwater quality conditions. In any monitoring assessment the background conditions are crucial to capture as they help identify the changes that have taken place within a system over time. Figure 4-8 shows the background FEC profile captured in the field (A) and the one captured during the laboratory test (B). In both profiles it is evident that lower FEC values were observed in the upper, more permeable layer of the aquifer system, and higher FEC values were recorded at the lower layer.

The transmissivity of the upper weathered layer allowed for inflow of formation water through the layer, which resulted in constant replenishment. Therefore, the water present in this section is representative of the aquifer water quality. On the contrary, the water found in the lower impermeable layer is considered stale due to the low transmissive nature of the layer, and it is not representative of the current aquifer water quality.

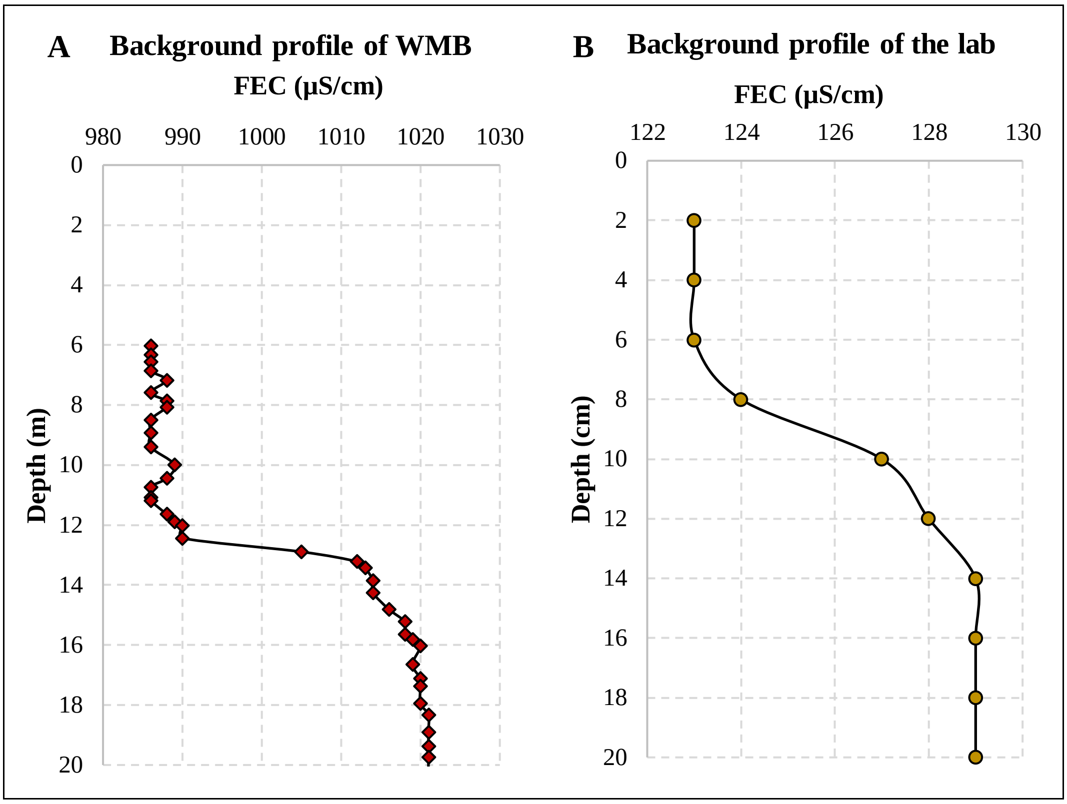

Figure 4-8 The background FEC profile captured in the field (A) and the one captured in the laboratory (B). Generally, low FEC values were observed in the upper more permeable layer.

4.4.2.2 First arrival of plume FEC profile

Once the background FEC profile was captured the saline contaminant was introduced into the system through the injection borehole (WIB). Slightly elevated FEC values were observed within the upper layer 20 minutes after injection as shown in Figure 4-9A. The increase in FEC values was visibly lower in the field FEC profile compared to the profile obtained in the laboratory (Figure 4-9B). Additionally, the effects of density in the field were significantly reduced. This can be accounted for by large scale of the field test. The shape of the first arrival plume profile obtained in the field was comparable to the one captured in the laboratory.

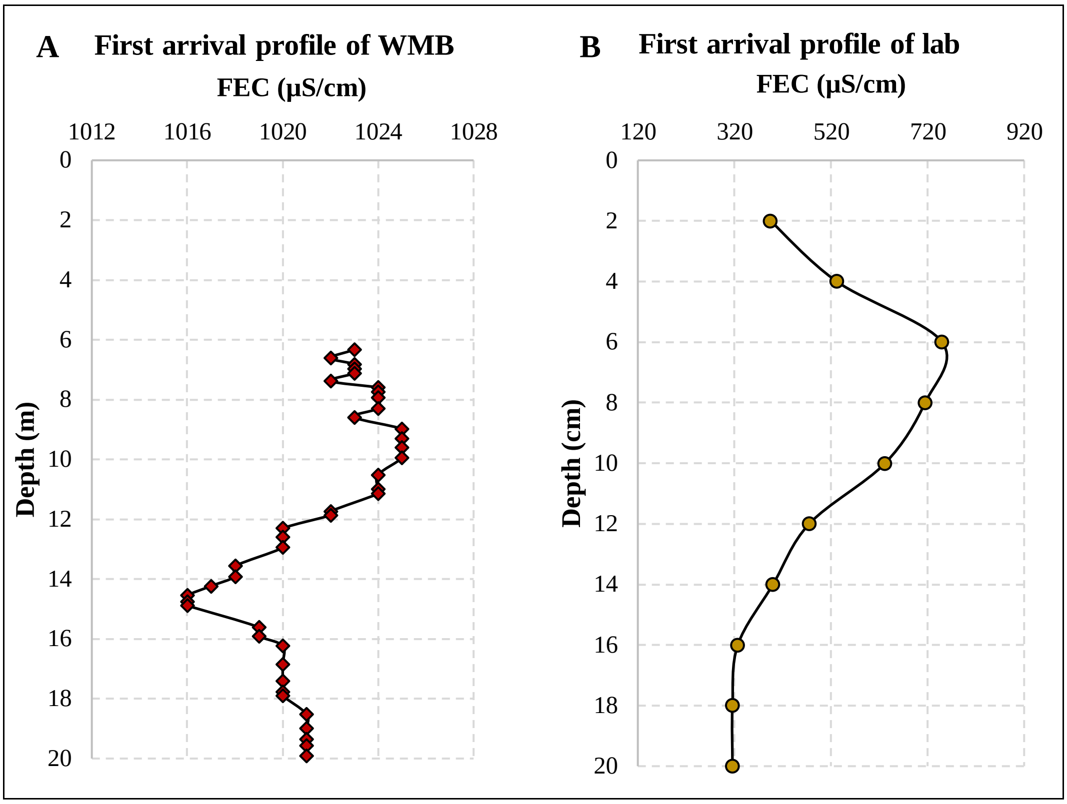

Figure 4-9 **The first arrival FEC profile captured in the field (A) and the one captured in the laboratory (B), elevated FEC values observed in the upper layer of both profiles.**

4.4.2.3 Plume peak FEC profile

As time progressed FEC values continuously increased within the system, particularly within upper- permeable layer. After 50 minutes maximum values of 1 585µS/cm were reached, and the profile shape displayed was similar to the one seen in the laboratory (Figure 4-10B). The effects of density were noticeably reduced in the field results, this could be due to (1) the large scale of the field test, (2) The technique of lowing the injection sock down and up the borehole changed the groundwater chemistry slowly instead of abruptly, and (3) the scale of the weathered aquifer in the field coupled with the effects of pumping enabled ample volume of formation water to enter the system at a faster rate which diluted the contaminant and reduced its mass concentration and density.

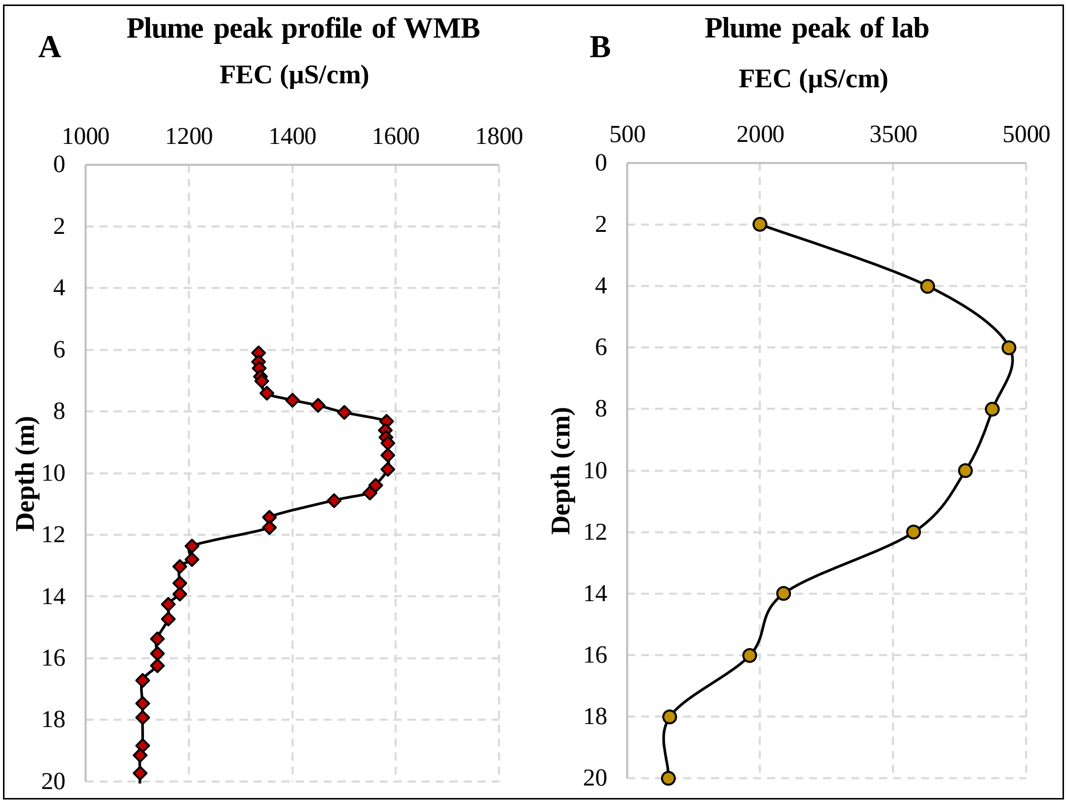

Figure 4-10 The plume peak FEC profile captured in the field (A) and the one captured in the laboratory (B), elevated FEC values observed in the upper layer of both profiles.

4.4.2.4 Residual plume FEC profile

Dilution continued taking place within the system until most of the plume had passed and only the tail end of it was still passing the monitoring point. The residual plume conditions were reflected by a decrease in FEC values from an average of 1 308.71 µS/cm to 1 151.13 µS/cm. Figure 4-11A shows the residual plume profile that was obtained in the field, it displayed a slight anomaly towards the upper section of the profile, this was comparable to the profile obtained in the laboratory (Figure 4-11B).

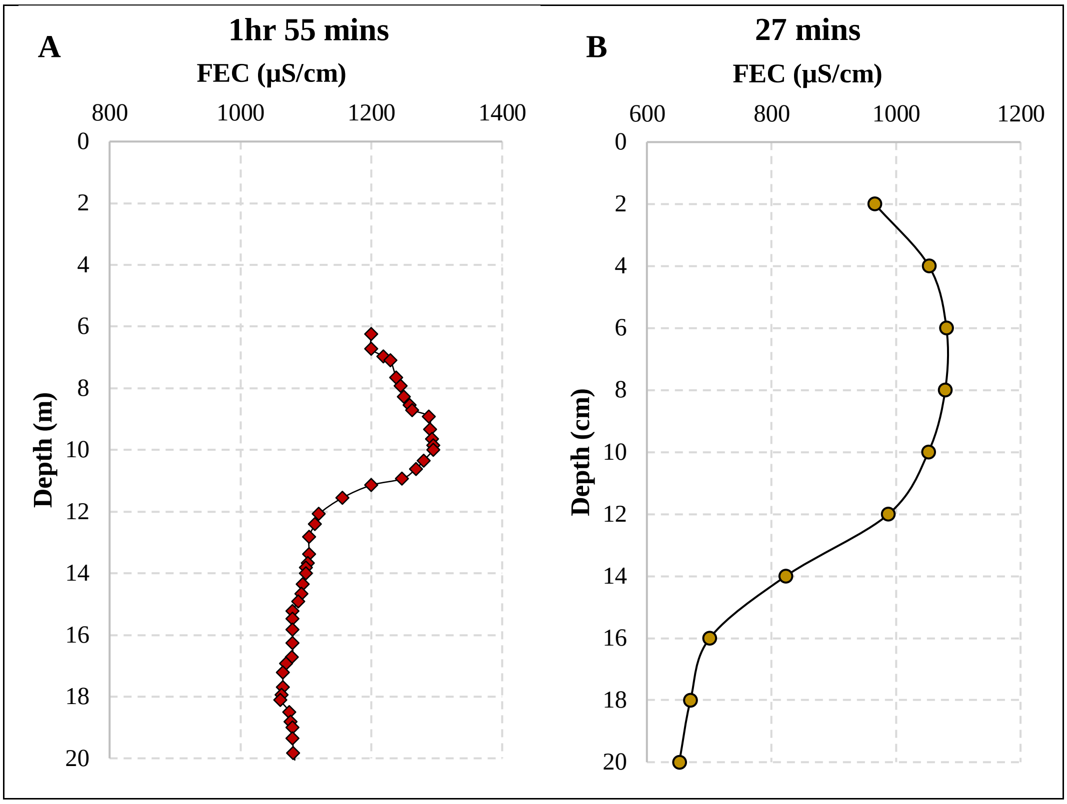

Figure 4-11 The residual plume obtained on site (A) compared to the one captured in the laboratory (B).

4.4.2.5 Near background FEC profile

Incoming natural water continually diluted the system until FEC values were similar to those of the background. Dilution and replenishment were more prevalent in the permeable upper weathered segment due to the high transmissivity of this layer. Figure 4-12 is the near-background profile versus the background profile (in blue) obtained in the field (A) and the laboratory (B), the two profiles were similar in shape, and both had an increasing trend towards the bottom.

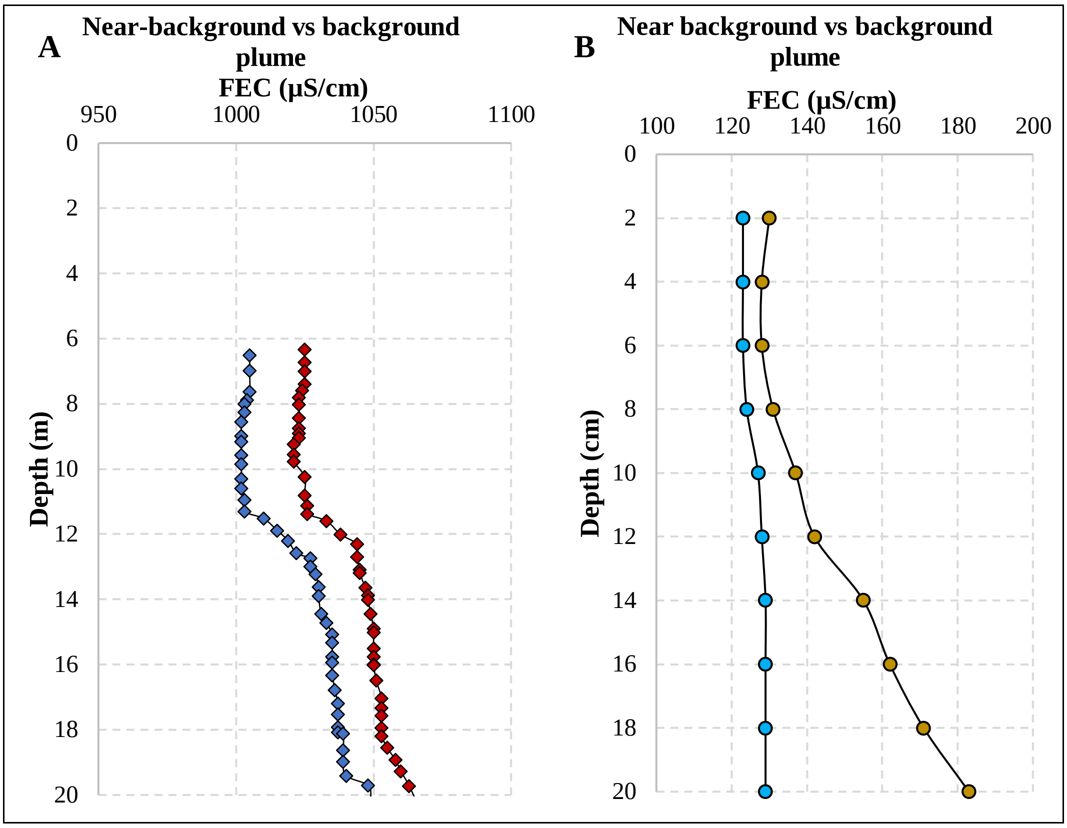

Figure 4-12 The near-background plume profile obtained in the field (A) compared to the one captured in the laboratory (B). The background profiles are shown in blue.

Chapter 5 CONCEPTUAL PROFILES

5.1 Introduction

Once the laboratory and field tests were conducted, assessed, and understood, there were distinct profiles that were observed from each stage of the contaminant plume in both the porous and weathered basement aquifer system. This chapter discusses the conceptual profiles associated with the two aquifer systems.

5.2 Conceptual FEC profiles of the porous aquifer system

The laboratory porous aquifer system made use of two monitoring points which enabled the analysis of whether the distance of a monitoring point from source would affect the outcome of the FEC profiles. The only two profiles that showed a notable difference were the “first arrival plume” and the “residual plume”, which displayed a sub-vertical FEC profile in the near-source monitoring point (BH1), and an FEC profile with a slight anomaly towards the centre in the far-source monitoring point (BH2). This observation brought to light the understanding of the effect of plume orientation during contaminant migration on the FEC profile. This concept is illustrated in detail in Section 5.2.1 and 5.2.2.

Figure 5-1 schematically illustrates how the plume migrated from the surface introduction throughout the entire system. It was evident that closer to the source the plume could have taken on a vertical to sub-vertical orientation. However, further away from the source as the plume continued to migrate, it aligned with the flow lines of the system, which resulted in a horizontal orientation, this was observed in FEC profiles obtained at BH2.

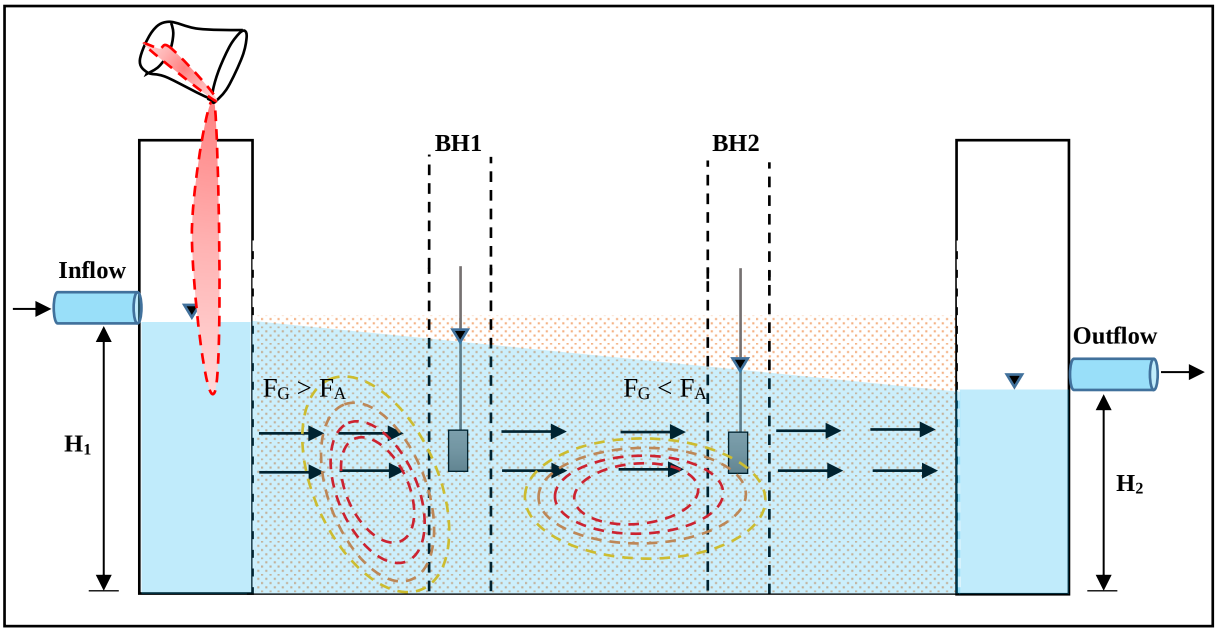

Figure 5-1 **Schematic illustration showing the contaminant plume migration from surface introduction throughout the porous aquifer system.**
Note: The red circles show the highest concentration within the plume and the yellow indicates the least concentration.

This sub-section presents a comprehensive explanation and illustration of conceptual FEC profiles obtained near the source (at BH1), and at a further distance from the source (at BH2) within the porous aquifer system. Five stages of the contaminant plume were identified at both monitoring points (i.e. the background, first arrival, plume peak, residual, and near-background stage), and it is based on these stages that conceptual profiles were developed. It is worth mentioning that the near-background profile was not conceptualised due to its close resemblance to the background profile.

5.2.1 Near to the source: vertical to sub-vertical plume

Closer to the source four distinct conceptual profiles associated with a saline contaminant plume in a borehole installed in a porous aquifer system were obtained. These are described and illustrated below:

5.2.1.1 Background FEC profile

The background profile was captured under natural water flow conditions. It displayed a vertically straight line as shown in Figure 5-2. This was because the FEC values were the same throughout the entire system due to the absence of contamination and the homogeneity of the system, particularly in the laboratory system. In a field system this profile is not expected to be as linear due to changes in homogeneity.

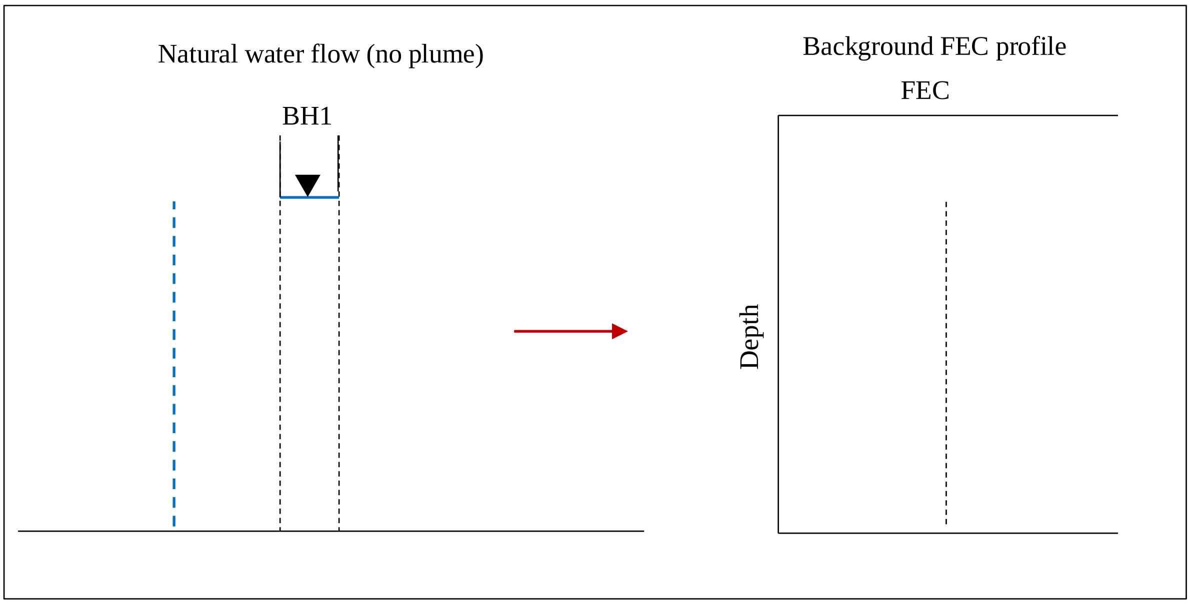

Figure 5-2 Conceptual background FEC profile near the source in a typical porous aquifer system, under natural groundwater quality conditions.

5.2.1.2 First arrival FEC profile

The introduction of a contaminant into the system resulted in a density contrast between the natural water already present in the system and the incoming contaminated water, thus the denser material migrated downward instead of only moving laterally. The downward or sinking motion of the plume is associated with the gravitational force, and the forward movement of the plume with the advection force. Therefore, it was apparent that at this point due to the high density of the contaminant plume the gravitational force acting upon the plume was more dominant than the advection force, consequently favouring the vertical to sub-vertical orientation of the plume. Figure 5-3 shows the conceptual profile associated with the first arrival of the plume at BH1. The dashed green line is an inferred extension of the plume, as it is possible that the plume may have been touching the base of the aquifer at that particular moment.

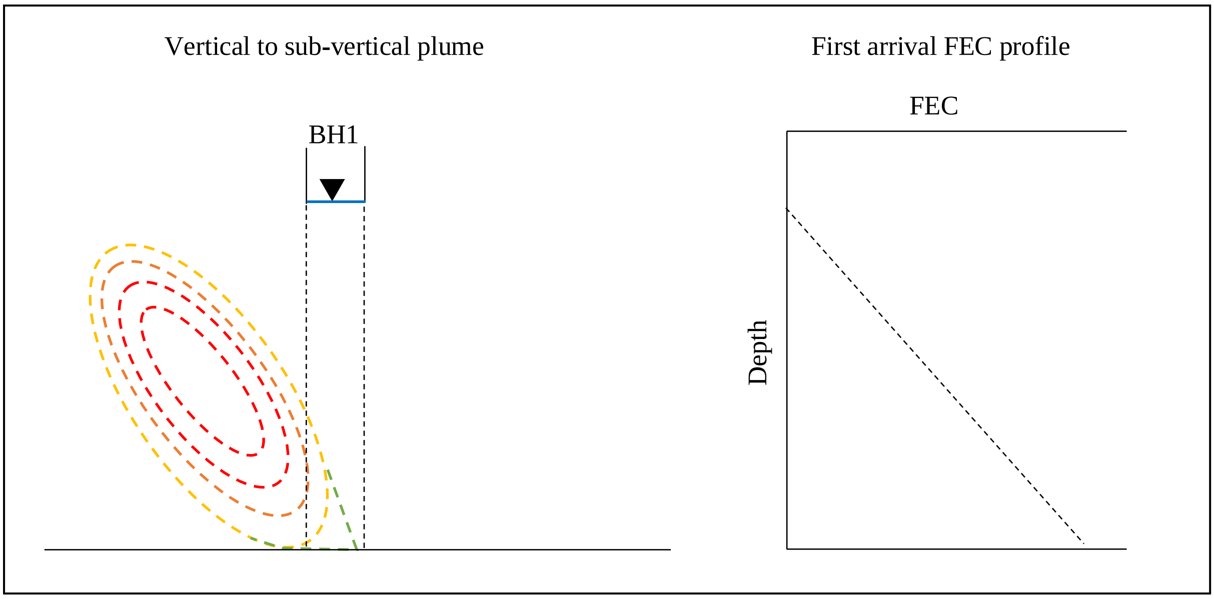

Figure 5-3 Conceptual profile associated with the first arrival of the plume at BH1 in a typical porous aquifer system under contaminated groundwater conditions.

Note: The dashed green line represents an inferred extension of the plume.

5.2.1.3 Plume peak FEC profile

When the centre of the contaminant plume reached BH1 elevated FEC values were observed as shown in Figure 5-4. The resulting profile was characterised by an anomaly located towards the bottom of the borehole. The shape of the profile indicated that the plume still maintained its vertical to sub-vertical orientation and was migrating more downward than forward.

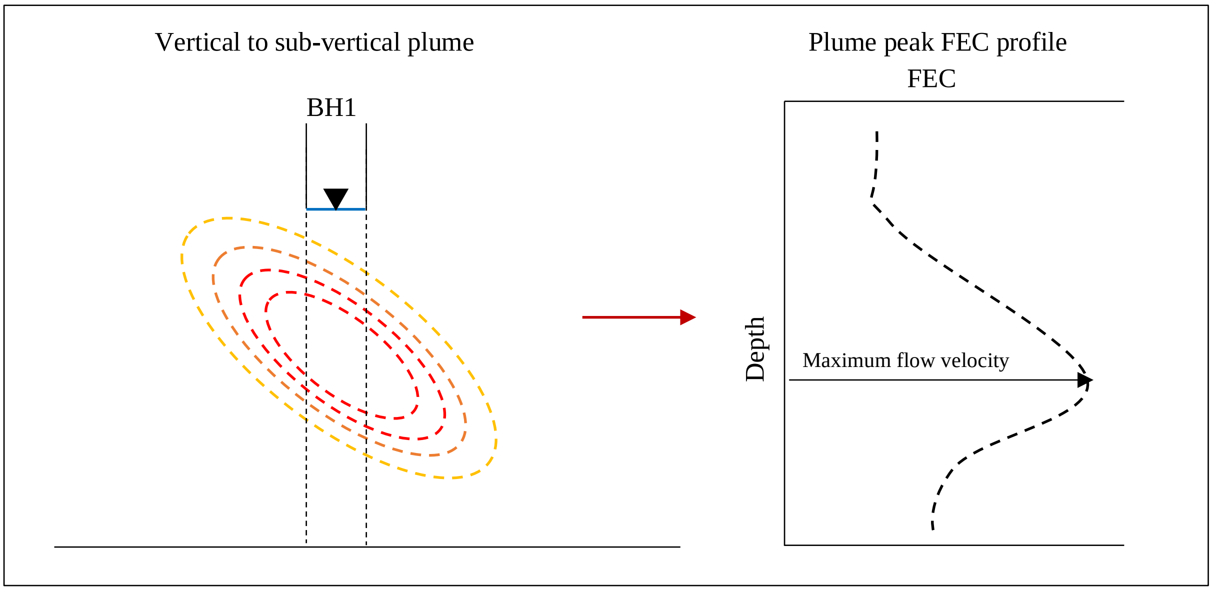

Figure 5-4 Conceptual model of the plume peak FEC profile near the source in a typical porous aquifer system under contaminated groundwater conditions.

The forward movement of the plume demonstrated that the advection force had increased at this point in time, however the downward movement of the plume indicated that the gravitational force was still relatively greater. Additionally, the increased presence of the advection force may have caused the plume to lift.

5.2.1.4 Residual FEC profile

The residual plume profile measured at BH1 was characterised by a diagonal profile shape (Figure 5-5) with FEC values decreasing towards the bottom. This indicated that at this point in time the greater quantity of the plume had already passed the monitoring point, and only its "tail" was left behind, thus resulting in notable FEC values on top and fairly low concentrations towards the bottom.

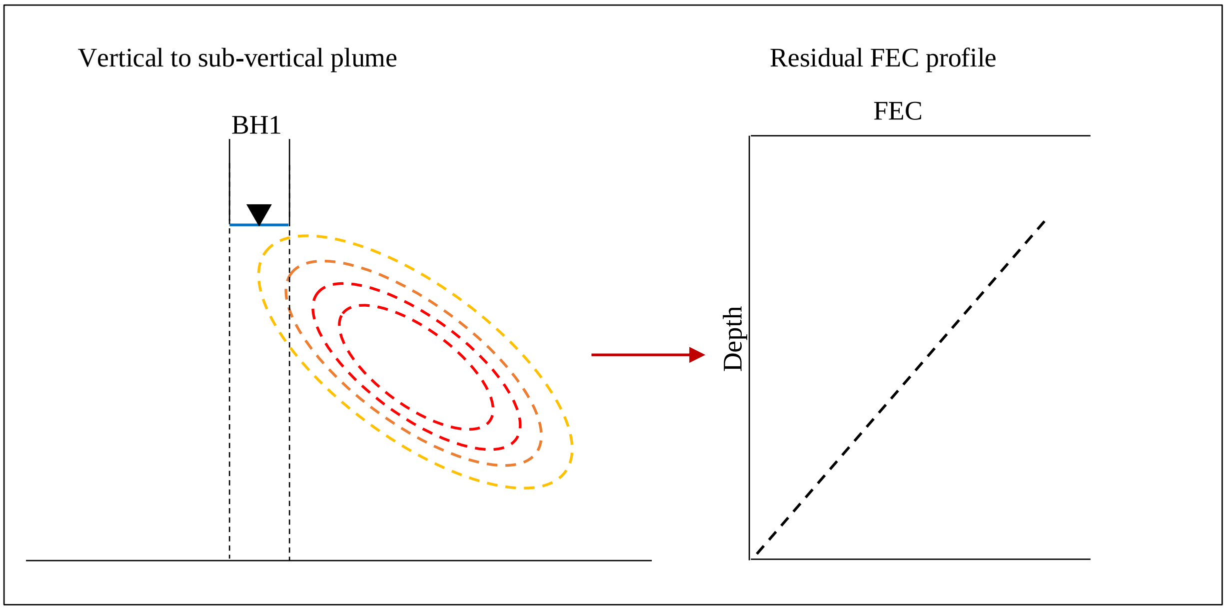

Figure 5-5 Conceptual model of the residual plume FEC profile near the source in a typical porous aquifer system under contaminated groundwater conditions.

5.2.2 Far from source: Horizontal plume

As the plume continued migrating through the system the advection force became greater than the gravitation force. This favoured the forward movement of the plume (instead of the sinking effect) and aligned it with the flow lines of the system, thus resulting in a horizontal orientation. It is for this reason that once the contaminant plume was introduced into the system, the profiles obtained at BH2 - which was located further from the source, were distinctly different from the ones observed at BH1. These are described and conceptualised below:

5.2.2.1 Background FEC profile

The background profile observed under natural water flow at BH2 was the same as that captured at a near-source borehole (BH1). It was characterised by a vertically straight line as shown in Figure 5-6. At this point in time the FEC values were the same throughout the entire system due to the absence of contamination and the homogeneity of the system itself.

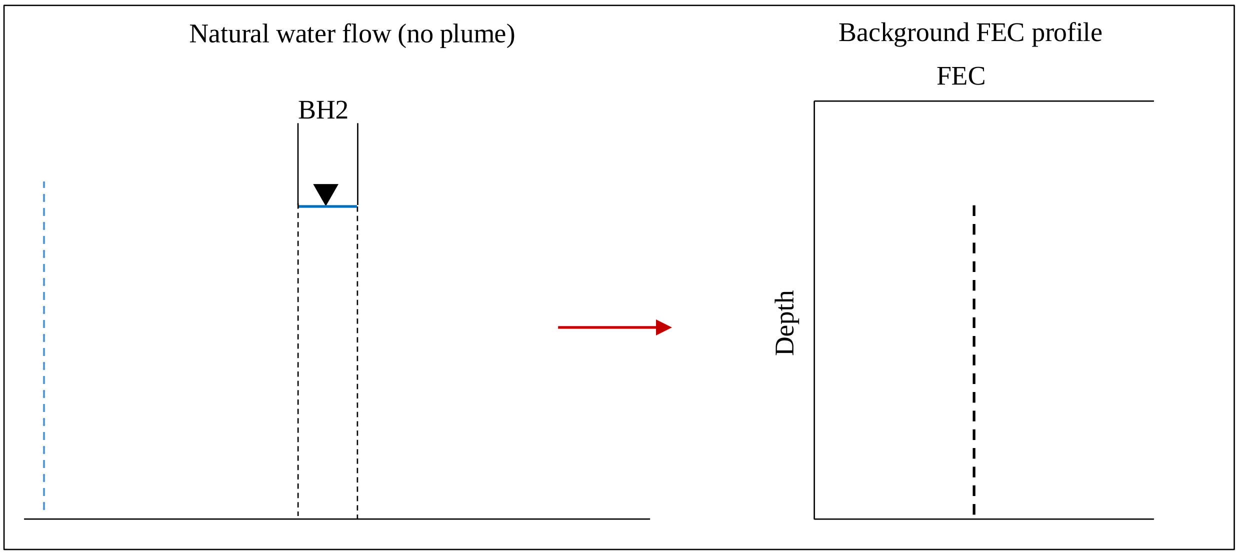

Figure 5-6 Conceptual model of the background FEC profile far from the source in a typical porous aquifer system under natural groundwater quality conditions.

5.2.2.2 First arrival FEC profile

The arrival of the contaminant plume at BH2 resulted in a different profile shape compared to BH1. Since BH2 was located further away from the source the effects of density were significantly reduced, hence decreasing the dominance of the gravitational force over the advection force. This caused the plume to align with the flow lines of the system and orientate itself horizontally. The resulting profile had a slight anomaly towards the centre as shown in Figure 5-7.

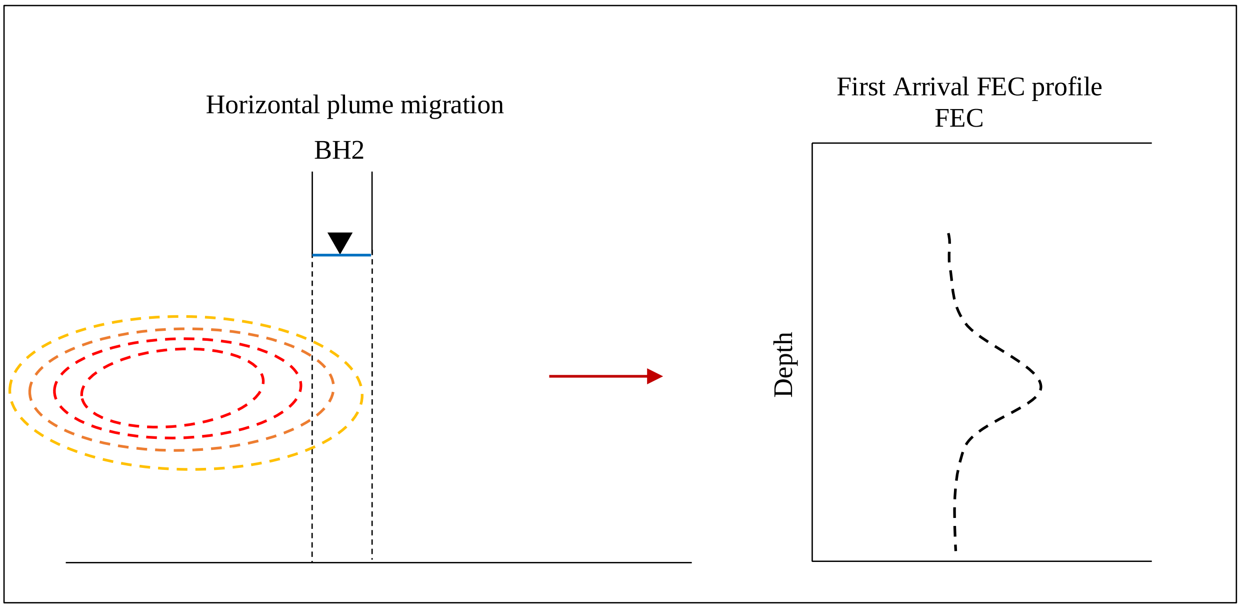

Figure 5-7 Conceptual model of the first arrival of the plume FEC profile far from the source in a typical porous aquifer system under contaminated groundwater conditions.

5.2.2.3 Plume peak FEC profile

Figure 5-8 shows the shape of the plume peak FEC profile captured at BH2, the profile was similar to the one observed at BH1. However, due to the dominance of the advection force at this point the plume did not display a downward movement but instead showed a pronounced anomaly towards the centre of the aquifer system, where the highest transporting velocity was expected.

The plume peak profiles obtained at BH1 and BH2 bring to light an interesting observation that regardless of where the monitoring point is located from the source, the shape of the plume peak FEC profile will always be represented by a pronounced anomaly. This was also observed in the fractured aquifer system (Moleme and Gomo, 2018). However, the closer to the source the monitoring point is, the more the effects of density will be observed on the profile.

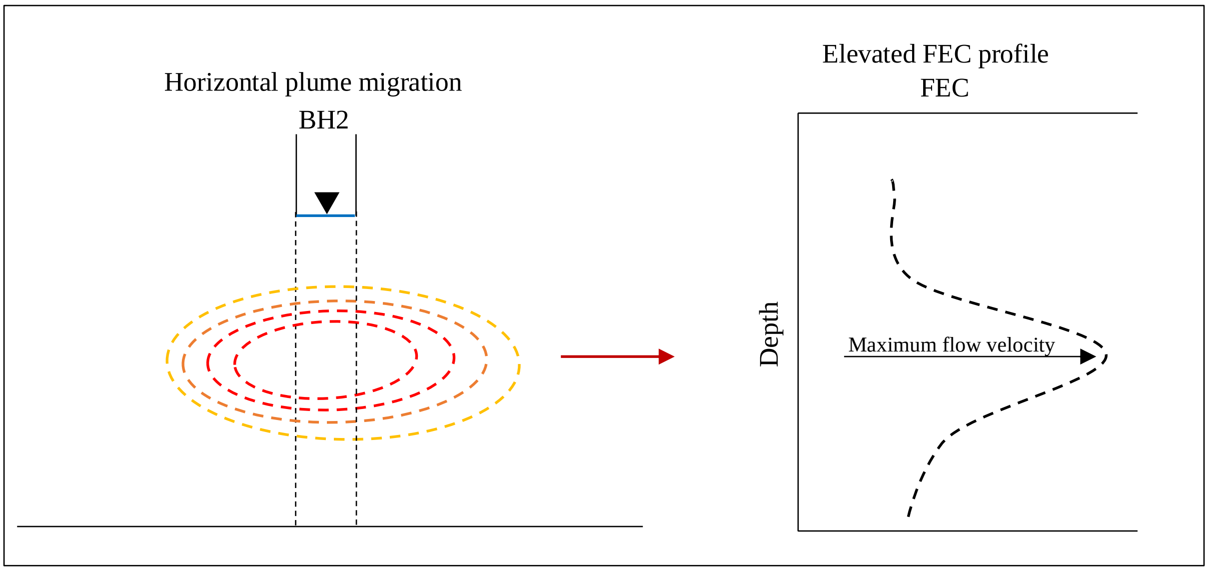

Figure 5-8 **Conceptual model of the plume peak FEC profile far from the source in a typical porous aquifer system under contaminated groundwater conditions.**

5.2.2.4 Residual FEC profile

The residual plume FEC profile represented conditions in the aquifer system where the majority of the contaminant plume had already passed the monitoring point (BH2). The shape of the resulting profile also displayed an anomaly towards the centre permeable zone as shown in Figure 5-9 . However, due to the continuous replenishment of natural water into the system the amplitude of the plume peak anomaly became smaller, and continued to decrease until the profile became a vertically straight-line once background conditions were reached.

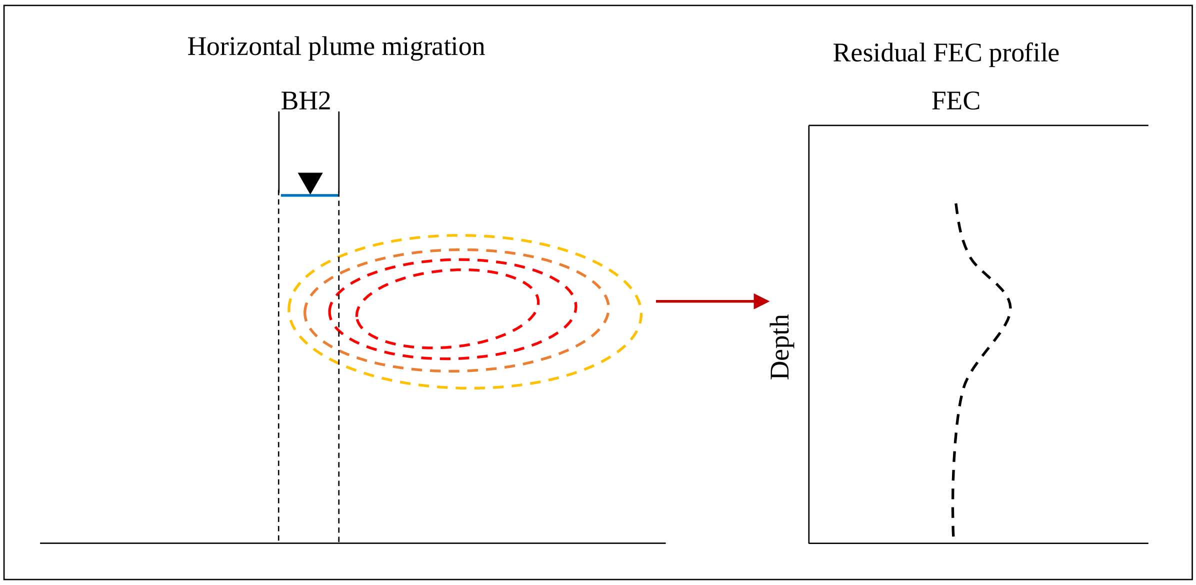

Figure 5-9 **Conceptual model of the residual plume FEC profile far from the source in a typical porous aquifer system under contaminated groundwater conditions.**

5.3 Conceptual FEC profiles of the weathered basement aquifer

Once FEC profiles obtained during the migration of a contaminant plume within the weathered basement aquifer system were established and understood, conceptual profiles were developed. Two distinct signatures were identified, namely the low FEC profile and the elevated FEC profile.

5.3.1 Low FEC profile

The shape of the background FEC profile closely resembled the one of the residual and near-background FEC profiles, for that reason these three profiles were conceptualised as one profile referred to as the low FEC profile (Figure 5-10). Therefore, this profile not only signified initial FEC conditions in system but also represented the stage where the majority of the plume had migrated passed the monitoring point, and the system was in the process of re-establishing initial conditions. The profile displayed increasing FEC values towards the bottom of the borehole, and three distinct zones were identified, namely the weathered zone, transition zone, and the impermeable zone.

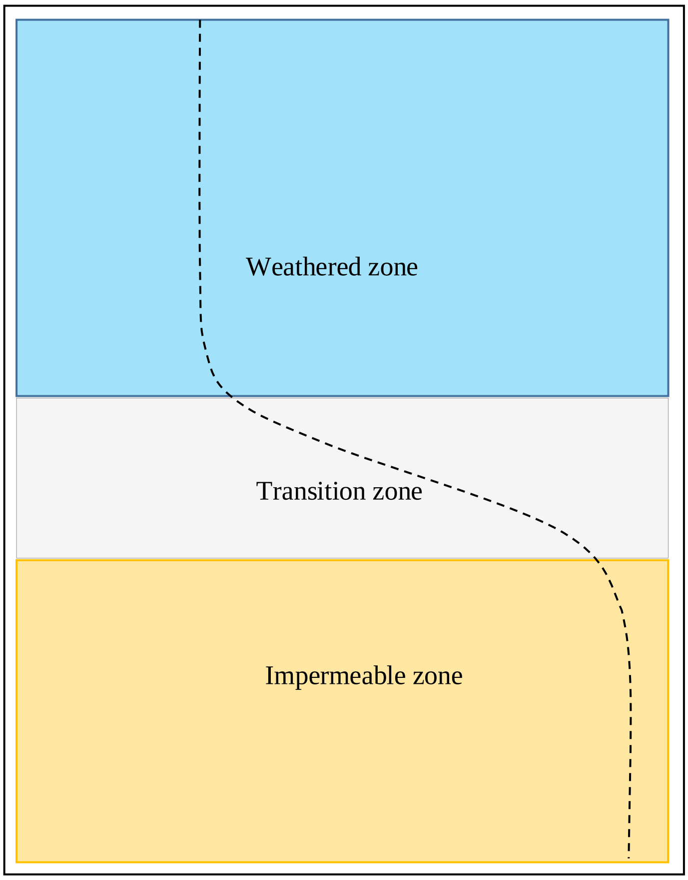

Figure 5-10 Conceptual low FEC profile obtained from a typical weathered basement aquifer system.

The weathered zone was located at the upper segment of the aquifer system and it was characterised by low FEC values. Due to its highly transmissive nature, natural water easily flowed through this zone effectively replenishing it, and as a result reduced its FEC values. In essence because continuous inflow takes place within this zone, representative aquifer water can be acquired from it.

The transition zone comprised of incoming aquifer water from the weathered zone, and stale water from the impermeable zone. The resulting FEC values of this zone were higher than the ones of the weathered zone but lower than the ones of the impermeable zone. The impermeable zone was characterised by elevated FEC values due to limited replenishment taking place within this segment.

The conceptual low FEC profile acquired from the weathered basement aquifer system was closely comparable to the one observed within the single-plane fractured rock aquifer system (Moleme, 2017) as shown in Figure 5-11. This highlights the importance of understanding the geology of the study area in order to effectively utilise the FEC profiling tool for improved site characterisation.

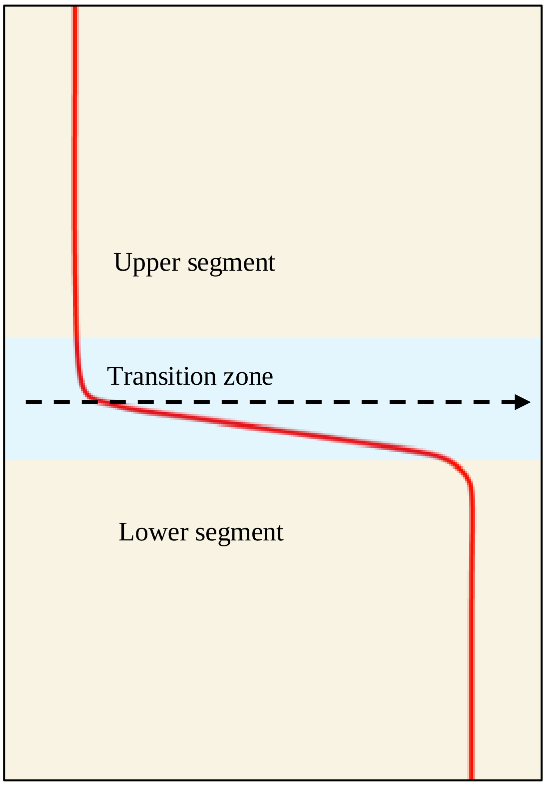

Figure 5-11 Conceptual low FEC profile obtained from atypical horizontal single-plane fractured rock aquifer system. Source: Moleme, 2017.

5.3.2 Elevated FEC profile

The shape of the first arrival and the plume peak FEC profile was highly comparable, therefore these two profiles were conceptualised as one profile referred to as the elevated FEC profile (Figure 5-12). This profile confirmed the presence of the contaminant plume within the aquifer system and was represented by increased FEC values. Two distinct zones were identified within this profile, the weathered zone and the impermeable zone.

In the presence of a contaminant plume elevated FEC values were observed at the weathered zone, which was located in the upper segment of the aquifer system. This zone was characterised by its highly transmissive property which enabled contamination to travel faster and in greater quantities, thus resulting in a pronounced anomaly situated towards the centre of the zone where the maximum transporting velocity was located. The thickness and amplitude of the anomaly would vary depending on the position of the plume at the time of profiling (i.e. first arrival or at the centre of the monitoring point).

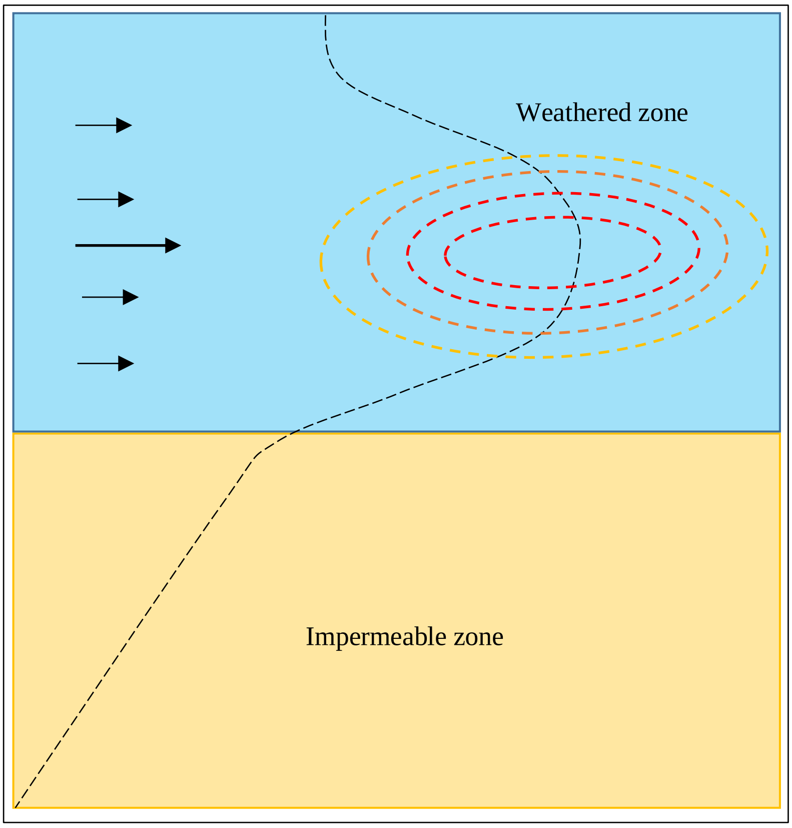

Figure 5-12 Conceptual elevated FEC profile in a typical weathered basement aquifer system due to saline contamination in the weathered basement aquifer

The impermeable zone was located at the lower segment of the aquifer system. Even though this layer did not allow fluid to flow through it, when a contaminant plume was present in the system FEC values still increased within this zone. This was due to density and diffusive effects and not because of the transmissivity of the layer. It is worth noting that in the absence of contamination elevated FEC values were found in the impermeable zone (as illustrated in Figure 5-10), however in the presence of contamination the highest FEC values were observed in the weathered zone (as shown in Figure 5-12).

When the majority of the contaminant plume had migrated passed the borehole and the system was re-establishing initial conditions, rapid dilution took place within the weathered zone as a result of constant replenishment. However, dilution within the impermeable zone was significantly slower since it was only facilitated by the process of diffusion.

Chapter 6
CONCLUSION AND RECOMMENDATIONS

6.1 Introduction

This study investigated the behaviour of FEC profiles associated with a saline contaminant plume in a typical unconfined porous and weathered basement aquifer systems using laboratory-based aquifer models and field tests. This was done to improve the conceptual understanding of contaminant migration patterns within these aquifer systems, and to essentially improve the interpretation of their FEC profiles. Additionally, this study aimed to investigate if the distance of a contaminant source (injection point) from a borehole had any effects on the evolution of FEC profiles.

As part of quality control, it was essential to assess the extent to which mass transport characteristics of the physical models conformed to those of the theoretical models observed in literature. The performance of the physical models was verified by conducting tracer breakthrough tests and comparing the obtained breakthrough curves to the ones of typical porous media breakthrough curves observed in literature. This was done to confirm the capacity of the model to simulate mass transport characteristics of a real system. All laboratory tests were repeated three times, using varying mass concentrations (i.e. 10, 15, and 20 g of salt diluted in 500 ml of tap water) in order to assess the repeatability of the outcomes. Once this was done, field tests were conducted for comparison and additional validation purposes.

Unlike previous studies that conventionally obtained FEC profiles while simultaneously low flow pumping the system, this study used a non-invasive approach of obtaining FEC profiles under natural gradient conditions without pumping during the laboratory tests.

6.2 Conclusions

6.2.1 Observations and conceptual profiles obtained from the unconfined porous aquifer system

In the porous aquifer system five stages of the plume evolution were identified at both BH1 and BH2 (i.e. the background, first arrival, plume peak, residual, and near-background stage), and it is based on these stages that conceptual profiles were developed. It is worth mentioning that the near-background profile was not conceptualised due to its close resemblance to the background profile.

Figure 6-1 shows the evolution of a contaminant plume in a porous aquifer system, and the resulting FEC profiles. The background profile was captured under natural water flow conditions, it displayed a vertically straight line in both boreholes as shown in Figure 6-1A and E. This was because the FEC values were the same throughout the entire system due to the absence of contamination and the homogeneity of the system.

Once the contaminant was introduced into the system the resulting FEC profiles obtained from BH1 and BH2, which were placed at varying distances from the source were distinctly different. Therefore, proving that the distance of a borehole from the source influences the shape of the FEC profile obtained. This insight brought to light the phenomenon of “plume orientation”. The orientation of the plume is usually disregarded in groundwater models and assessments, however this study showed that it is an important aspect which can be used to assist with FEC data interpretation in contaminated site characterisation studies. The magnitude of two main forces strongly influenced the orientation of the plume, namely the gravitational force and the advection force.

The general observation was that as the plume was introduced into the system it was primarily under the influence of the gravitational force due to its high density, this resulted in its vertical to sub-vertical orientation as displayed on Figure 6-1 B to D. However, as the plume continued to migrate and natural water continued entering the system, the magnitude of the advection force increased and ultimately became greater than that of the gravitational force, thus causing the plume to lift and re-orientate itself parallel to the groundwater flow direction shown in Figure 6-1 F to H.

Understanding the concept of plume orientation and factors that attribute to it greatly assisted with the interpretation of FEC profiles obtained in the porous aquifer system, at boreholes located at varying distances from the source. The arrival of the contaminant plume at BH1 was characterised by a diagonally shaped FEC profile (Figure 6-1B) due to the downward sinking of the plume.

On the contrary, since the effects of density were significantly reduced by the time the plume reached BH2 and the plume had aligned with the flow lines of the system, the resulting profile displayed a slight anomaly at the centre of the profile (Figure 6-1F) where the maximum transporting velocity was located. Since the plume no longer exhibited a sinking effect, it was evident that the advection force was significantly greater than the gravitational force at BH2.

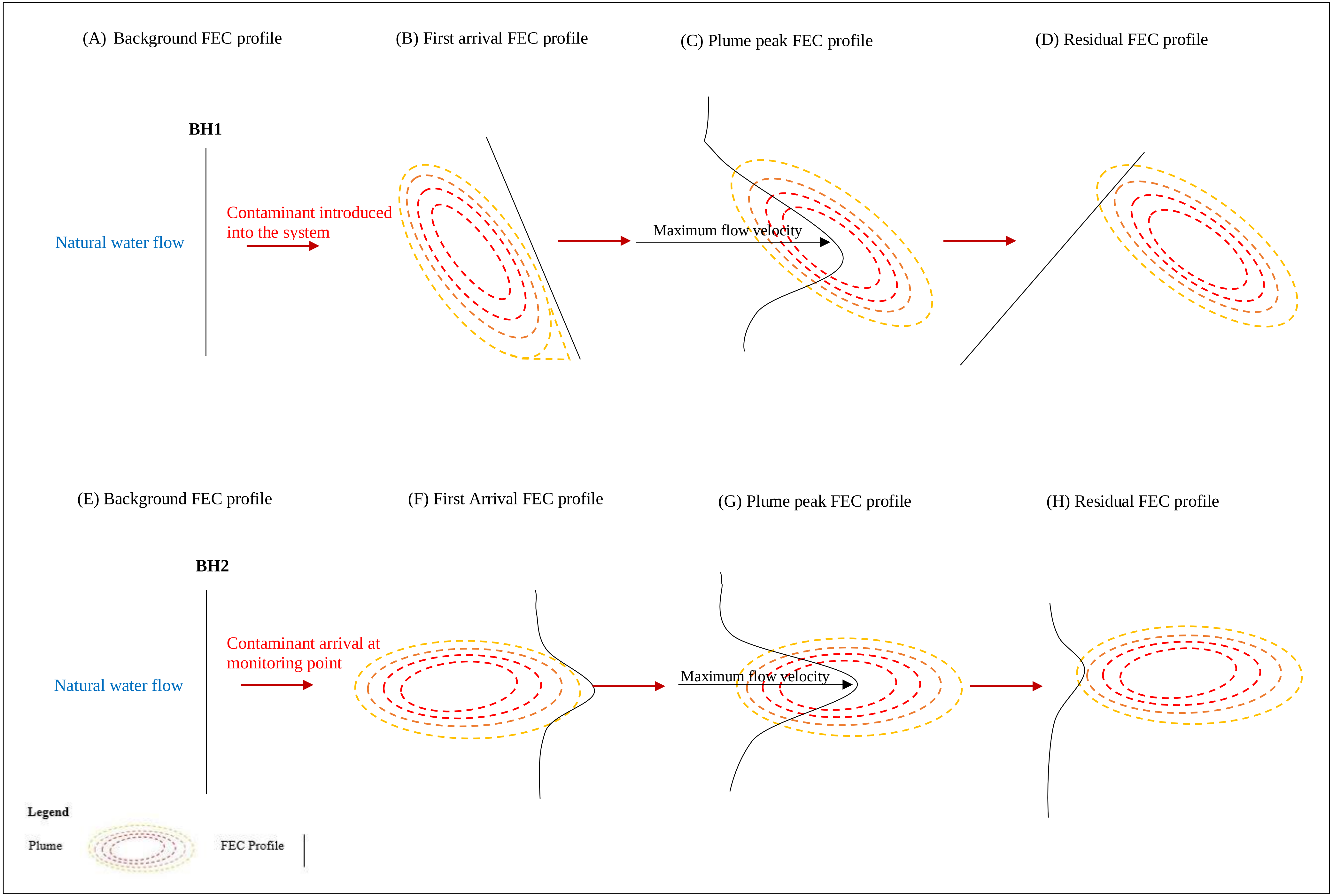

Figure 6-1 Conceptual profiles illustrating the evolution of a contaminant plume in a porous aquifer system, and the resulting FEC profiles.

Note: Profile A to D were obtained in a borehole near to the source (BH1), and profile E to H in a borehole further away from the source (BH2).

Once the centre of the contaminant plume reached the monitoring points maximum FEC values were observed, and the resulting profile was classified as the plume peak profile. This profile was observed at different times at BH1 and BH2 due to the distance between the two boreholes. The plume peak profile at BH1 displayed an anomaly slightly towards the bottom of the profile (Figure 6-1C), therefore illustrating that although the magnitude of the advection force had increased at that point in time, the gravitational force was still greater. However, the anomaly of the plume peak profile at BH2 was situated at the centre of the profile where the maximum transporting velocity was located as shown in Figure 6-1G.

As natural water continued flowing through the system, dilution took place and FEC values decreased, thus illustrating the fourth conceptual profile, namely the residual plume FEC profile (Figure 6-1D and H). At this point in time, the greater quantity of the plume itself had already passed the monitoring point. The plume observed at BH1 was diagonal with most of the FEC values measured towards the top of the aquifer system (Figure 6-1D), whereas at BH2 the plume displayed an anomaly decreased in amplitude towards the centre of the aquifer system (Figure 6-1H). Once the plume had passed the monitoring points and natural water had completely replenished the aquifer system, initial aquifer conditions were reinstated, and this was represented by a profile analogous to the background profile. The results obtained in the field closely resembled results associated with monitoring point that is further from the source (i.e. BH2).

6.2.2 Observations and conceptual profiles obtained from the weathered basement aquifer system

The second part of this study focused on investigating the behaviour of FEC profiles associated with a contaminant plume within the weathered basement aquifer system. Two distinct signatures were observed, these were defined and conceptualised as the low FEC profile and the elevated FEC profile.

The low FEC profile not only represented initial FEC conditions of the system but also referred to the stage where the majority of the plume had migrated passed the borehole, and the system was in the process of re-establishing initial conditions. The profile showed three zones which were classified as the weathered zone, transition zone, and the impermeable zone. These are illustrated in Figure 6-2.

The weathered zone was identified at the upper segment of the aquifer system. The highly transmissive property of the weathered layer enabled natural water to easily flow through it, thus effectively replenishing it and as a result decreasing the FEC values of this zone. The transition zone represented a mixture between the incoming aquifer water from the weathered zone, and stale water from the impermeable zone. The impermeable zone was observed in the lower segment of the aquifer system. This segment restricted the flow of incoming natural water, as a result, stale water with increased FEC values accumulated within this zone.

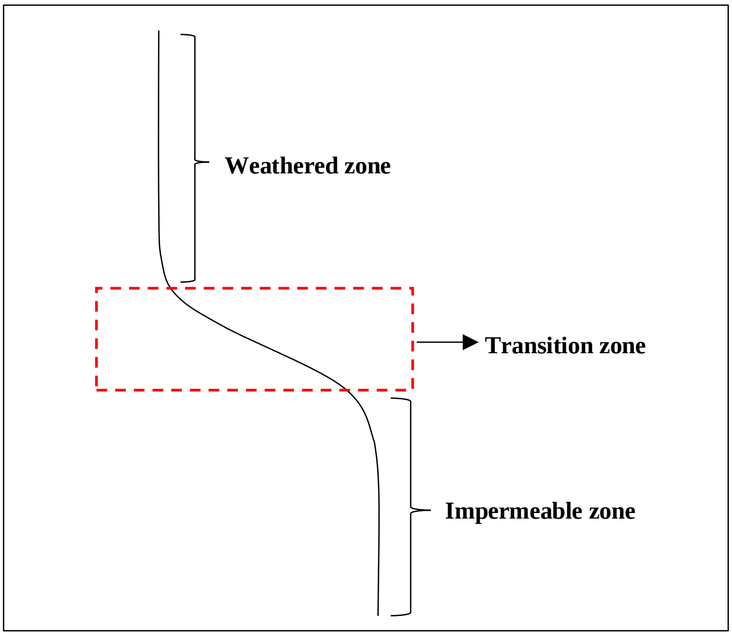

Figure 6-2 The conceptual low FEC profile obtained in the weathered basement aquifer system.

The second conceptual profile was the elevated FEC profile. It represented contaminated groundwater conditions and had two distinct zones, the weathered zone and the impermeable zone as shown in Figure 6-3. The weathered zone showed highly elevated FEC values because the high transmissivity of the weathered segment enabled the contamination to travel faster than in the impermeable zone. It also displayed a pronounced anomaly with the highest FEC values measured at the centre of the weathered zone where the maximum transporting velocity was located. The thickness and amplitude of the anomaly varied depending on the position of the plume at the time of profiling.

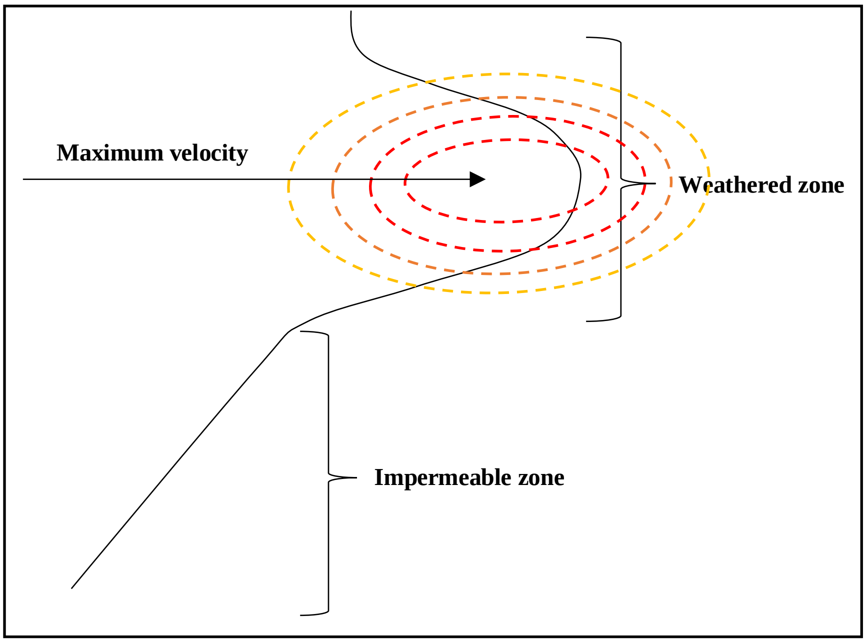

Figure 6-3 The conceptual elevated FEC Profile obtained within the weathered basement aquifer system.

Although the impermeable segment also displayed increased FEC values, these were significantly lower compared to the ones observed in the weathered segment. The increase of FEC values within the impermeable zone was accounted for by density and diffusive effects rather than the transmissivity of the layer.

These profiles were seen under a controlled laboratory environment and were verified in the field. The insight gained from this study can be used as a guideline for interpreting FEC profiles within the above-mentioned aquifer systems. It can further assist with identifying the stage of the contaminant plume within the aquifer system at the time of FEC profiling. In general, this study demonstrates that the application of the FEC profiling technique is quite versatile and should not just be restricted to fractured aquifer systems, and limited to its conventional use of determining hydrogeological properties and locating inflow zones.

6.3 Recommendations

The FEC profiling method is a powerful tool in groundwater studies. The method offers valuable information even under non-invasive conditions. Given the versatility of the method, which has been demonstrated in this study, the following additional applications of the FEC profiling technique in groundwater studies are recommended:

- When conducting groundwater quality monitoring, it would be of value to also conduct FEC profiling. The profiles obtained over time can offer some guidelines in terms of the state of the aquifer system and the movement of the contaminant plume.

- FEC profiles can also assist in building hydrogeological conceptual models to complement drilling data, or in instances where geological data from drilling is not readily available. This can be done by analysing the FEC profile and identifying changes within the profile; areas with sharp anomalies could be indicative of highly transmissive layers such as sandstone, chalk or even fractures, and areas with no distinct anomalies could be indicative of impermeable formations such as shale, clay and silt.

This study does not suggest that the use of the developed FEC profiles is sufficient to independently determine geological lithology or the contribution of aquifer layers to groundwater transport or flow. Instead, the developed conceptual FEC profiles should be used as a guideline, coupled with a sound geo-hydrological understanding of the aquifer system to complement other contaminant site characterisation tools.

Future studies may consider the following:

- Conducting the tests in bigger laboratory models, this would facilitate the recording of more measurements which could help eliminate any variations encountered due to the scale factor.
- Conducting the test in a confined aquifer system to determine the extent to which the breakthrough curves as well as the FEC profiles would change.
- Using two monitoring points within the weathered basement aquifer system and analyse how the near-source profile differs from the far-source profile. Using multiple boreholes within the porous aquifer system gave interesting insight on the plume orientation phenomenon, therefore implementing multiple boreholes within the weathered basement aquifer system could increase our understanding of the plume movement in this aquifer system, and possibly bring to light new insights.
- Assessing the progression of FEC profiles in different aquifer systems, using other tracer types to help improve understanding on contaminant migration across various aquifer systems.

REFERENCES

Abbott, M.B., Bathrust, J.C., Cunge, J.A., O'Connell, P.E. and Rasmussen, J. (1986). An introduction to Europeen hydrological system - systeme hydrologique Europeen (SHE) Part 2. Structure of a physically based distributed modeling system. *Journal of Hydrology* 87, pp. 61-77.

Abelin, H., Birgersson, L., Moreno, L., Widen, H., Agren, T. and Neretnieks, I. (1991). A large-scale flow and tracer experiment in granite 2. Results and interpretation. *Water Resources Research*, 27(12), pp. 3019–3135.

Allaby, A., Allaby, M. (1999). A dictionary of Earth Sciences (2nd Ed), Oxford University Press.

APHA. (1998). Standard Methods for the Examination of Water and Wastewater (20th Ed), Am. Public Health Association, Washington DC.

Back, W. and Cherry J.A. (1976). Chemical aspects of present and future hydrogeological problems in proceedings advances in groundwater hydrology. American Water Resources Association, Chicago, Ill, pp. 153-172.

Baran, E. and Jonch, F. (2000). Hydrogeological map series of the Republic of South Africa.

Barber, T. and Rosthal, R.A. (1991). Using a multiarray induction tool to achieve high-resolution logs with minimum environmental effects. Trans. SPE.10.2118/22725-MS.

Bauer, G.D. and LoCoco, JJ. (1996). Hydro-geophysics determines aquifer characteristics, *International Ground Water Technology*, Vol. 2, No. 7, pp. 12-16.

Bear, J. (1972). *Dynamics of fluids in porous media*. New York: Elsevier.

Beauheim, R.L. and Pedler, W.H. (2009). Fluid electrical conductivity logging in borehole DGR-1 at the Bruce site. Technical report: TR-07-14. DGR Site Characterization Document Intera Engineering Project 06-219.

Beauheim, R. L., Meigs, L. C. and Davies, P. B. (1997). Rationale for the H-19 and H-l 1 tracer tests at the WIPP site, field tracer transport experiments, field tracer experiments: Role in the prediction of radionuclide migration, synthesis and proceedings of an NEA/EC Workshop, Cologne Germany, 28-30 August 1996, OECD/NEA, pp. 107-118.

Beven, K. (1981). Kinematic subsurface stormflow, Waf. Resources. Res., 17, 1419-1424.

Beven K. (2001). Rainfall-Runoff modelling. The Primer. John Wiley and Sons, Chichester, UK, pp. 1-360.

Beven K. (2004). Robert E. Horton's perceptual model of infiltration processes, Hydrological processes, 18, pp. 3447-3460.

Bloschl, G., Grayson, R. B., and Sivapalan, M. (1995). On the representative elementary area (REA) concept and its utility for distributed rainfall-runoff modelling, Hydrol. Process., 9, 000-000.

Bockelmann, A., Zamfirescu, D., Ptak, T., Grathwohl, P. and Teutsch, G. (2003). Quantification of mass fluxes and natural attenuation rates at an industrial site with a limited monitoring network: a case study. *Journal of Contaminant Hydrology*. 60, pp. 97–121.

Botha, J. F., Verwey, J. P., Van der Voort, I., Vivier, J. J. P., Colliston, W. P. and Loock, J. C. (1998). Karoo Aquifers. Their Geology, Geometry and Physical Behaviour. *Water Research Commission*. South Africa.

Brown, B. H., Barber, D. C. and Seagar, A. D. (1985). Applied Potential Tomography: Possible Clinical Applications, Clin, Phys. Physiol. Meas. 6, pp. 109-121.

Carleton G.B., Welty, C. and Buxton, H.T. (1999). Technical Report: Design and Analysis of Tracer Tests to Determine Effective Porosity and Dispersivity in Fractured Sedimentary Rocks, Newark Basin, New Jersey. Water-Resources Investigation Report 98-4126A.

Chappell, N. and Ternan, L. (1992). Flow path dimensionality and hydrological modelling, Hydrol. Process., 6, 327-345.

Church, E.E. and Friesz, E.J. (1993). Deleation of a Road-salt Plume in Ground Water, and Travel time Measurements for Estimating Hydraulic Conductivity by use of Borehole-induction Logs', Minerals and Geotech. Logging Sot., 5th Intern. Syrup. on Geophysics for Minerals, Geotech. And Environmental Applications, Proe., Soc. Prof. Well Log Anal., paper Y, pp. 1-16.

Crawford, N.H. and R.K. Linsley. (1966). Digital Simulation in Hydrology: Stanford Watershed Model IV. Technical Report No. 39, Department of Civil Engineering, Stanford University, pp. 210.

Darcy, H.P.G. (1856). Determination of the Laws of Water Flow through Sand, the Public Fountains of the City of Dijon, Appendix D- Filtration, section 2 of Appendix D on Natural Filtration. Translated from French by Patricia Bobeck. Kendall/ Hunt Publishing Company, lowa, pp. 455-459.

Dawson C.W., Abrahart R.J., Shamseldin A.Y. and Wilby R.L. (2006). Flood estimation at ungauged sites using artificial neural networks, *Journal of Hydrology* 319 (1-4), pp. 391-409.

Department of Water Affairs and Forestry (2012). 1:3 000 000 Aquifer Classification of South Africa.

DeSimone, L.A. and Barlow, E.M. (1993). 'Borehole Induction Logging for Delineation of a seepage-effluent Contaminant Plume in Glacial Outwash, Cape Cod, Massachusetts', Minerals and Geotech. Logging Sot., 5th Intern. Symp. on Geophysics for Minerals, Geotech. And Environmental Applications, Proc., Soc. Prof. Well Log Anal., paper X, pp. 1-13.

Diersch, H.J.G. and Kolditz, O. (2002). High density flow and transport in porous media: approaches and challenges. Advanced Water Resources 25 (8-12), pp. 899-944.

Doll, G. H. (1949). The SP Log: Theoretical Analysis and Principles of Interpretation, Trans. AIME 179, Tech. Paper 2463.

Dooge, J. C. I. 1982. 'Parameterization of hydrologic processes' in Eagleson, P. S. (Ed.), Land Surface Processes in Atmospheric General Circulation Models. Cambridge University Press, London, pp. 243-288.

Dooge, J. C. I. (1986). Looking for hydrologic laws, Wat. Resour. Res., 22, 46s-58s.

Doughty, C. and Tsang, C.-F. (2000). BORE II – A code to compute dynamic wellbore electrical conductivity logs with multiple inflow/outflow points including the effects of horizontal flow across the well. Rep. LBL-46833. Lawrence Berkeley National Laboratory, Berkeley, CA. https://escholarship.org/uc/item/3sh5f8kg

Doughty, C. and Tsang, C.-F. (2002). Inflow and outflow signatures in flowing wellbore electrical conductivity logs. Technical Report. Rep. LBNL-51468.U.S. Department of Energy, Office of Scientific and Technical Information. https://doi.org/10.2172/833944

Doughty, C. and Tsang, C.-F. (2005). Signatures in flowing fluid electric conductivity logs. *Journal of Hydrology*, 310(1−4), pp. 157−180. https://doi.org/10.1016/j.jhydrol. 2004.12.003

Doughty, C., Takeuchi, S., Amano, K., Shimo, M. and Tsang, C.-F. (2005). Application of multi-rate flowing fluid electric conductivity logging method to well DH-2, Tono Site, Japan. *Water Resources Research*. 41 (10), pp. 1-16.

Doughty, C., Tsang, C.-F., Hatanaka, K., Yabuuchi, S. and Kurikami, H. (2008). Application of direct-fitting, mass integral, and multirate methods to analysis of flowing fluid electric conductivity logs from Horonobe, Japan, Water Resources Research., 44, W08403. https://doi.org/10.1029/2007WR006441.

Doveton, J. H. and Prensky, S. E. (1992). Geological Applications of Wireline Logs: A Synopsis of Developments and Trends. The Log Analyst, 33 (3), pp. 286-30.

Dovers, S. R. (1995). A framework for scaling and framing policy problems in sustainability, Ecological Econ., 12, pp. 93-106.

Dozier, J. (1992). Opportunities to improve hydrologic data, Rev. Geophysics., 30, 315-331.

Drost, W., Klotz, D., Koch, A., Moser, H., Neumaier, F. and Rauert, W. (1968). Point dilution methods of investigating ground water flow by means of radioisotopes. *Water Resource Research* 4(1), pp. 125–146.

Drost, W and Neumaier, F. (1974). Application of single borehole methods in groundwater research. In Proceedings, Symposium on Isotope Techniques in Groundwater Hydrology, Vienna, pp. 241-254.

Dunn S.M., Freer J., Weiler M., Kirkby M. J., Seibert J., Quinn P.F., Lischeid G., Tetzlaff D. and Soulsby C. (2008). Conceptualization in catchment modelling: simply learning, Hydrological Processes, 22(13), pp. 2389-2393.

Evans, D.G. (1995). Inverting fluid conductivity logs for fracture inflow parameters. *Water Resource Research* 31 (12), pp. 2905–2915.

Field, M.S. (2003). A review of some tracer-test design equations for tracer-mass estimation and sample-collection frequency. *Environmental Geology*, 43, pp. 867−881. https://doi.org/10.1007/s00254-002-0708-7

Freeze, R.A. and J.A. Cherry. (1979). *Groundwater*. Englewood Cliffs, N.J.: Prentice-Hall.

Gebrekristos, R.A. (2007). Site characterisation methodologies for DNAPLs in fractured South African aquifers. Doctoral thesis. University of the Free State, Bloemfontein, South Africa. http://hdl.handle.net/11660/1220

Gelhar, L.W., Welty, Claire, and Rehfeldt, K.R. (1992). A critical review of field-scale dispersion in aquifers: *Water Resources Research*, v. 28, no. 7, pp. 1955–1974.

Germann, P. F. (1990). Macropores and hydrologic hillslope processes in Anderson, M. G. and Burt, T. P. (Eds), Process Studies in Hillslope Hydrology. Wiley, Chichester, pp. 327-367.

Gillham, R.W. and O'Hannesin, S.F. (1984). Apparatus for demonstrating confined and unconfined aquifer characteristics. *Journal of Geological Education,* v.32. No.4, pp. 261−264. https://doi.org/10.5408/0022-1368-32.4.261

Gochioco, L.M., Magill, C. and Marks, F. (2002). The Borehole Camera: An Investigative Geophysical Tool Applied to Engineering, Environmental, and Mining Challenges. – The Leading Edge 21(5), pp. 474 – 477.

Gomo, M. (2009). Site characterisation of LNAPL-contaminated fractured-rock aquifer. Master's dissertation, University of the Free State, Bloemfontein, South Africa. http://hdl.handle.net/11660/1888

Gomo, M. (2011). A groundwater-surface water interaction study of an alluvial channel aquifer. Ph.D. thesis. Institute for Groundwater Studies. Faculty of Natural and Agricultural Sciences. University of the Free State, Bloemfontein, South Africa.

Gomo, M. and Vermeulen, D. (2015). An investigative comparison of purging and non-purging groundwater sampling methods in Karoo aquifer monitoring wells. *Journal of African Earth Sciences*, 103, pp.81–88. https://doi.org/10.1016/j.jafrearsci.2014.11.011

Gomo, M., Vermeulen, D. and Lourens P. (2017). Groundwater sampling: Flow-through bailer passive method versus conventional purge method. *Natural Resources Research*, 27, pp. 51−65. https://doi.org/10.1007/s11053-017-9332-9

Gondouin, M. and Scala, C. (1958). Streaming Potential and the SP Log, Trans. AIME, Tech. Paper 8023.

Gorokhovski, V. (2014). Transformation of Geological Objects' Properties into Effective Model Parameters. In: Effective Parameters of Hydrogeological Models. Springer Hydrogeology. Springer, Cham. https://doi.org/10.1007/978-3-319-03569-7_5

Haggerty, R., McKenna, S.A. and Meigs, L.C. (2000). Late time behaviour of tracer test breakthrough curves. *Water Resources Research*, 36(12), pp. 3467−3479. https://doi.org/10.1029/2000WR900214

Haimson, B. C. and Lee, M.Y. (1984). Development of a Wireline Hydrofracturing Technique and Its Use at a Site of Induced Seismicity, in Proc. 25th US Rock Mech. Symp., Soc. Mining Engrs, New York, NY, pp. 194-203.

Hale, F.V. and Tsang, C.-F. (1988). A code to compute borehole conductivity profiles from multiple feed points. Report no. LBL-24928, Lawrence Berkeley Laboratory, Berkeley, CA. https://doi.org/10.2172/5100624

Haury, L. R., McGowan, J. A,, and Wiebe, P. H. (1977). Patterns and processes in the time-space scales of plankton distributions in Steele, J. H. (Ed.), Spatial Pattern in Plankton Communities. Plenum Press, New York and London, pp. 277-327.

Hess, A. E. (1986). Identifying hydraulically conductive fractures with a slow-velocity borehole flowmeter. *Canadian Geotechnical Journal*, 23(1), pp. 69-78.

Hill, A.D. (1990). Production logging - Theoretical and interpretive elements, Society of Petroleum Engineers Monograph 14, Richardson, Texas.

Hillel, D., and Elrick, D. E. (1990). Scaling in Soil Physics: Principles and Applications. Soil Science Society of America, Vol. 25, pp. 122.

Hwang, S., Shin, J., Park, I. and Lee, S. (2004). Assessment of Seawater Intrusion Using Geophysical Well Logging and Electrical Soundings in a Coastal Aquifer. – Youngkwang-gun, Korea. Exploration Geophysics 35, pp. 99 – 104.

Jain A., Sudheer K.P. and Srinivasulu S. (2004). Identification of physical processes inherent in artificial neural network rainfall runoff models, Hydrological Processes 18, pp. 571–583.

Jiao, J. and Zhang, Y. (2014). Two-dimensional physical-based inversion of confined and unconfined aquifers under unknown boundary conditions. *Advances in Water Resources*, 65, pp. 43−57. https://doi.org/10.1016/j.advwatres.2013.10.011

Jones, M.J. (1985). The weathered zone aquifers of the basement complex areas of Africa. *Quarterly Journal of Engineering Geology and Hydrogeology*, 18(1), pp. 35−46. https://doi.org/10.1144/GSL.QJEG.1985.018.01.06

Jorgensen, D.G. and Petricola, M. (1995). Research Borehole-Geophysical Logging in Determining Geohydrologic Properties. – *Ground Water* 33(4). pp. 589 – 596.

Kazumasa, I., Naoto, T., Yoji, S., Kazuki, N. and Yoshio, W. (2006). AIST, Research Centre for Deep Geological Environment. 1-1-1 Higashi Tsukuba, Ibaraki, 305 – 8567, Japan.

Proceedings, tough symposium 2006, Lawrence Berkeley National Laboratory, Berkeley, California, May 15-17, 2006.

Käss, W. (1998). Tracing Techniques in Geohydrology, A.A. Balkema, Rotterdam.

Keller, G.V. and Frischknecht, F.C. (1966). *Electrical methods in geophysical prospecting*. Oxford: Pergamon Press.

Kelly, V.A., Lavanchy, J.M., and Loew, S. (1991). Transmissivities and heads derived from detailed analysis of Siblingen 1989 fluid logging data. Nagra, Wettington, Switzerland.Nagra Tech. Rep. NTB 90-09, pp. 184.

Keys, W.S. (1989). Borehole Geophysics Applied to Ground-Water Investigations. Dublin, OH: National Water Well Association.

Keys, W.S. (1996). A practical guide to borehole Geophysics in Environmental Investigations. – Lewis Publishers, Boca Raton, Florida.

Kinzelbach, W. (1992). Continuous groundwater velocity fields and path lines in linear, bilinear, and trilinear finite elements. *Water Resources Research*, 28(11), pp. 2903−2911. https://doi.org/1029/92WR01686.

Klemes, V. (1983). Conceptualisation and scale in hydrology, *J. Hydrol*., 65, pp. 1-23.

Kruseman, G. P, and de Ridder, N A. (1994). Analysis and Evaluation of Pumping Test Data. Wageningen: International Institute for Land Reclamation and Improvement.

Kurikami, H., Takeuchi, R. and Yabuuchi, S. (2008). Scale effects and heterogeneity of hydraulic conductivity of sedimentary rocks at Horonobe URL site. *Physics and Chemistry of the Earth*, 33(2008) S37−S44. http://dx.doi.org/10.1016/j.pce.2008.10.016

Lacy, L.L., and Smith, X. (1989). Fracture azimuth and geometry determinations. Pp. 357–375 in SPE Monograph 12: Recent Advances in Hydraulic Fracturing. Richardson, Tex.: Society of Petroleum Engineers.

LeBlanc, D.R., Garabedian, S.P., Hess, K.M., Gelhar, L.W., Quadri, R.D., Stollenwerk, K.G. and Wood, W.W. (1991). Large-scale natural gradient tracer test in sand and gravel, Cape Cod, Massachusetts. 1. Experimental design and observed tracer movement. *Water Resources Research*, 27(5), pp. 895–910. https://doi.org/10.1029/91WR00241

Lekkas D. (2008). Using complementary methods for improved flow forecasting, Hydrological Sciences Journal, 53(4), pp.696-705.

Löw, S., Tsang, C.-F., Hale, F.V. and Hufschmied, P. (1990). The application of moment methods to the analysis of fluid electrical conductivity logs in boreholes, Rep. LBL-28809, Lawrence Berkeley Laboratory, Berkeley, CA.

MacDonald, A.M., Bonsor, H.C., Dochartaigh, B.É.Ó. and Taylor, R.G. (2012). Quantitative maps of groundwater resources in Africa. 1. Approach and overview of plume movement. *Environmental Research Letters*, 7(2), 024009. https://doi.org/10.1088/1748-9326/7/2/024009

MacKay, D.M., Freyberg, D.L., Roberts, P.V. and Cherry, J.A. (1986). A natural gradient experiment on solute transport in a sand aquifer. *Water Resources Research*, 22(13), pp. 2017-2029. http://dx.doi.org/10.1029/WR022i013p02017

MacKay, R. and Riley, M. S. (1991). The problem of scale in the modelling of groundwater flow and transport processes in Chemodynamics of Groundwaters. Proc. Workshop November 1991, Mont Sainie-Odile. France. EAWAG, EERO, PIR "Environment" of CNRS, IMF Universite Louis Pasreur Strasbourg. pp. 17-51.

Malaguerra, F., Albrechtsen, H., and Binning, P. (2013). Assessment of the contamination of drinking water supply wells by pesticides from surface water resources using a finite element reactive transport model and global sensitivity analysis techniques. *Journal of Hydrology*. 476, pp. 321–331. http://doi.org/10.1016/j.jhydrol.2012.11.010.

Malloszewski, P. and Zuber, A. (1992). The calibration and validation of mathematical models for the interpretation of tracer experiments in groundwater. *Advances in Water Resources*, 15(1), pp. 47–62. https://doi.org/10.1016/0309-1708(92)90031-V

Mares, S., Zboril, A. and Kelly, W.E. (1994). Logging for the determination of aquifer hydraulic properties. *The Log Analyst* 35(6), pp. 28–36. https://pubs.usgs.gov/wsp/2453/report.pdf

Marschall, P. and Vomvoris, S. (1995). Grimsel Test Site: Developments in hydrotesting, fluid logging and combined salt/heat tracer experiments in the BK Site (Phase III), Nagra Tech. Rep. 93–47, Nagra, Wettingen, Switzerland.

Martin, D.W., Spencer, M.C., and Patel, H. (1984). The digital induction – A new approach in the response of the induction measurement. 25th annual logging symposium transactions. Society of Professional Well Log Analysts paper M, pp. 11-11.

Mau, E.R. (1992). Particle transport in flow through porous media: Advection, longitudinal dispersion, and filtration. Doctoral thesis, California Institute of Technology, California. https://resolver.caltech.edu/CaltechETD:etd-08202007-142809

Maute, R.E. (1992). Electrical logging: State-of-theart. – The Log Analyst 33(3), pp. 206 – 227.

McCarty, P.L., Reinhard, M. and Rittmann, B.E. (1981). Trace organics in groundwater. Environmental Science & Technology, 15(1), 40−51. https://doi.org/10.1021/es00083a003

McIntyre N. and Al-Qurashi A. (2009). Performance of ten rainfall-runoff models applied to an arid catchment in Oman, *Environmental Modelling & Software*, 24(6), pp. 726-738.

McNeely, R.N., Neimanis V.P. and Dwyer, L. (1979). Water quality sourcebook: A guide to water quality parameters. Inland waters Directorate Ottawa, Canada, pp. 32-70.

Mohr, S.D. and Smith, L. (2019). Flowing Fluid Electrical Conductivity Profiling – An inventive and cost-effective alternative to conventional downhole hydraulic profiling techniques. South African Groundwater Conference.

Moir, R.S., Parker, A.H., and Bown, R.T. (2014). A simple inverse method for the interpretation of pumped flowing fluid electrical conductivity logs. *Water Resources Research*, 50, pp.6466 – 6478.

Moleme, MF. (2017). Evolution of fluid electrical conductivity (FEC) profiles associated with a contaminant plume in a horizontal single-plane fractured rock aquifer system. Master's dissertation, University of the Free State, Bloemfontein, South Africa. http://hdl.handle.net/11660/7741

Moleme, M.F. and Gomo, M. (2018). Evolution of fluid electrical conductivity profiles associated with a saline contaminant plume in a horizontal single-plane fractured-rock aquifer system. *Natural Resources Research*, 28, pp. 79–90. https://doi.org/10.1007/s11053-018-9372-9

Molz, F.J. and Young, S.C. (1993). Development and Application of Borehole Flowmeters for Environment Assessment. – The Log Analyst 34(1), pp. 13 – 23.

Molz, F. J., Bowman, G.K., Young, S.C. and Waldrop, W.R. (1994). Borehole flowmeters—Field application and data analysis, *Journal of Hydrology*, 163, pp. 347–371.

Muniruzzaman, M. and Rolle, M. (2017). Experimental investigation of the impact of compound-specific dispersion and electrostatic interactions on transient transport and solute breakthrough. *Water Resources Research*, 53(2), pp. 1189–1209. https://doi.org/10.1002/2016WR019727

Nadiri, A.A., Sedghi, Z., Khatibi, R. and Sadeghfam, S. (2018). Mapping specific vulnerability of multiple confined and unconfined aquifers by using artificial intelligence to learn from multiple DRASTIC frameworks. *Journal of Environmental Management*, 227, pp. 415−428. https://doi.org/10.1016/j.jenvman.2018.08.019

National Research Council. (1984). Panel on groundwater contamination, National Academy of Science, Washington, D.C.

National Research Council. (1991). Opportunities in the Hydrologic Sciences. National Academy of Science, Washington, D.C.

National Research Council. (1996). Rock fractures and fluid flow: Contemporary understanding and applications. National Academy of Science, Washington, D.C.

Ogden, F.L. (2021). Geohydrology: Hydrological Modelling. *Encyclopaedia of Geology*, 2 (6), pp. 457-475. https://doi.org/10.1016/B978-0-08-102908-4.00115-6

Pacome, A.D. (2010). *Fracture characterisation of Karoo aquifers*. Master's dissertation, University of the Free State, Bloemfontein, South Africa. http://hdl.handle.net/11660/1464

Paillet, F.L, Cheng, C.H. and Pennington W.D. (1992). Acoustic-waveform Logging-advances in Theory and Application. – The Log Analyst 33(3), pp. 239 – 258.

Patil, S.B. and Chore, H.S. (2014). Contaminant transport through porous media: An overview of experimental and numerical studies. *Advances in Environmental Research*, 3(1), 45−69. https://doi.org/10.12989/aer.2014.3.1.045

Paunescu, D., Puddu, M., Soellner, J. O. B., Stoessel, P. R. and Grass, R. N. (2013). Reversible DNA encapsulation in silica to produce ROS-resistant and heat-resistant synthetic DNA "fossils". Nature Protocols, 8(12), pp. 2440–8. http://doi.org/10.1038/nprot.2013.154

Pechlivanidis, I., Jackson, B. and Mcintyre, N. (2011). Catchment scale hydrological modelling: A review of model types, calibration approaches and uncertainty analysis methods in the context of recent developments in technology and applications. GlobalINEST International Journal. Vol 13, pp. 193-214.

Pedler, W.H., Barvenik, M.J., Tsang, C.-F. and Hale, F.V. (1990). Determination of bedrock hydraulic conductivity and hydrochemistry using a wellbore fluid logging method. Proceedings of the Outdoor Action Conference – 1990, NWWA, pp. 39-53.

Pedler, W.H., Head, C.L. and Williams, L.L. (1992). Hydro-physical logging: A new wellbore technology for hydro-geologic and contaminant characterization of aquifers, National Outdoor Action Conference, National Ground Water Association, Las Vegas, Nevada.

Perina, T. and Lee, T.-C. (2006). General well function for pumping from a confined, leaky, or unconfined aquifer. *Journal of Hydrology*, 317(3-4), pp. 239−260. https://doi.org/10.1016/j.jhydrol.2005.05.020

Pretorius, J.A. (2007). DNAPLS in South African fractured aquifers: Occurrence, fate and management. PhD Thesis at the Institute for Groundwater Studies, University of the Free State, South Africa.

Ptak, T., Piepenbrink, M. and Martac, E. (2004). Tracer tests for the investigation of heterogeneous porous media and stochastic modelling of flow and transport – a review of some recent developments. *Journal of Hydrology 294*, pp. 122 – 163. https://doi:10.1016/j.jhydrol.2004.01.020

Ratto M., Young P.C., Romanowicz R., Pappenberger F., Saltelli A. and Pagano A. (2007), Uncertainty, sensitivity analysis and the role of data based mechanistic modelling in hydrology, *Hydrology and Earth System Sciences*, 11, pp. 1249-1266.

Raupach, M. R. and Finnigan, J. J. (1995). Scale issues in boundary layer - meteorology: surface energy balances in heterogenous terrain, *Hydrological Process*., 9, pp. 589 - 612.

Rauen, A. and Lastovickova, M. (1995). Investigation of Electrical Anisotropy in the Deep Borehole KTB, Surv. in Geophys. 16, pp. 37-46.

Repsold, H. (1989). Well Logging in Groundwater Development. – International Contributions to Hydrogeology 9; Verlag Heinz Heise, Hannover.

Riemann, K. (2002). Aquifer Parameter Estimation in fractured-Rock Aquifers using a Combination of Hydraulic and Tracer Tests. PhD, Thesis. Faculty of Natural and Agricultural Sciences, Department of Geohydrology at the University of the Free State, Bloemfontein, South Africa.

Robledo, A.R., Ryder, P.L., Fenelon, J.M., and Paillet, F.L. (1997). Geohydrology of Monitoring Wells Drilled in Oasis Valley near Beatty, Nye Country, Nevada: Water Resourced Investigations Report 98-4184.

Shakhane, T. (2011). Coupled flow in groundwater systems: The study of bulk flow parameters. Unpublished MSc Thesis at the Institute for Groundwater Studies, University of the Free State, South Africa.

Sherman L.K. (1932). Stream flow from rainfall by the unit-graph method, Engineering News Record,108, pp. 501-505.

Simmons, C.T., Fenstemaker, T.R. and Sharp, J.M. (2001). Variable density groundwater flow and solute transport in heterogeneous porous media: approaches, resolutions and future challenges. *Journal of Contaminant Hydrology* 52:1-4, pp. 245-275.

Singh, A. (2018). A concise review on introduction to hydrological models. *Global Research and Development Journal for Engineering*, 3 (10), pp.14 -19.

Singh, V.P. (1995). Computer models of watershed hydrology, *Water Resources Publications*, LLC, USA.

Singh, V.P. and Woolhiser D.A. (2002). Mathematical modeling of watershed hydrology. *Journal of Hydrologic Engineering*, 7(4), pp. 270-292.

Singh, V.P. and Frevert D. (2006). Watershed models. Boca Raton, Taylor & Francis.

Smart, C.C. and Worthington, S.R.H. (2003). Electrical conductivity profiling of boreholes as a means of identifying karst aquifers. Ninth Multidisciplinary Conference on Sinkholes and the Engineering and Environmental Impacts of Karst. Geotech Special Publication no. 122, American Society of Civil Engineers, pp 265–276. https://doi.org/10.1061/40698(2003)24

Smits, A. R., Fincher, D. V., Nishida, K., Mullins, O. C., Schroeder, R. J. and Yamate, T. (1993). In-situ Fluid Analysis as an Aid to Wireline Formation Sampling, 68th Ann. Conf., Soc. Petrol. Eng., SPE 26496.

Spies, B. R. (1996). Electrical and Electromagnetic Borehole Measurements: A Review. Surveys in Geophysics, 17, pp. 517-556.

Stewart, L.M. (2000). Laboratory analytical results for groundwater sampling at Southern Polytechnic State University, Marietta, Georgia, 1997: U.S. Geological Survey Open-File Report 00–277, pp. 28.

Stommel, H. (1963). Varieties of oceanographic experience, Science, 139, pp. 572-576.

Stumm, F., Chu, A., Lange, A.D., Paillet, F.L., Williams, J.H. and Lane, J.W. (2001). Use of advanced borehole geophysical techniques to delineate fractured-rock ground-water flow and fractures along water-tunnel facilities in northern Queens County. New York: U.S. Geological Survey Water-Resources Investigations Report 01-4276. p.12.

Taylor, K., Hess, J. and Wheatcraft, S. (1990). Evaluation of Selected Borehole Geophysical Methods for Hazardous Waste Site Investigations and Monitoring. – Final Report, United States Environmental Protection Agency, EPA/600/4-90/029, Las Vegas, Nevada.

Thiem, G. (1906). Hydrologische methoden [Hydrological methods]. PhD Thesis, University of Stuttgart, Stuttgart, Germany.

Toerien, D.K. (1979). Die geologie van die gebied Oudtshoorn [The geology of the Oudtshoorn area]. Department of Mines, Geological Survey, Government Printer, South Africa.

Tsang, C. F. (1985). Lessons learned in the verification and validation studies of a coupled heat and fluid flow code, paper presented at the Symposium on Groundwater Flow and Transport Modeling for Performance Assessment of Deep Geologic Disposal of Radioactive Waste: A Critical Evaluation of the State of the Art. Albuquerque, New Mexico.

Tsang, C.-F. and Doughty, C. (2003). Multirate flowing fluid electric conductivity logging method. *Water Resources Research*, 39(12), pp. 1354–1362. https://doi.org/10.1029/2003WR002308

Tsang, C.-F., Hufschmied, P. and Hale, F.V. (1990). Determination of fracture inflow parameters with a borehole fluid conductivity profiling method. *Water Resources Research*, 26(4), 561–578. https://doi.org/10.1029/WR026i004p00561

Tsang, Y. W., and C. F. Tsang. (1989). Flow channelling in a single fracture as a two-dimensional, strongly heterogeneous permeable medium. *Water Resources Research*, 25 (9), pp. 2076–2080.

Usher, B.H., Pretorius, J.A., Gebrekristos, R.A., Jagals, P., Traoré, H.N., Robertson, N., Tshitenge, C., Zadoroshnaya, V., Groenewald, J., Lenong, S., and Pienaar, M. (2008). Field and laboratory investigations to study the fate and transport of dense non-aqueous phase liquids (DNAPLS) in groundwater. Final Report, WRC Project, Pretoria.

Van Tonder, G.J., Bardenhagen, I., Riemann, K., van Bosch, J., Dzanga, P. and Xu, Y. (2001). Manual on Pumping Test Analysis in fractured-Rock Aquifers. Final Report, WRC Project, Pretoria.

Van Werkhoven K., Wagener T., Reed P. and Tang Y., (2009), Sensitivity-guided reduction of parametric dimensionality for multi-objective calibration of watershed models, *Advances in Water Resources*, 32(8), pp.1154-1169.

Van Wyk, A.E. (1998). Tracer experiments in fractured-rock aquifers. Master's dissertation, University of the Free State, South Africa.

Wagener, T., Wheater, H.S., and Gupta H.V. (2004). Rainfall-Runoff Modelling in Gauged and Ungauged Catchments. Imperial College Press, London, UK, pp. 1-306.

Ward, S. H. (1980). History of Geophysical Exploration- Electrical, Electromagnetic and Magneto-telluric Methods, Geophysics 45, pp. 1659-1666.

Welty, D. and Gelhar, L. W. (1989). Evaluation of longitudinal dispersivity from tracer test data. Report 320, Ralph M. Parsons Laboratory for Water Resources and Hydrodynamics, Massachusetts Institute of Technology, Cambridge.

Wheater, H.S., Jakeman, A.J., Beven, K.J., Beck, M.B., and McAleer, M.J. (1993). Progress and directions in rainfall-runoff modelling. Modelling change in environmental systems. New York, pp. 101-132.

Wheater, H.S. (2002). Progress in and prospects for fluvial flood modelling. Philosophical Transactions of the Royal Society of London, Series A-Mathematical Physical and Engineering Sciences. 360 (1796).

Williams, J.H. and Johnson, C.D. (2004). Acoustic and optical borehole-wall imaging for fractured-rock aquifer studies: Journal of Applied Geophysics, vol. 55, Issue 1-2, p. 151-159.

Wonik, T. and Hinsby, K. (2006). Borehole logging in hydrogeology. In: Kirsch, R., Rumpel, H.-M., Scheer, W. and Wiederhold, H. (Eds), Groundwater resources in buried valleys: A challenge for geosciences. BurVal Working Group. Leibniz Institute for Applied Geosciences. Hannover, pp. 107−122.

Wonik T. and Olea R.A. (2007). Borehole Logging. In: Environmental Geology. Springer, Berlin, Heidelberg. https://doi.org/10.1007/978-3-540-74671-3_13

Worthington, S.R.H. and Smart, C.C. (2017). Transiet bacterial contamination of the dual-porosity aquifer at Walkerton, Ontario, Canada. *Hydrogeology Journal*, 25, 1003–1016. https://doi.org/10.1007/s10040-016-1514-8

Wyllie, M.R.J. (1948). A Quantitative Analysis of the Electrochemical Component of the SP Curve, Trans. SPE, AIME 186.

Xu, Y., van Tonder, G.J., van Wyk, B., van Wyk, E. and Aleobua, B. (1997). Borehole dilution experiment in a Karoo aquifer in Bloemfontein. ISSN 0378-4738. Water SA. 23 (2).

Young P.C., Jakeman A.J. and Post D.A. (1997). Recent advances in the data-based modelling and analysis of hydrological systems, *Water Science and Technology*, 36(1), pp. 99-116.

Zemanak, J.R., Glenn, E.E., Norton, L.J., and Caldwell, R.L. (1970). Formation evaluation by inspection with the borehole televiewer. Geophysics 35 (2), pp. 254 – 269.

Zlotnik,V., Zurbuchen,B., Ptak,T., and Teutsch,G. (2000). Supportvolume and scale effect in hydraulic conductivity: Experimental aspects. Geological Society of America, Boulder, Colorado, Special Paper 348. In: Zhang, D., Winter, C.L. (Eds.), Theory, Modeling, and Field Investigation in Hydrogeology: A Special Volume in Honor of Shlomo P. Neuman's 60th Birthday, pp. 215–231.

Appendix A LABORATORY TRACER BREAKTHROUGH TEST

Table A 1. 1 BH1 and BH2 Porous aquifer system tracer breakthrough test data Model 1 (10 g).

BH1				BH2			
Time (mins)	FEC (μS/cm)			Time (mins)	FEC (μS/cm)		
	T1	T2	T3		T1	T2	T3
0	141	141	141	0	141	141	141
1	150	153	155	1	141	141	141
2	870	859	753	2	146	145	145
3	970	952	966	3	160	155	156
4	1100	1083	1092	4	200	185	198
5	1180	1154	1169	5	300	293	275
6	1190	1179	1184	6	430	417	428
7	1199	1190	1179	7	600	577	568
8	1220	1211	1214	8	700	689	701
9	1214	1209	1204	9	800	768	788
10	1205	1200	1192	10	930	915	915
11	1170	1158	1165	11	1010	1011	1015
12	1120	1055	1115	12	1030	1022	1024
13	970	969	961	13	1040	1036	1038
14	729	725	718	14	1050	1047	1049
15	500	505	498	15	1044	1042	1037
16	300	289	293	16	1035	1036	1030
17	209	235	200	17	1000	1008	989
18	212	215	197	18	950	958	944
20	200	192	182	20	800	784	798
22	180	187	171	22	650	646	625
24	163	161	160	24	400	385	389
26	152	155	153	26	300	285	288
27	148	144	148	27	250	244	222
29	146	145	145	29	200	215	194
30	145	146	144	30	191	184	187
31	145	143	144	31	180	178	177
33	141	142	141	33	164	168	160
35	141	141	141	35	146	144	150
36	142	141	141	36	142	140	143
37	141	141	141	37	148	144	145
39	141	141	141	39	146	145	145
40	141	141	141	40	145	143	142
42	141	142	141	42	142	141	141
43	141	141	141	43	145	145	143
45	141	141	141	45	145	142	144
46	141	141	141	46	144	141	142
47	141	141	141	47	141	141	141

49	141	141	141	49	141	141	141
50	141	141	141	50	141	141	141
52	141	141	141	52	141	141	141
54	141	141	141	54	141	141	141
56	141	141	141	56	141	141	141
58	141	141	141	58	141	141	141
60	141	141	141	60	141	141	141
62	141	141	141	62	141	141	141
64	141	141	141	64	141	141	141
66	141	141	141	66	141	141	141
68	141	141	141	68	141	141	141
70	141	141	141	70	141	141	141
72	141	141	141	72	141	141	141
74	141	141	141	74	141	141	141
76	141	141	141	76	141	141	141
78	141	141	141	78	141	141	141
80	141	141	141	80	141	141	141
82	141	141	141	82	141	141	141
84	141	141	141	84	141	141	141
86	141	141	141	86	141	141	141
88	141	141	141	88	141	141	141
90	141	141	141	90	141	141	141
92	141	141	141	92	141	141	141
94	141	141	141	94	141	141	141
96	141	141	141	96	141	141	141
98	141	141	141	98	141	141	141
100	141	141	141	100	141	141	141
102	141	141	141	102	141	141	141
104	141	141	141	104	141	141	141
106	141	141	141	106	141	141	141
108	141	141	141	108	141	141	141
110	141	141	141	110	141	141	141
112	141	141	141	112	141	141	141
114	141	141	141	114	141	141	141
116	141	141	141	116	141	141	141
118	141	141	141	118	141	141	141
120	141	141	141	120	141	141	141

Table A 1. 2 BH1 and BH2 Porous aquifer system tracer breakthrough test data Model 2 (15 g).

BH1				BH2			
Time (mins)	FEC (µS/cm)			Time (mins)	FEC (µS/cm)		
	T1	T2	T3		T1	T2	T3
0	141	141	141	0	141	141	141
1	440	527	550	1	141	141	141
2	1365	1545	1540	2	248	401	411
3	2270	2235	2269	3	750	744	688
4	3000	2851	2983	4	1151	1080	1149
5	3300	3211	3277	5	1453	1433	1450
6	3401	3288	3400	6	1723	1720	1689
7	3488	3433	3468	7	2014	2001	2011
8	3490	3473	3460	8	2257	2235	2238
9	3454	3411	3448	9	2517	2498	2477
10	3405	3300	3375	10	2732	2664	2711
11	3240	3211	3238	11	2819	2799	2789
12	3107	3011	3100	12	2910	2804	2801
13	2820	2800	2811	13	2936	2825	2824
14	2613	2578	2600	14	2950	2900	2830
15	2380	2211	2368	15	2935	2851	2822
16	2089	2013	2077	16	2855	2838	2815
17	1890	1854	1868	17	2827	2801	2798
18	1625	1616	1620	18	2716	2700	2707
20	1150	1135	1143	20	2354	2504	2291
22	908	728	883	22	1800	1764	1799
24	723	603	701	24	1450	1488	1371
26	514	492	500	26	981	1 180	1077
27	478	463	466	27	751	843	764
29	393	390	385	29	521	682	520
30	342	333	338	30	325	555	315
31	304	287	310	31	287	345	280
33	240	248	247	33	234	300	341
35	208	216	213	35	197	277	190
36	182	178	180	36	180	178	187
37	155	150	155	37	172	160	170
39	148	150	147	39	169	158	163
40	148	145	148	40	164	150	160
42	143	141	141	42	157	148	155
43	143	142	143	43	155	147	151
45	141	142	141	45	150	145	148
46	143	141	141	46	146	148	146
47	141	141	141	47	148	145	148
49	142	141	141	49	152	147	147
50	141	141	141	50	147	144	150
52	141	141	141	52	148	143	148
54	141	141	141	54	145	144	145
56	141	141	141	56	143	143	144
58	141	141	141	58	142	141	143

60	141	141	141	60	145	142	144
62	141	141	141	62	143	141	142
64	141	141	141	64	142	141	141
66	141	141	141	66	141	141	142
68	141	141	141	68	141	141	141
70	141	141	141	70	141	141	141
72	141	141	141	72	141	141	141
74	141	141	141	74	141	141	141
76	141	141	141	76	141	141	141
78	141	141	141	78	141	141	141
80	141	141	141	80	141	141	141
82	141	141	141	82	142	141	141
84	141	141	141	84	141	141	141
86	141	141	141	86	141	141	141
88	141	141	141	88	141	141	141
90	141	141	141	90	141	141	141
92	141	141	141	92	141	141	141
94	141	141	141	94	141	141	141
96	141	141	141	96	141	141	141
98	141	141	141	98	141	141	141
100	141	141	141	100	141	141	141
102	141	141	141	102	141	141	141
104	141	141	141	104	141	141	141
106	141	141	141	106	141	141	141
108	141	141	141	108	141	141	141
110	141	141	141	110	141	141	141
112	141	141	141	112	141	141	141
114	141	141	141	114	141	141	141
116	141	141	141	116	141	141	141
118	141	141	141	118	141	141	141
120	141	141	141	120	141	141	141

Table A 1. 3 BH1 and BH2 Porous aquifer system tracer breakthrough test data Model 3 (20 g).

BH1				BH2			
Time (mins)	FEC (µS/cm)			Time (mins)	FEC (µS/cm)		
	T1	T2	T3		T1	T2	T3
0	141	141	141	0	141	141	141
1	887	880	928	1	141	141	141
2	2030	2160	2189	2	580	570	582
3	2815	2792	2810	3	911	898	900
4	3729	3711	3715	4	1237	1230	1235
5	4623	4620	4589	5	1 702	1680	1645
6	4924	4899	4835	6	513	2500	2444
7	5125	4934	5011	7	3124	3024	3033
8	5208	4977	5089	8	3 624	3555	3510
9	5108	4953	4988	9	052	3899	3888
10	4917	4854	4863	10	4207	4058	4012
11	4629	4597	4647	11	4510	4333	4385
12	3773	3759	3691	12	4650	4577	4608
13	3323	3320	3360	13	4698	4607	4658
14	3023	2890	3067	14	4731	4728	4730
15	2823	2615	2769	15	4680	4601	4482
16	2623	2409	2553	16	4420	4338	4014
17	2407	2210	2382	17	4030	3900	3406
18	2001	1845	1983	18	3407	3244	2890
20	1562	1414	1482	20	2602	2357	2380
22	1373	1164	1283	22	2180	1801	2011
24	1257	1001	1083	24	1713	1319	1590
26	953	720	883	26	1208	970	1111
27	757	620	743	27	800	798	731
29	515	481	505	29	621	605	611
30	409	397	408	30	540	535	520
31	387	375	317	31	438	428	428
33	343	339	336	33	395	388	382
35	320	318	307	35	312	309	309
36	298	288	274	36	293	292	288
37	263	260	225	37	273	270	268
39	240	235	243	39	251	247	248
40	211	209	213	40	239	233	230
42	209	204	201	42	221	218	228
43	183	180	168	43	219	209	220
45	165	170	161	45	201	205	200
46	157	158	157	46	192	190	198
47	149	148	145	47	190	187	189
49	145	147	144	49	188	180	180
50	143	144	147	50	184	183	179
52	141	143	141	52	175	170	170
54	145	144	143	54	166	159	160
56	143	142	142	56	157	155	155
58	141	141	141	58	150	148	149

60	141	141	141	60	147	149	148
62	141	141	141	62	145	144	145
64	141	141	141	64	145	143	144
66	141	141	141	66	143	150	143
68	141	141	141	68	141	142	148
70	141	141	141	70	145	144	142
72	141	141	141	72	141	143	141
74	141	141	141	74	146	142	143
76	141	141	141	76	143	141	141
78	141	141	141	78	141	141	141
80	141	141	141	80	141	141	141
82	141	141	141	82	141	141	141
84	141	141	141	84	141	141	141
86	141	141	141	86	141	141	141
88	141	141	141	88	141	141	141
90	141	141	141	90	141	141	141
92	141	141	141	92	141	141	141
94	141	141	141	94	141	141	141
96	141	141	141	96	141	141	141
98	141	141	141	98	141	141	141
100	141	141	141	100	141	141	141
102	141	141	141	102	141	141	141
104	141	141	141	104	141	141	141
106	141	141	141	106	141	141	141
108	141	141	141	108	141	141	141
110	141	141	141	110	141	141	141
112	141	141	141	112	141	141	141
114	141	141	141	114	141	141	141
116	141	141	141	116	141	141	141
118	141	141	141	118	141	141	141
120	141	141	141	120	141	141	141

Table A - 2. 1 Weathered basement aquifer system tracer breakthrough test data Model 1 (10 g).

BH			
Time (mins)	FEC (μS/cm)		
	T1	T2	T3
0	123	123	123
1	123	123	123
2	130	135	128
3	138	140	128
4	158	150	148
5	315	309	288
6	485	477	488
7	548	521	533
8	715	700	714
9	805	977	828
10	1028	1011	1020
11	1107	1100	1100
12	1183	1172	1173
13	1160	1148	1170
14	1155	1133	1163
15	1149	1128	1150
16	1128	1119	1130
17	1100	1063	1100
18	970	949	957
20	858	850	844
22	716	703	705
24	635	628	630
26	500	470	491
27	471	381	441
29	305	290	300
30	272	270	267
31	254	245	250
33	248	220	233
35	229	218	230
36	216	212	211
37	204	200	200
39	188	184	181
40	172	170	167
42	161	160	160
43	153	150	158
45	148	146	147
46	143	144	140
47	141	142	140
49	138	136	140
50	135	133	138
52	134	131	138
54	132	130	135
56	131	130	131
58	131	131	135

60	130	129	130
62	129	127	129
64	129	129	129
66	130	129	129
68	129	127	129
70	128	127	127
72	129	130	129
74	128	127	130
76	129	127	128
78	128	128	128
80	126	127	128
82	127	127	126
84	126	125	126
86	126	125	125
88	126	126	126
90	126	126	128
92	126	126	128
94	128	127	126
96	128	127	126
98	127	127	125
100	127	127	126
102	127	127	127
104	127	127	127
106	126	127	126
108	126	127	126
110	126	127	127
112	128	127	127
114	128	127	127
116	127	127	127
118	127	127	127
120	127	127	127

Table A - 2. 2 Weathered basement aquifer system tracer breakthrough test data Model 2 (15 g).

BH			
Time (mins)	FEC (µS/cm)		
	T1	T2	T3
0	125	125	125
1	125	124	125
2	338	488	430
3	900	867	883
4	1300	1189	1284
5	1700	1563	1677
6	2021	2001	2023
7	2262	2201	2254
8	2621	2611	2600
9	2888	2798	2790
10	3137	3162	3122
11	3190	3183	3171
12	3239	3216	3230
13	3214	3119	3200
14	3198	3105	3178
15	3140	3100	3133
16	3010	3001	3051
17	2896	2699	2876
18	2801	2601	2745
20	2400	2533	2511
22	2100	2200	2186
24	1611	1834	1774
26	1205	1198	1365
27	997	1002	1012
29	780	774	820
30	618	600	701
31	468	587	580
33	363	381	435
35	304	301	427
36	252	250	249
37	247	250	247
39	236	244	240
40	230	238	238
42	221	229	228
43	215	221	220
45	209	210	209
46	197	200	201
47	174	197	199
49	171	183	183
50	169	175	180
52	163	170	178
54	159	168	160
56	152	160	160
58	147	155	155

60	143	150	158
62	139	148	161
64	135	135	148
66	137	137	141
68	135	137	145
70	131	137	141
72	129	130	138
74	127	130	135
76	129	128	129
78	129	127	130
80	129	128	128
82	127	126	127
84	129	127	127
86	130	129	127
88	129	130	127
90	129	130	127
92	129	129	127
94	128	127	127
96	129	127	127
98	127	127	127
100	130	127	127
102	129	127	127
104	127	127	127
106	127	127	127
108	129	127	127
110	129	127	129
112	127	127	127
114	127	127	127
116	127	127	129
118	127	127	129
120	127	127	127

Table A - 2. 3 Weathered basement aquifer system tracer breakthrough test data Model 3 (20 g).

BH			
Time (mins)	FEC (µS/cm)		
	T1	T2	T3
0	125	125	125
1	125	125	125
2	765	720	738
3	1238	1212	1222
4	1653	1648	1430
5	2416	2400	2420
6	2855	2867	2664
7	3427	3212	3682
8	4010	3814	3995
9	4412	4011	4410
10	4603	4463	4600
11	4804	4678	4711
12	4918	4766	4800
13	4907	4754	4890
14	4870	4866	4881
15	4801	4787	4872
16	4780	4773	4760
17	4580	4565	4551
18	4400	4386	4321
20	3600	3501	3620
22	2800	2789	2520
24	1850	1843	1712
26	1310	1311	1311
27	1079	1083	1077
29	935	910	930
30	865	832	866
31	761	742	767
33	656	650	653
35	552	551	555
36	432	441	430
37	329	322	320
39	309	300	311
40	285	283	280
42	260	253	254
43	245	242	243
45	220	219	220
46	218	215	220
47	201	212	213
49	198	209	190
50	183	194	188
52	170	184	177
54	168	166	164
56	163	160	166
58	157	155	161

60	149	153	159
62	154	150	155
64	150	148	152
66	147	148	149
68	142	145	150
70	138	141	147
72	143	144	145
74	137	132	146
76	133	130	144
78	145	138	139
80	143	143	140
82	138	137	140
84	134	135	139
86	131	130	135
88	129	126	130
90	128	128	131
92	131	139	129
94	129	130	133
96	128	127	129
98	129	129	128
100	129	129	129
102	128	127	129
104	128	126	129
106	128	128	127
108	128	127	128
110	128	129	128
112	128	128	128
114	128	128	128
116	128	128	128
118	128	128	128
120	128	128	128

Appendix B

POROUS AQUIFER SYSTEM FLUID ELECTRICAL CONDUCTIVITY DATA

Table B - 1. 1 Porous aquifer system background data Model 1 (10 g).

Background FEC data for both BH1 and BH2									
2 minutes				4 minutes			8 minutes		
Depth (cm)	FEC (µS/cm)			FEC (µS/cm)			FEC (µS/cm)		
	T1	T2	T3	T1	T2	T3	T1	T2	T3
1	142	142	143	141	141	141	141	141	141
2	141	142	142	141	141	141	141	141	141
4	141	141	141	141	141	141	141	141	141
6	142	141	142	141	141	141	141	141	141
8	141	142	141	141	141	141	141	141	141
10	142	142	141	141	141	141	141	141	141
12	141	141	141	141	141	141	141	141	141

Table B - 1. 2 Porous aquifer system background data Model 2 (15 g).

Background FEC data for both BH1 and BH2									
2 minutes				4 minutes			8 minutes		
Depth (cm)	FEC (µS/cm)			FEC (µS/cm)			FEC (µS/cm)		
	T1	T2	T3	T1	T2	T3	T1	T2	T3
1	142	144	144	142	141	141	141	141	141
2	141	142	141	141	141	142	141	141	141
4	143	143	143	141	141	141	141	141	141
6	141	141	142	141	141	141	141	141	141
8	143	142	143	141	141	141	141	141	141
10	141	141	141	141	141	141	141	141	141
12	141	142	142	141	141	141	141	141	141

Table B - 1. 3 Porous aquifer system background data Model 3 (20 g).

Background FEC data for both BH1 and BH2									
2 minutes				4 minutes			8 minutes		
Depth (cm)	FEC (µS/cm)			FEC (µS/cm)			FEC (µS/cm)		
	T1	T2	T3	T1	T2	T3	T1	T2	T3
1	143	141	143	141	142	141	141	141	141
2	143	142	143	141	141	141	141	141	141
4	141	141	142	141	141	141	141	141	141
6	142	143	142	141	141	141	141	141	141
8	141	141	142	141	141	141	141	141	141
10	141	141	141	141	141	141	141	141	141
12	141	141	141	141	141	141	141	141	141

Table B - 2. 1 Porous aquifer system plume arrival data Model 1 (10 g).

Plume arrival at BH1							Plume arrival at BH2						
	1 minute			2 minutes				2 minutes			4 minutes		
Depth (cm)	FEC (µS/cm)			FEC (µS/cm)			Depth (cm)	FEC (µS/cm)			FEC (µS/cm)		
	T1	T2	T3	T1	T2	T3		T1	T2	T3	T1	T2	T3
1	141	141	141	744	750	738	0	-	-	-	-	-	-
2	141	141	142	746	743	742	2	142	141	142	600	570	585
4	142	144	141	877	869	863	4	144	144	143	700	625	668
6	142	145	148	1049	1037	1040	6	145	146	145	900	873	881
8	163	158	153	1214	1203	1211	8	145	145	145	800	748	776
10	189	180	189	1699	1705	1681	10	143	144	143	600	514	593
12	189	188	201	2023	2 018	2 020	12	141	143	142	200	285	350

Table B - 2. 2 Porous aquifer system plume arrival data Model 2 (15 g).

Plume arrival at BH1							Plume arrival at BH2						
	1 minute			2 minutes				2 minutes			4 minutes		
Depth (cm)	FEC (µS/cm)			FEC (µS/cm)			Depth (cm)	FEC (µS/cm)			FEC (µS/cm)		
	T1	T2	T3	T1	T2	T3		T1	T2	T3	T1	T2	T3
1	148	152	147	946	924	943	0	-	-	-	-	-	-
2	148	153	150	968	947	955	2	265	248	259	687	653	669
4	287	281	288	1148	1137	1133	4	380	335	360	1085	996	1078
6	287	288	315	1350	1339	1342	6	423	411	419	1167	1089	1154
8	581	579	570	1550	1538	1541	8	399	370	378	1061	1008	1048
10	581	588	577	2150	2031	2134	10	306	285	297	742	740	739
12	581	603	593	2268	2143	2240	12	268	255	260	553	558	547

Table B - 2. 3 Porous aquifer system plume arrival data Model 3 (20 g).

Plume arrival at BH1							Plume arrival at BH2						
	1 minute			2 minutes				2 minutes			4 minutes		
Depth (cm)	FEC (µS/cm)			FEC (µS/cm)			Depth (cm)	FEC (µS/cm)			FEC (µS/cm)		
	T1	T2	T3	T1	T2	T3		T1	T2	T3	T1	T2	T3
1	365	343	351	1350	1287	1339	0	-	-	-	-	-	-
2	386	359	357	1371	1338	1344	2	405	410	407	943	933	939
4	543	511	539	1590	1553	1581	4	431	428	428	1118	1137	1125
6	890	793	855	1879	1780	1880	6	588	578	581	1243	1229	1238
8	926	920	953	2241	2155	2228	8	541	550	539	1216	1205	1208
10	1157	1098	1168	2358	2328	2305	10	480	451	469	978	949	967
12	1202	1182	1190	2573	2497	2529	12	320	319	311	450	438	444

Table B - 3. 1 Porous aquifer system plume peak data Model 1 (10 g).

Plume peak at BH1				Plume peak at BH2			
Depth (cm)	8 minutes			Depth (cm)	14 minutes		
	FEC (μS/cm)				FEC (μS/cm)		
	T1	T2	T3		T1	T2	T3
1	1182	1180	1175	0	-	-	-
2	1199	1194	1185	2	930	927	930
4	1210	1209	1201	4	1035	1028	1030
6	1215	1211	1210	6	1081	1059	1076
8	1219	1215	1213	8	1045	1033	1042
10	1167	1160	1158	10	950	940	939
12	1150	1153	1147	12	930	911	923

Table B - 3. 2 Porous aquifer system plume peak data Model 2 (15 g).

Plume peak at BH1				Plume peak at BH2			
Depth (cm)	8 minutes			Depth (cm)	14 minutes		
	FEC (μS/cm)				FEC (μS/cm)		
	T1	T2	T3		T1	T2	T3
1	2159	2140	2143	0	-	-	-
2	2343	2311	2339	2	2311	2298	2300
4	2935	2928	2890	4	2750	2703	2739
6	3194	3088	3165	6	2901	2873	2831
8	3486	3466	3457	8	2846	2830	2803
10	2958	2921	2934	10	2178	2350	2166
12	1766	1743	1732	12	2139	2305	2127

Table B - 3. 3 Porous aquifer system plume peak data Model 3 (20 g).

Plume peak at BH1				Plume peak at BH2			
Depth (cm)	8 minutes			Depth (cm)	14 minutes		
	FEC (μS/cm)				FEC (μS/cm)		
	T1	T2	T3		T1	T2	T3
1	3291	3250	3271	0	-	-	-
2	3543	3382	3520	2	3419	3398	3416
4	4288	3889	4257	4	4425	4273	4415
6	4991	4684	4957	6	4800	4779	4789
8	5198	4982	5097	8	4742	4700	4757
10	5037	4832	4786	10	3980	3864	3900
12	3043	2932	2876	12	3790	3698	3699

Table B - 4. 1 Porous aquifer system residual plume data Model 1 (10 g).

Residual plume at BH1				Residual plume at BH2			
Depth (cm)	16 minutes			Depth (cm)	18 minutes		
	FEC (µS/cm)				FEC (µS/cm)		
	T1	T2	T3		T1	T2	T3
1	297	298	299	0	-	-	-
2	295	295	295	2	224	224	224
4	294	295	295	4	224	224	224
6	288	289	288	6	225	226	225
8	285	286	286	8	224	225	224
10	282	281	283	10	224	224	224
12	277	279	280	12	224	224	224

Table B - 4. 2 Porous aquifer system residual plume data Model 1 (15 g).

Residual plume at BH1				Residual plume at BH2			
Depth (cm)	16 minutes			Depth (cm)	18 minutes		
	FEC (µS/cm)				FEC (µS/cm)		
	T1	T2	T3		T1	T2	T3
1	2142	2133	2144	0	-	-	-
2	2135	2128	2130	2	1788	1789	1786
4	2111	2111	2115	4	1790	1787	1791
6	2094	2084	2090	6	1803	1805	1801
8	2083	2077	2080	8	1802	1803	1800
10	2078	2070	2077	10	1765	1758	1760
12	2065	2066	2066	12	1750	1746	1748

Table B - 4. 3 Porous aquifer system residual plume data Model 1 (20 g).

Residual plume at BH1				Residual plume at BH2			
Depth (cm)	16 minutes			Depth (cm)	18 minutes		
	FEC (µS/cm)				FEC (µS/cm)		
	T1	T2	T3		T1	T2	T3
1	2683	2677	2680	0	-	-	-
2	2651	2650	2643	2	2102	2100	2108
4	2575	2570	2566	4	2138	2140	2140
6	2490	2487	2480	6	2158	2165	2160
8	2456	2450	2455	8	2140	2138	2144
10	2351	2355	2351	10	2088	2079	2073
12	2319	2322	2315	12	2052	2053	2050

Table B - 5. 1 Porous aquifer system near-background data Model 1 (10 g).

Near-background FEC profile at BH1												
	27 minutes			33 minutes			47 minutes			62 minutes		
Depth (cm)	FEC (µS/cm)			FEC (µS/cm)			FEC (µS/cm)			FEC (µS/cm)		
	T1	T2	T3	T1	T2	T3	T1	T2	T3	T1	T2	T3
1	148	148	148	141	141	141	141	141	141	141	141	141
2	148	148	148	141	141	141	141	141	141	141	141	141
4	148	148	148	141	141	141	141	141	141	141	141	141
6	148	148	148	141	141	141	141	141	141	141	141	141
8	148	148	148	141	141	141	141	141	141	141	141	141
10	148	148	148	141	141	141	141	141	141	141	141	141
12	148	148	148	141	141	141	141	141	141	141	141	141
	82 minutes			111 minutes			116 minutes					
Depth (cm)	FEC (µS/cm)			FEC (µS/cm)			FEC (µS/cm)					
	T1	T2	T3	T1	T2	T3	T1	T2	T3			
1	141	141	141	141	141	141	141	141	141			
2	141	141	141	141	141	141	141	141	141			
4	141	141	141	141	141	141	141	141	141			
6	141	141	141	141	141	141	141	141	141			
8	141	141	141	141	141	141	141	141	141			
10	141	141	141	141	141	141	141	141	141			
12	141	141	141	141	141	141	141	141	141			

Table B - 5. 2 Porous aquifer system near-background data Model 2 (15 g).

Near-background FEC profile at BH1												
	27 minutes			33 minutes			47 minutes			62 minutes		
Depth (cm)	FEC (µS/cm)			FEC (µS/cm)			FEC (µS/cm)			FEC (µS/cm)		
	T1	T2	T3	T1	T2	T3	T1	T2	T3	T1	T2	T3
1	530	528	533	247	250	248	141	141	141	141	141	141
2	505	500	503	243	244	240	141	141	141	141	141	141
4	490	488	491	240	238	238	141	141	141	141	141	141
6	480	483	485	235	231	233	141	141	141	141	141	141
8	463	460	465	230	228	230	141	141	141	141	141	141
10	455	458	453	227	227	228	141	141	141	141	141	141
12	450	451	451	219	220	221	141	141	141	141	141	141
	82 minutes			111 minutes			116 minutes					
Depth (cm)	FEC (µS/cm)			FEC (µS/cm)			FEC (µS/cm)					
	T1	T2	T3	T1	T2	T3	T1	T2	T3			
1	141	141	141	141	141	141	141	141	141			
2	141	141	141	141	141	141	141	141	141			
4	141	141	141	141	141	141	141	141	141			
6	141	141	141	141	141	141	141	141	141			
8	141	141	141	141	141	141	141	141	141			
10	141	141	141	141	141	141	141	141	141			
12	141	141	141	141	141	141	141	141	141			

Table B - 5. 3 Porous aquifer system near-background data Model 3 (20 g).

Near-background FEC profile at BH1												
	27 minutes			33 minutes			47 minutes			62 minutes		
Depth (cm)	FEC (µS/cm)			FEC (µS/cm)			FEC (µS/cm)			FEC (µS/cm)		
	T1	T2	T3	T1	T2	T3	T1	T2	T3	T1	T2	T3
1	963	960	959	430	428	425	155	155	153	141	141	141
2	830	855	825	423	420	418	153	152	151	141	141	141
4	775	768	770	390	388	387	150	151	150	141	141	141
6	602	588	600	343	340	344	149	150	149	141	141	141
8	548	533	550	311	315	320	148	148	148	141	141	141
10	521	519	520	294	290	288	149	149	149	141	141	141
12	450	450	455	272	271	270	149	150	149	141	141	141

	82 minutes			111 minutes			116 minutes		
Depth (cm)	FEC (µS/cm)			FEC (µS/cm)			FEC (µS/cm)		
	T1	T2	T3	T1	T2	T3	T1	T2	T3
1	141	141	141	141	141	141	141	141	141
2	141	141	141	141	141	141	141	141	141
4	141	141	141	141	141	141	141	141	141
6	141	141	141	141	141	141	141	141	141
8	141	141	141	141	141	141	141	141	141
10	141	141	141	141	141	141	141	141	141
12	141	141	141	141	141	141	141	141	141

Appendix C

WEATHERED BASEMENT AQUIFER SYSTEM FLUID ELECTRICAL CONDUCTIVITY DATA

Table C - 1. 1 Weathered basement aquifer system background data Model 1 (10 g).

Background FEC data									
	2 minutes			4 minutes			8 minutes		
Depth (cm)	FEC (µS/cm)			FEC (µS/cm)			FEC (µS/cm)		
	T1	T2	T3	T1	T2	T3	T1	T2	T3
0	-	-	-	-	-	-	-	-	-
2	126	126	126	123	123	123	123	123	123
4	126	126	126	123	123	123	123	123	123
6	126	127	126	123	123	123	123	123	123
8	127	126	128	124	124	124	124	124	124
10	129	129	129	126	126	126	126	126	126
12	130	131	130	128	128	127	128	128	127
14	132	132	132	128	129	128	129	129	129
16	133	133	133	130	130	130	129	129	129
18	133	133	133	130	130	130	129	129	129
20	133	133	133	130	130	130	129	129	129

Table C - 1. 2 Weathered basement aquifer system background data Model 2 (15 g).

Background FEC data									
	2 minutes			4 minutes			8 minutes		
Depth (cm)	FEC (µS/cm)			FEC (µS/cm)			FEC (µS/cm)		
	T1	T2	T3	T1	T2	T3	T1	T2	T3
0	-	-	-	-	-	-	-	-	-
2	127	126	126	123	123	123	123	123	123
4	128	126	125	123	123	123	123	123	123
6	125	125	125	124	124	123	123	123	123
8	124	124	125	122	124	123	124	124	124
10	124	126	125	122	124	123	125	127	126
12	129	130	129	130	128	128	128	128	128
14	130	130	130	130	130	130	129	129	129
16	130	130	130	130	130	130	129	129	129
18	129	130	130	130	130	130	129	129	129
20	130	130	130	129	130	130	129	129	129

Table C - 1. 3 Weathered basement aquifer system background data Model 3 (20 g).

Background FEC data									
	2 minutes			4 minutes			8 minutes		
Depth (cm)	FEC (µS/cm)			FEC (µS/cm)			FEC (µS/cm)		
	T1	T2	T3	T1	T2	T3	T1	T2	T3
0	-	-	-	-	-	-	-	-	-
2	125	125	126	124	123	124	123	123	123
4	126	126	126	124	123	124	123	123	123
6	127	126	126	124	123	123	123	123	123
8	126	126	126	123	123	123	124	124	124
10	126	128	128	128	126	127	127	127	127
12	133	130	133	129	129	129	128	127	128
14	133	133	133	130	130	130	129	129	129
16	133	133	133	131	131	131	129	129	129
18	133	133	133	131	131	131	129	129	129
20	132	133	133	131	131	131	129	129	129

Table C - 2. 1 Weathered basement aquifer system plume arrival and plume peak data Model 1 (10 g).

First arrival of plume FEC data				Plume peak FEC data			
Depth (cm)	2 minutes FEC (µS/cm)			Depth (cm)	12 minutes FEC (µS/cm)		
	T1	T2	T3		T1	T2	T3
0	-	-	-	0	-	-	-
2	135	135	135	2	1050	1030	1046
4	142	142	145	4	1121	1091	1102
6	148	146	148	6	1173	1160	1165
8	143	143	143	8	1158	1133	1160
10	130	130	130	10	1110	1108	1111
12	128	128	128	12	1050	1035	986
14	127	129	128	14	859	850	801
16	129	129	129	16	610	615	607
18	129	129	129	18	543	545	544
20	129	129	129	20	519	525	520

Table C - 2. 2 Weathered basement aquifer system plume arrival and plume peak data Model 2 (15 g).

First arrival of plume FEC data				Plume peak FEC data			
Depth (cm)	2 minutes FEC (µS/cm)			Depth (cm)	12 minutes FEC (µS/cm)		
	T1	T2	T3		T1	T2	T3
0	-	-	-	0	-	-	-
2	340	350	338	2	1303	1290	1298
4	498	501	490	4	2042	2033	2022
6	532	530	526	6	3239	3227	3229
8	489	500	485	8	3203	3188	3220
10	421	458	435	10	3073	2987	3098
12	298	310	301	12	2694	2513	2585
14	256	260	254	14	2162	2085	2153
16	235	249	240	16	1363	1401	1357
18	221	227	221	18	825	812	820
20	221	223	220	20	796	799	790

Table C - 2. 3 Weathered basement aquifer system plume arrival and plume peak data Model 3 (20 g).

First arrival of plume FEC data				Plume peak FEC data			
Depth (cm)	2 minutes FEC (µS/cm)			Depth (cm)	12 minutes FEC (µS/cm)		
	T1	T2	T3		T1	T2	T3
0	-	-	-	0	-	-	-
2	395	390	386	2	2002	1978	1988
4	532	532	525	4	3890	3853	3877
6	750	721	743	6	4812	4781	4801
8	715	693	705	8	4623	4510	4600
10	632	645	628	10	4316	4300	4290
12	475	470	462	12	3733	3687	3600
14	400	374	389	14	2265	2015	2197
16	327	320	321	16	1886	1833	1691
18	316	315	318	18	983	974	991
20	316	316	320	20	965	955	970

Table C - 3. 1 Weathered basement aquifer system residual plume data Model 1 (10 g).

Residual plume FEC data												
	27 minutes			30 minutes			33 minutes			36 minutes		
Depth (cm)	FEC (µS/cm)			FEC (µS/cm)			FEC (µS/cm)			FEC (µS/cm)		
	T1	T2	T3	T1	T2	T3	T1	T2	T3	T1	T2	T3
0	-	-	-	-	-	-	-	-	-	-	-	-
2	415	415	414	290	288	291	245	244	245	203	205	202
4	428	435	430	280	281	283	245	244	243	201	200	200
6	435	440	438	280	283	285	243	240	240	201	200	201
8	430	435	430	292	290	290	250	248	247	207	209	205
10	417	420	415	311	308	310	257	254	255	211	215	217
12	390	384	388	320	315	322	271	270	273	228	226	230
14	378	375	376	338	336	334	289	290	286	246	250	251
16	362	365	363	344	348	348	308	310	311	278	280	277
18	362	364	363	347	350	347	314	314	313	284	286	288
20	362	363	362	347	350	348	328	330	330	297	292	290

	40 minutes			60 minutes			70 minutes		
Depth (cm)	FEC (µS/cm)			FEC (µS/cm)			FEC (µS/cm)		
	T1	T2	T3	T1	T2	T3	T1	T2	T3
0	-	-	-	-	-	-	-	-	-
2	156	153	157	128	130	130	124	122	123
4	155	153	155	128	130	128	124	123	123
6	155	153	155	128	130	128	124	124	123
8	167	168	170	133	135	131	125	126	125
10	180	178	181	140	138	138	129	130	128
12	195	193	193	163	160	162	145	143	144
14	229	230	230	180	178	180	162	161	161
16	235	240	238	189	188	187	168	167	166
18	248	250	248	193	191	190	170	171	173
20	253	250	251	200	198	201	173	172	173

Table C - 3. 2 Weathered basement aquifer system residual plume data Model 1 (15 g).

Residual plume FEC data												
	27 minutes			30 minutes			33 minutes			36 minutes		
Depth (cm)	FEC (µS/cm)			FEC (µS/cm)			FEC (µS/cm)			FEC (µS/cm)		
	T1	T2	T3	T1	T2	T3	T1	T2	T3	T1	T2	T3
0	-	-	-	-	-	-	-	-	-	-	-	-
2	899	890	895	532	530	528	423	425	428	331	328	330
4	950	953	944	601	605	587	402	406	408	319	320	325
6	986	990	980	635	628	633	371	370	372	305	310	308
8	898	910	890	617	610	620	362	368	366	307	315	311
10	813	850	825	569	570	568	403	405	408	358	360	362
12	687	680	688	515	517	520	421	420	422	398	400	403
14	651	650	653	507	503	511	447	450	449	415	418	428
16	624	635	628	494	498	495	463	466	460	429	435	438
18	615	610	618	490	490	488	468	470	466	443	440	444
20	605	606	610	489	490	487	472	470	470	448	450	453

	40 minutes			60 minutes			70 minutes		
	FEC (µS/cm)			FEC (µS/cm)			FEC (µS/cm)		

Depth (cm)	T1	T2	T3	T1	T2	T3	T1	T2	T3
0	-	-	-	-	-	-	-	-	-
2	245	244	238	143	145	147	132	135	133
4	240	241	240	142	141	142	130	132	132
6	235	230	233	143	143	144	130	132	133
8	233	233	234	166	168	159	138	138	140
10	270	265	275	222	217	225	161	160	157
12	325	321	319	271	260	268	187	190	183
14	350	338	341	295	287	300	216	220	211
16	392	377	381	322	314	319	267	260	261
18	405	402	402	330	325	328	284	277	281
20	418	415	420	335	330	331	295	300	301

Table C - 3. 3 Weathered basement aquifer system residual plume data Model 1 (20 g).

Residual plume FEC data												
	27 minutes			30 minutes			33 minutes			36 minutes		
Depth (cm)	FEC (µS/cm)			FEC (µS/cm)			FEC (µS/cm)			FEC (µS/cm)		
	T1	T2	T3	T1	T2	T3	T1	T2	T3	T1	T2	T3
0	-	-	-	-	-	-	-	-	-	-	-	-
2	966	950	958	729	730	730	574	568	570	461	455	460
4	1053	1048	1051	816	801	814	631	628	633	440	438	444
6	1081	1077	1088	871	866	865	667	651	661	428	430	431
8	1079	1068	1071	853	851	850	658	644	660	420	420	425
10	1052	1055	1041	805	800	811	611	600	612	432	433	433
12	988	980	962	673	662	682	534	532	528	455	461	455
14	823	821	850	605	578	594	518	520	519	463	466	466
16	701	687	700	587	580	580	515	516	515	469	470	470
18	670	658	677	572	575	576	508	510	510	471	472	471
20	652	650	653	570	571	568	493	490	491	473	475	474

	40 minutes			60 minutes			70 minutes		
Depth (cm)	FEC (µS/cm)			FEC (µS/cm)			FEC (µS/cm)		
	T1	T2	T3	T1	T2	T3	T1	T2	T3
0	-	-	-	-	-	-	-	-	-
2	325	330	328	179	180	183	143	143	145
4	311	315	311	173	177	179	145	144	146
6	290	294	291	167	167	168	140	141	141
8	288	278	278	164	163	165	141	141	140
10	309	301	300	192	190	191	157	155	155
12	356	350	348	243	240	244	193	190	192
14	384	381	377	317	323	319	275	277	276
16	400	405	411	338	345	340	301	298	305
18	411	420	415	351	355	352	322	320	319
20	425	423	432	379	382	380	329	330	333

Table C - 4. 1 Weathered basement aquifer system near-background data Model 1 (10 g).

Near-background FEC data									
	80 minutes			108 minutes			130 minutes		
Depth (cm)	FEC (µS/cm)			FEC (µS/cm)			FEC (µS/cm)		
	T1	T2	T3	T1	T2	T3	T1	T2	T3
0	-	-	-	-	-	-	-	-	-
2	123	124	123	123	123	123	123	123	123
4	124	124	123	123	124	123	123	123	123
6	123	123	123	123	123	124	123	123	124
8	124	124	128	123	125	126	123	123	124
10	126	130	127	129	127	128	125	126	126
12	138	136	138	134	130	131	129	127	130
14	152	155	153	139	138	140	132	130	131
16	157	160	159	148	149	147	141	142	143
18	160	165	166	150	153	151	148	145	149
20	169	172	171	156	155	155	148	148	148

Table C - 4. 2 Weathered basement aquifer system near-background data Model 1 (15 g).

Near-background FEC data									
	80 minutes			108 minutes			130 minutes		
Depth (cm)	FEC (µS/cm)			FEC (µS/cm)			FEC (µS/cm)		
	T1	T2	T3	T1	T2	T3	T1	T2	T3
0	-	-	-	-	-	-	-	-	-
2	129	129	130	127	127	127	126	126	126
4	130	129	131	128	127	127	126	126	126
6	129	130	129	127	127	127	126	127	126
8	135	132	133	131	130	134	128	127	128
10	138	137	138	133	135	133	129	131	130
12	147	148	147	143	146	144	135	136	138
14	162	163	161	159	160	161	147	150	148
16	169	171	170	162	161	163	153	155	156
18	173	175	172	170	173	171	159	161	163
20	180	180	179	176	176	177	161	163	163

Table C - 4. 3 Weathered basement aquifer system near-background data Model 1 (20 g).

Near-background FEC data									
	80 minutes			108 minutes			130 minutes		
Depth (cm)	FEC (µS/cm)			FEC (µS/cm)			FEC (µS/cm)		
	T1	T2	T3	T1	T2	T3	T1	T2	T3
0	-	-	-	-	-	-	-	-	-
2	141	140	142	131	129	129	130	128	131
4	138	137	141	129	129	129	128	128	128
6	138	138	138	129	129	129	128	128	129
8	143	145	138	135	132	135	131	132	133
10	149	150	151	140	138	139	137	138	140
12	155	153	154	149	149	150	142	141	144
14	168	172	170	163	161	164	155	156	158

16	178	175	175	174	172	173	162	163	162
18	189	185	187	182	180	181	171	172	171
20	193	192	191	190	188	190	183	180	182